Fall 12-2016

Design and Synthesis of Dynamic Covalent Polymer Scaffolds with Controlled Architectures

Emily Annette Hoff
University of Southern Mississippi

DESIGN AND SYNTHESIS OF DYNAMIC COVALENT POLYMER SCAFFOLDS WITH CONTROLLED ARCHITECTURES

by

Emily Annette Hoff

A Dissertation
Submitted to the Graduate School
and the School of Polymers and High Performance Materials
at The University of Southern Mississippi
in Partial Fulfillment of the Requirements
for the Degree of Doctor of Philosophy

Approved:

_____
Dr. Derek L. Patton, Committee Chair
Associate Professor, Polymers and High Performance Materials

_____
Dr. Sarah E. Morgan, Committee Member
Professor, Polymers and High Performance Materials

_____
Dr. Charles L. McCormick, Committee Member
Professor, Polymers and High Performance Materials

_____
Dr. Robson F. Storey, Committee Member
Professor, Polymers and High Performance Materials

_____
Dr. Yoan C. Simon, Committee Member
Assistant Professor, Polymers and High Performance Materials

_____
Dr. Karen S. Coats
Dean of the Graduate School

December 2016

Published by the Graduate School

ABSTRACT

DESIGN AND SYNTHESIS OF DYNAMIC COVALENT POLYMER SCAFFOLDS WITH CONTROLLED ARCHITECTURES

by Emily Annette Hoff

December 2016

The design and synthesis of functional, controlled polymer architectures is essential to the development of new materials with precise and tailorable properties or applications. The work described in this dissertation focuses on the development of controlled polymer architectures with dynamic linkages for the design of multifunctional materials and surfaces via robust, efficient, and stimuli-responsive strategies.

In Chapter III, a post-polymerization modification strategy based on ambient temperature nucleophilic chemical deblocking of polymer scaffolds bearing N-heterocycle blocked isocyanate moieties is reported. Room temperature RAFT polymerization of three azole-*N*-carboxamide methacrylates, including 3,5-dimethyl pyrazole, imidazole, and 1,2,4-triazole derivatives, afforded reactive polymer scaffolds with well-defined molecular weights and narrow dispersities ($Đ < 1.2$). The reactivity of the azole-*N*-carboxamide moieties towards nucleophiles can be tuned simply by varying the structure of the azole blocking agents. DBU-catalyzed reactions of thiols with imidazole- and 1, 2, 4-triazole-blocked isocyanate scaffolds were shown to occur rapidly and quantitatively under ambient conditions. Reactivity differences of 1,2,4-triazole and 3,5-dimethyl pyrazole-blocked isocyanate copolymers with various nucleophiles at room temperature facilitated sequential post-polymerization modification. This strategy

advances the utility of blocked isocyanates and promotes the chemistry as a powerful postmodification tool to access multifunctional polymeric materials.

Aqueous RAFT (aRAFT) polymerization at pH=0 mediated by a novel imidazolium-containing chain transfer agent is reported in Chapter IV. In 1 M HCl, unprecedented controlled polymerization and chain-extension of unprotected acyl hydrazide methacrylamides is achieved enabling the synthesis of well-defined acyl hydrazide functionalized polymer scaffolds of interest for dynamic covalent and bioconjugation strategies. Additionally, the well-controlled aRAFT polymerization of 4-vinylimidazole is demonstrated in water for the first time. Futhermore, methods for low pH aRAFT polymerizations will afford new access to controlled polymerization of monomers with low pKa values such as 4-vinylimidazole.

In Chaper V, hydrazide-functional brush surfaces are synthesized via a combination of surface-initiated atom-transfer radical polymerization (SI-ATRP) and post-polymerization modification (PPM). Hydrazone formation, cleavage, and exchange reactions on surfaces were achieved via these hydrazide-functional brush surfaces. The dynamic nature of the hydrazone linkage was leveraged toward reversible control of surface properties. The work in this chapter serves as a powerful and robust strategy for dynamic surfaces with pH-responsive linkages.

ACKNOWLEDGMENTS

I would first like to thank my family, friends, and colleagues for the invaluable support, guidance, knowledge, and wisdom they have shared with me.

I would especially like to thank my advisor, Dr. Derek L. Patton. He has been an excellent role model and mentor. I am very grateful for all of the opportunities to write, research, and present my work that he has provided and facilitated throughout my graduate career. I appreciate the freedom and trust he placed in me to conduct the research found in this dissertation. The high standards to which he holds himself and his students continually challenge me to be a better scientist.

I would like to extend my sincere gratitude to past and current members of the Patton Research Group. You have been outstanding colleagues and friends. I want to extend an extra thank you to Chase Tretbar for his part in all of research presented in this dissertation.

I would like to thank my committee members, Dr. Sarah Morgan, Dr. Charles McCormick, Dr. Robson Storey, Dr. Yoan Simon, and Dr. Daniel Savin, for their continued support in my professional and scientific development. A special thank you also goes to Jody Wiggins, Candy Sigler, Beverly McNeese, and Dr. Bret Calhoun for all of the support outside the lab that has been a huge asset to my graduate career.

I'd like to thank all of my collaborators: Dr. Brooks Abel, Chase Tretbar, Dr. Charles McCormick, Dr. Ryan Hensarling, Dr. Stephen Foster, Dr. Jacob Ray, and Dr. Daniel Savin. I would also like to acknowledge financial support from the NSF Graduate Research Fellowship Program (DGE-1445151).

DEDICATION

This dissertation is dedicated to my family and my husband. To my parents, I do not have the words to adequately express my gratitude for all you have done for me. I would be lost without your unconditional love. You have always been my biggest motivators, role models, and champions. To my husband, Brooks, thank you for all your love and support. I am so grateful you are my best friend and my partner in everything. To Olivia and Ethan, thank you for your love, friendship, and support. I admire and look up to both of you. You have always challenged me to be better and have provided comic relief and morale support over the years. I am also grateful to all of the wonderful friends I have made throughout graduate school as you have made this journey much more meaningful and enjoyable. I would also like to thank Penenlope, Meeka, and Bruce for being especially loyal and loving friends through this journey.

TABLE OF CONTENTS

LIST OF TABLES

LIST OF ILLUSTRATIONS

LIST OF SCHEMES

LIST OF ABBREVIATIONS

4VIM	4-vinylimidazole
aRAFT	Aqueous reversible addition-fragmentation chain-transfer
ATRP	Atom-transfer radical polymerization
$BnNH_2$	Benzylamine
BnSH	Benzyl mercaptan
$CDCl_3$	Deuterated choroform
CH_2Cl_2	Dichloromethane
CPCB	2-Cyano-2-propyl-4-cyanobenzodithioate
CRP	Controlled radical polymerization
CTA	Chain transfer agent
DBU	1,8-Diazabicyco[5.4.0]undec-7-ene
DCC	Dynamic covalent chemistry
$Đ_M$	Molar-mass dispersity
DMF	Dimethylformamide
Et_2O	Diethyl ether
FTIR	Fourier transform infrared spectroscopy
gATR-FTIR	Grazing-angle attenuated total reflectance Fourier transform infrared
HEMA	2-Hydroxylethyl methacrylate
HxSH	1-Hexanethiol
IEM	2-Isocyanatoethyl methacrylate
MAEH	(2-Methacrylamidoethyl) carbohydrazide hydrochloride
MAH	Methacryloyl hydrazide hydrochloride

MALLS	Multi-angle laser light scattering
MeOH	Methanol
M_n	Number-average molecular weight
mNCOI	Imidazole-blocked isocyanate model compound
mNCOP	3,5-Dimethylpyrazole-blocked isocyanate model compound
mNCOT	1,2,4-Triazole-blocked isocyanate model compound
NCO	Isocyanate
NCOI	Imidazole-blocked isocyanato methacrylate
NCOP	3,5-Dimethylpyrazole-blocked isocyanato methacrylate
NCOT	1,2,4-Triazole-blocked isocyanato methacrylate
NMP	Nitroxide-mediated polymerization
NMR	Nuclear magnetic resonance
PD	Piperidine
PEG	Poly(ethylene glycol)
PPM	Post-polymerization modification
PrSH	1-Propanethiol
RAFT	Reversible addition-fragmentation chain-transfer
RDRP	Reversible-deactivation radical polymerization
SAMs	Self-assembled monolayers
SEC	Size-exclusion chromatography
SI-ATRP	Surface-initiated atom-transfer radical polymerization
SIP	Surface-initiated polymerization
TFA	Trifluoroacetic acid

THF	Tetrahydrofuran
TTC	Trithiocarbonate
V-70	2,2'-Azobis(4-methoxy-2,4-dimethylvaleronitrile)
VA-044	2,2'-Azobis[2-(2-imidazolin-2-yl)propane]dihydrochloride
WCA	Water contact angle
XPS	X-ray photoelectron spectroscopy

CHAPTER I - INTRODUCTION

1.1 Functional and Controlled Polymer Architectures

Methods to achieve precise synthesis of materials are progressively providing access to complex functional polymers with well-defined architectures for advanced applications where high demands are placed on polymer composition, molecular weight, distribution of chain lengths, microstructure, topology, and response to environment. It is well-known that manipulation of polymer structure greatly influences polymer function. In this way, scientists are driving creation of sophisticated materials by controlling polymer architecture to address pressing issues in areas of energy use, drug delivery, renewable and biodegradable materials, programmable materials, material interfaces, sensors, as well as in other applications where advanced material properties are required.[1-5]

Technological advances in reversible-deactivation radical polymerization (RDRP) techniques have enabled the synthesis of functionally-complex polymers with controlled architectures, including telechelic polymers, homopolymers, copolymers (e.g. alternating, statistical, gradient, and multiblock microstructures), cyclic polymers, molecular brushes, surface brushes, and multiarm star polymers (Scheme 1.1).[6] An additional level of architectural control can be imparted when chemoselective handles with latent reactivity are specifically incorporated along the polymer backbone, side chains, or chain-ends. Emphasis is placed on using simple, efficient, and/or dynamic reactions to bring about chemical transformations post-polymerization. Ongoing advances in these areas have facilitated the synthesis of highly tailorable polymers to take advantage of the close relationship between polymer structure and function.

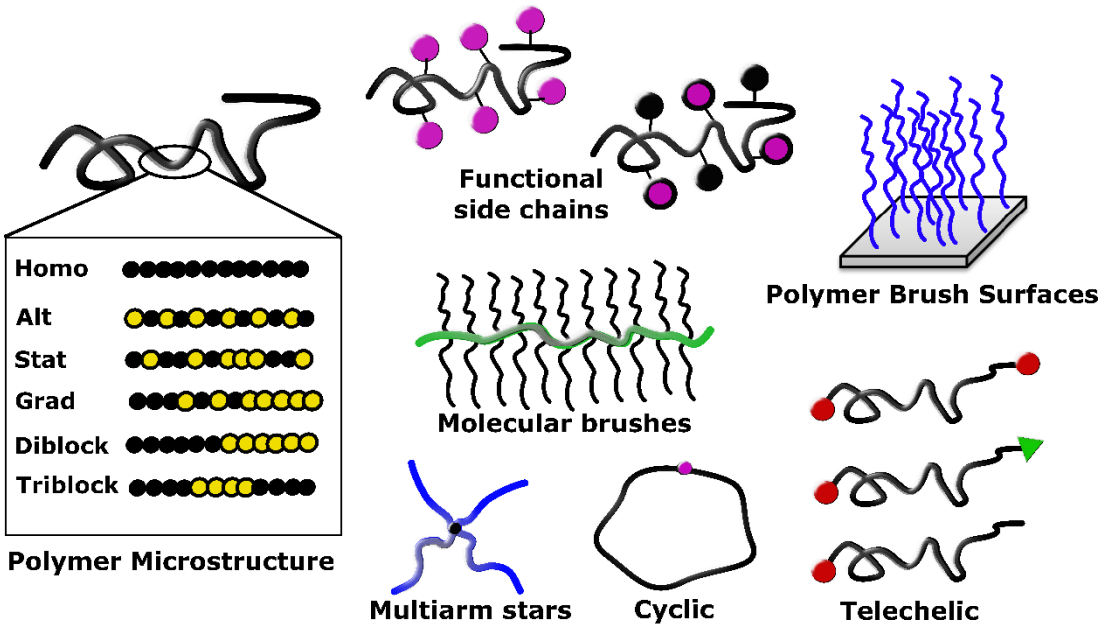

Scheme 1.1 Complex polymer architectures accessible via RDRP techniques.

In this introduction chapter, controlled polymer architectures from two perspectives will be discussed: (i) design and synthesis of solution polymers by RDRP techniques with modifiable and stimuli-responsive functional groups and (ii) design and synthesis of polymer brush surfaces by surface-initiated polymerization for dynamic control of surface properties. Interconnecting themes of post-polymerization modification (PPM) and dynamic covalent chemistry (DCC) that span solution and surface polymer engineering will also be summarized as a strategy to tailor polymer functionality with efficient, versatile, and dynamic methods.

1.2 Reversible-Deactivation Radical Polymerization (RDRP)

Reversible-deactivation radical polymerizations, a type of controlled radical polymerizations (CRP), afford polymers with well-defined molecular weights, dispersities, topologies, compositions, and side-chain and end-group identities.[7-11] Many of the complex architectures afforded by RDRP techniques are shown in Scheme 1.1.

The most well-known RDRP techniques include nitroxide-mediated radical polymerization (NMP), atom-transfer radical polymerization (ATRP), and reversible addition-fragmentation chain-transfer (RAFT) polymerization. Characteristics of RDRP polymerizations include rapid initiation with respect to propagation via a radical source, controlled addition of monomers to propagating radicals, and an absence, or very low occurrence, of irreversible termination or undesirable chain transfer events.[12] Each polymerization technique utilizes a rapid, reversible active/dormant equilibrium of propagating chain-ends, via a persistent radical effect or degenerative chain transfer, to reduce the effective concentration of propagating radicals. Reducing the radical concentration substantially reduces disadvantageous termination or chain transfer reactions that lead to uncontrolled polymer architectures. Furthermore, uniform addition of monomer to growing chain ends is achieved. The combined outcome of reducing the effective concentration of propagating radicals and controlling monomer addition is the synthesis of polymers with well-defined molecular weights and narrow dispersities. ATRP and RAFT are by far the most widely employed of these techniques due to a significantly broader selection of monomers and solvents as compared to NMP. The equilibria for RAFT and ATRP processes are shown in Scheme 1.2. The ability to obtain well-defined polymer architectures via RDRP processes leads to narrow property distributions and provides a means by which to closely study and tailor physicochemical properties.

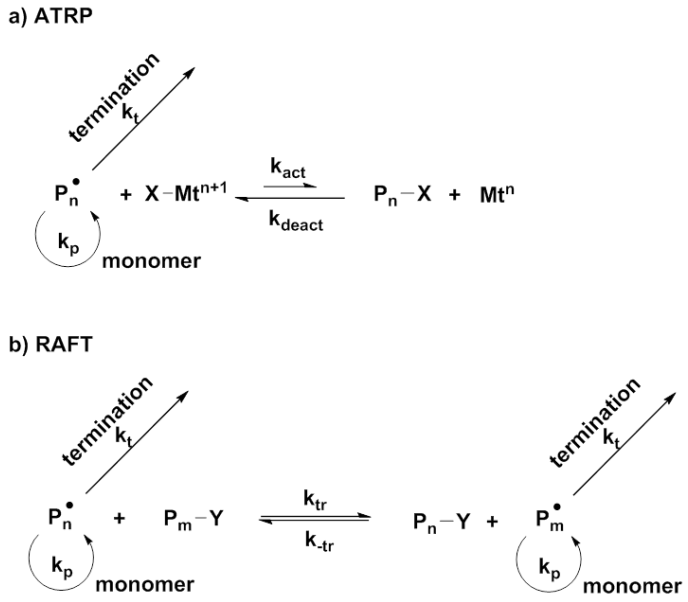

Scheme 1.2 (a) Activation/deactivation equilibrium for ATRP. (b) Reversible degenerative chain transfer equilibrium for RAFT process.

The atom/group transfer process during ATRP typically involves a low molecular weight alkyl halide initiator and a reductive transition metal catalyst. During initiation, the transition metal catalyst (typically a Cu(I)X-ligand species) promotes initiator reduction by single electron transfer to form an initiator-derived radical and a Cu(II)X_2 deactivator species which influences the active-dormant polymerization equilibrium. Propagation occurs when monomers add to initiator radicals while deactivation occurs when a halide (e.g. Cl or Br) is transferred from the oxidized transition metal halide complex (e.g. Cu(II)X_2) to the growing polymer chain-end to form a dormant polymer and a reduced transition metal complex. An equilibrium is rapidly established between active and deactivated polymers and is shifted to favor chains in their dormant state, effectively reducing [$P_n\cdot$] and therefore termination. This mechanism affords polymers with well-defined molecular weights, low dispersities, and halogenated end-groups that can be easily modified for design of functional polymers.[13] While the scope of

monomers and solvent conditions for ATRP polymerizations has increased significantly since it was first introduced, sensitivity to functional groups that will competitively complex with the metal catalyst remains a limitation. Despite this however, ATRP is still a powerful polymerization tool and can be combined with surface-initiated polymerization (SIP)[14] as will be discussed in further detail later in this introduction.

RAFT polymerization is arguably the most versatile RDRP technique owing to its superior functional group tolerance and compatibility with organic, aqueous, and heterogeneous solvent conditions. Vinyl monomer – types including (meth)acrylamides, (meth)acrylates, styrenics, acrylonitriles, vinyl esters, and vinyl amides – have been successfully polymerized via RAFT. Rather than an atom- or group-transfer process, RAFT is governed by degenerative chain transfer usually involving thiocarbonylthio compounds that serve as chain-transfer agents (CTA).[15-17] RAFT end-groups bearing thiocarbonylthio moieties can be readily converted to reactive functional groups (e.g. thiol, alkene, hydroxyl, etc.) and facilitate a host of efficient chemistries for subsequent modification.[18-23] The versatility of RAFT polymerizations is also well-suited for direct polymerization of monomers with nucleophilic functional groups (e.g. primary and secondary amines),[24-27] a feature that will be utilized in the following chapters to synthesize multifunctional and dynamic polymer scaffolds. For this purpose, a more in-depth discussion of the RAFT process is given in the following section.

1.2.1 Reversible Addition-Fragmentation Chain-Transfer (RAFT) Polymerization

In RAFT polymerizations, propagating chains achieve an active/dormant equilibrium via reversible degenerative chain transfer in simultaneous activation/deactivation steps. The proposed mechanism for the RAFT process is shown

in Scheme 1.3. Typically, RAFT polymerizations are mediated by thiocarbonythio-containing CTAs which are designed with Z- and R-groups that influence the rates of addition and fragmentation from the CTA.[28] During RAFT polymerization, the R-group is displaced by a propagating chain that concomitantly becomes dormant when added to the CTA. Meanwhile, the Z-group stabilizes the intermediate radical formed in the addition-fragmentation process. Since the majority of polymer chains are initiated by the CTA-derived R-group, polymer molecular weight is a function of the initial ratio of CTA to monomer ($[CTA]_0$:$[M]_0$) and monomer conversion.

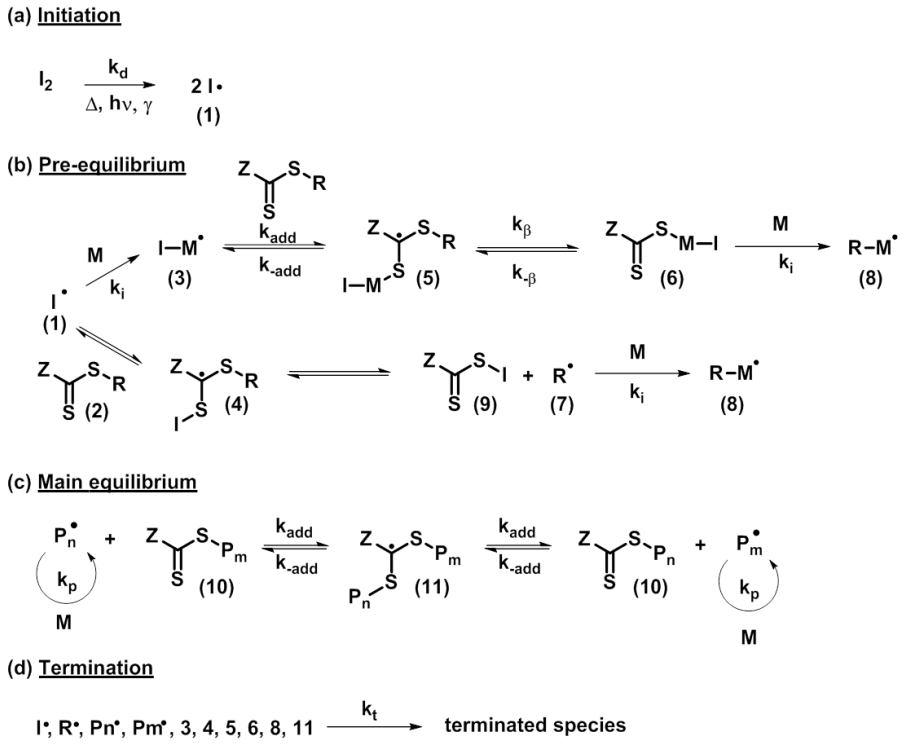

Scheme 1.3 Proposed RAFT polymerization mechanism.

The first step in RAFT polymerization is decomposition of a radical initiator most commonly through the application of heat or UV-light (Scheme 1.3a). In the initiation/pre-equilibrium step (Scheme 1.3b), initiator radicals (1) can then react with the

CTA (2) (the CTA fragments and generates an R-group derived radical (7) that can initiate propagation via monomer addition), or react with monomer (3) (generates propagating chains) until all molecules of CTA have been converted to macro-CTA (6). An initialization period during the pre-equilibrium step, as described by Klumperman et al.,[29, 30] is observed in cases where R-group derived radicals preferentially add to CTA rather than initiating monomer propagation. This initialization period results in prolonged pre-equilibrium stages as conversion of CTA to macro-CTA is slower. Slow fragmentation of the intermediate radical – effects often observed in ambient temperature RAFT polymerizations, may also lead to prolonged pre-equilibrium stages.[31, 32] The timeframe of the pre-equilibrium ideally should be short with respect to the main equilibrium step in which the majority of chain propagation occurs.

In the main equilibrium of RAFT (Scheme 1.3c), propagation occurs by addition of monomer to active polymer chains. As discussed previously for ATRP, the number of active chains is significantly lower than dormant chains and the rapid equilibrium between dormant and active species allows chains to grow uniformly. The CTA intermediate (11) formed in the addition-fragmentation process can fragment in either direction (degenerate) also assuring that RAFT polymers grow uniformly. Characteristic features of RDRP technieques, such as RAFT, include pseudo-first-order kinetic behavior indicative of a steady state radical concentration and a linear relationship between molecular weight and monomer conversion. These features are evidence of a well-controlled polymerization. The theoretical molecular weight ($M_{n,theory}$) of RAFT polymers can then be calculated by the following equation:

$$M_{n,theory} = \frac{[M]_0 \rho}{[CTA]_0} M_{MW} + CTA_{MW} \quad (1)$$

where $[M]_0$ is the initial monomer concentration, ρ is monomer conversion, $[CTA]_0$ is the initial CTA concentration, M_{MW} is the monomer molecular weight, and CTA_{MW} is the CTA molecular weight. This equation is a simplified version that applies when the number of CTA-derived polymer chains relative to initiator-derived polymer chains is high as is the case in nearly all RAFT polymerizations.[33] Furthermore, CTA degradation during RAFT polymerization can lead to deviations of experimentally derived molecular weights ($M_{n,exp}$) when compared to $M_{n,theory}$.[34]

RAFT polymerization has been used to polymerize a large class of monomers possessing functional groups including amines, hydroxyls, carboxylic acids, sulfonates, sulfonamides, and isocyanates among others.[8, 35-37] Furthermore, aqueous RAFT polymerization has been developed to provide a powerful method of generating water-soluble polymers and afford controlled polymerization of nucleophilic functional groups that are traditionally difficult to polymerize directly in organic media.[38] The next section will focus on aqueous RAFT (aRAFT) polymerizations as aRAFT is key to polymerizing water-soluble, nucleophilic functional groups discussed later in this introduction.

1.2.1.1 Aqueous RAFT Polymerization

To date, RAFT polymerization has enabled the synthesis of functional polymers with controlled molecular weights, low dispersities and complex architectures, and offers excellent utility for the controlled polymerization of monomers bearing strongly nucleophilic functional groups.[4, 8, 22, 39] aRAFT polymerization further expands the scope of accessible functional groups via polymerization of water-soluble monomers directly in water. In developing aRAFT polymerization, consideration of hydrolysis and aminolysis of the CTA, primary pathways for CTA degradation in aqueous RAFT polymerizations,

led to significant advances in the success of the technique. Multiple groups have examined the influence of pH and temperature on hydrolysis of thiocarbonylthio chain-ends and found that rates of hydrolysis increase with increasing temperature and pH.[38, 40-43] Hydrolysis studies of small molecule CTAs have also revealed that they are more susceptible to hydrolysis than the CTA end-groups of polymers.[41] Alternatively, at lower pH values, thiocarbonylthio-based CTAs are stable toward hydrolysis for extended periods of time.[40, 41] Additionally, trithiocarbonate CTAs have been shown to be more stable than dithiobenzoates.[43, 44]

Lowering the pH of aRAFT polymerizations also prevents aminolysis which occurs when amine-containing monomers react with the thiocarbonyl of small molecule or polymeric CTA end-groups. aRAFT has enabled the direct polymerization of amide- or amine-containing monomers (pK_a values ≈ 9) by employing pH 5 buffer solutions as the polymerization medium – conditions that protonate the nucleophilic sites and suppress aminolysis of thiocarbonylthio-based CTAs.[24, 35, 40, 41, 45]

Recent interest in controlled polymerization of nucleophilic monomers with low pK_a values has sparked investigation into the use of more acidic polymerization media to ensure protonation of the nucleophilic functional groups. Buffer solutions of pH = 5 are typically used for controlled aRAFT polymerization of nucleophilic monomers; however, aRAFT polymerizations of nucleophilic monomers with pK_a values < 7 require substantially more acidic polymerization conditions to prevent CTA aminolysis. For example, Allen et al.[46] recently attempted aRAFT of 4-vinylimidazole (pk_a ≈ 6) in pH 5.2 acetate buffer with limited success, but found polymerizations conducted in glacial acetic acid (pK_a = 4.76) afforded excellent control over MW and dispersity. CTA stability has

been demonstrated at values as low as pH = 2, yet few examples exist of aRAFT polymerizations under more acidic conditions (i.e. pH < 2). This dissertation will investigate low pH (pH = 0) aRAFT polymerizations as a strategy to achieve direct, controlled polymerization of unprotected acyl hydrazide-containing monomers ($pK_a < 4$), a class of low pK_a monomers previously inaccessible by RDRP techniques.

1.3 Surface-Initiated Polymerization (SIP)

Surface-initiated polymerization (SIP) represents one of the most effective and versatile methods for tailoring the physico-chemical properties of surfaces.[47] SIP offers a direct means to control the density, thickness, and functionality of ultrathin films by growing polymer chains directly from surface bound initiators. At high grafting density, the macromolecules adopt a highly stretched conformation extending perpendicular to the substrate surface in order to avoid chain overlap, or the so-called "polymer brush" conformation (Scheme 1.4b).[48] The ability of SIP to conformally modify substrates of any geometry with outstanding film homogeneity at nanometer thicknesses offers many advantages over solution cast films. Additionally, the three-dimensional brush conformation of SIP brushes greatly enhances the functionality of the surface by providing not only an opportunity to present functional groups at the interface, but also throughout the film – as each monomer unit is capable of carrying a functional moiety (Scheme 1.4a).[49] This feature makes SIP vastly superior to self-assembled monolayers (SAMs) where functionality is limited to the outermost edge of the interface. The ability to endow a surface with 3D functionality has tremendous advantages for applications where high functional group densities are required, e.g. membranes and biosensor chips.[50] When properly designed, polymer films fabricated by SIP are extremely stable

under a variety of environmental conditions owing to the covalent interaction of the polymer chains with the substrate surface. The SIP technique can also be combined with RDRP techniques to provide a means of growing precisely defined polymer structures from surfaces. The most widely used RDRP method for growing surface brushes is surface-initiated atom-transfer radical polymerization (SI-ATRP) which has been applied in a variety of ways to install covalently attached polymers to surfaces and bestow specific functionality in a controlled fashion.[51,52] SI-ATRP also has the benefit of allowing the synthesis of polymers with end-groups capable of reinitiating polymerization which is useful should copolymer structures with controlled block sizes be desired.

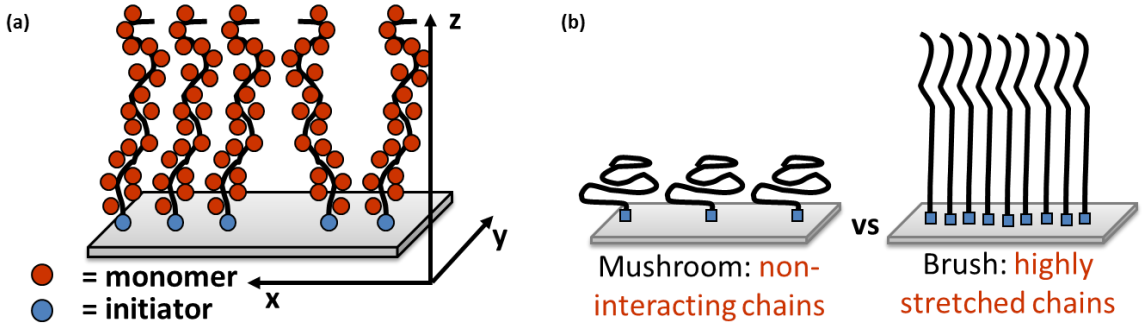

Scheme 1.4 (a) 3D brush conformation of SIP polymer brush surfaces and (b) polymer conformations at low grafting density (mushroom) and high grafting density (brush).

1.4 Post-Polymerization Modification (PPM)

This section will focus on modular and efficient PPM platforms for functionalizing RDRP polymers, with an emphasis on RAFT polymers, and controlling surface properties by PPM of surface-tethered polymer chains. PPM is a concept whereby latent chemoselective handles are installed along the polymer backbone, as pendent groups, or chain-ends are modified after polymerization (Scheme 1.5).[53-57]

Despite the development of techniques for controlled polymerization possessing high functional group tolerances such as RAFT and ATRP, some functional groups remain inaccessible by direct polymerization of a functional monomer (i.e. polymers with pendant thiols). PPM can also be used to preserve latent functionality until the desired reaction time, avoid costly or challenging monomer synthesis, and provide multiple reaction sites per monomer unit. Efficient or "click" chemistries are useful for PPM strategies due to near quantitative conversions as well as the ease with which they are applied. Additionally, by incorporation of two or more reactive moieties on the same polymer scaffold, new strategies that allow for orthogonal,[58] sequential,[59, 60] or cascade transformations[61] have been achieved for the synthesis of multifunctional materials. These features make PPM strategies, especially those with mild, simple, and efficient chemistries, a powerful tool to access functional materials. Approaches that address synthesis of functional polymers via PPM of RDRP and SI-ATRP scaffolds will be discussed in the following sections.

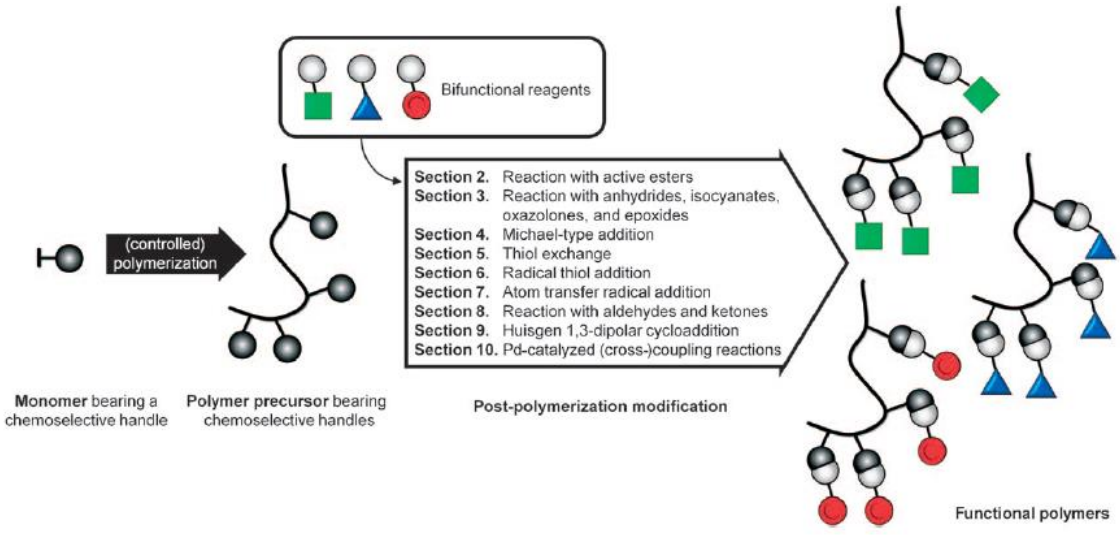

Scheme 1.5 Post-polymerization modification process (reproduced from ref. 62 with permission).

1.4.1 Synthesis of PPM Precursors

Multiple reviews demonstrate the synergism achieved when PPM is combined with RDRP techniques.[62-64] Polymer scaffolds bearing pendant groups such as activated esters, maleimides, alkynes, alkenes, substituted succinic anhydrides, disulfides, isocyanates, epoxides, azides, and aldehydes as side chains and/or end-groups are among the precursors prepared by RDRP techniques for PPM.[5] Of these RDRP techniques, RAFT is arguably the most versatile controlled radical polymerization for these precursors via direct polymerization of functional monomers.

Amidst the different "click" reactions included above, thiol-click reactions have emerged as valuable tools for the synthetic polymer chemist. Specifically, electron rich alkenes (radical), alkynes (radical), electron poor alkenes (Michael addition), isocyanates (carbonyl addition), epoxies (S_N2 ring opening), and halogens[65-67] (S_N2 nucleophilic substitution) all readily react with thiols, thus comprising a *toolbox* of efficient chemical reactions.[68] Recently, we and others have shown thiol-based click reactions – such as thiol-ene,[69-73] thiol-yne,[72, 74-78] and thiol-isocyanate[79, 80] – to be a powerful approach for engineering multifunctional materials and surfaces in a modular fashion. Of these thiol-click approaches, isocyanates react readily with amines and alcohols, in addition to thiols, thereby possessing features ideal for versatile PPM routes. Our group has demonstrated thiol-isocyanate reactions as a modular strategy for surface modification via PPM, yet few examples exist of isocyanate-functional RDRP polymers despite the high reactivity and versatility of isocyanate. To address the relatively unexplored isocyanate functionality as a PPM approach for RDRP scaffolds, the combination of blocked isocyanates and RAFT polymers is explored in the following section.

1.4.2 Blocked Isocyanates as a PPM Strategy

Isocyanates are highly reactive, inherently sensitive to water, and undergo rapid hydrolysis under ambient conditions if no precautions (i.e. dry nitrogen atmosphere) are implemented (Scheme 1.6a). In an unprotected form, isocyanates readily react with alcohols, amines and thiols to form urethane, urea, and thiourethane linkages, respectively, as shown in Scheme 1.6a. Collectively, these reactions underpin many industrial technologies such as polyurethane coatings, foams, and thermoplastic elastomers. The isocyanate functional group can be protected, or "blocked", by reacting the isocyanate with an active hydrogen compound such as phenols, ketoximes, amides, and nitrogen heterocycles (i.e. imidazole,[81] pyrazole[82]).[83] In a typical application, blocked isocyanates are exposed to heat and undergo an elimination reaction to regenerate the reactive isocyanate and the active hydrogen compound. In the presence of a nucleophile (i.e. alcohols, amines and thiols), the regenerated isocyanate can proceed as previously described to form urethane, urea, and thiourethane linkages. The elimination-addition blocking scheme, as shown in Scheme 1.6a, has been used in coatings applications for shelf-stable formulations that can be activated at elevated temperatures; however, relatively high temperatures (100 – 200 °C) are often necessary to facilitate the deblocking reaction which can limit the applicability of blocked NCOs for certain applications. The deblocking temperature depends on the structure of both the isocyanate and the blocking compound.

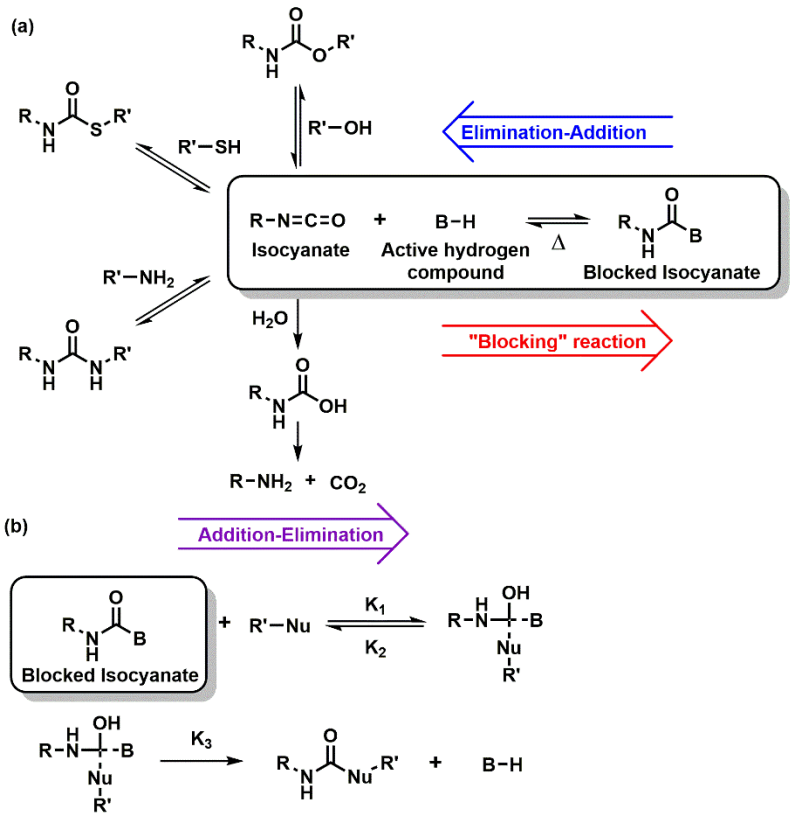

Scheme 1.6 (a) Formation of a blocked isocyanate as well as isocyanate reactions with alcohols, thiols, amines, and hydrolysis to generate an amine and CO_2. (b) Addition-elimination pathway for blocked isocyanates.

An alternate scheme to utilize blocked NCOs is shown in Scheme 1.6b. In the addition-elimination route, the nucleophile reacts directly with the blocked NCO to yield a tetrahedral intermediate followed by elimination of the blocking agent. While blocked NCOs have been widely used at elevated temperatures for crosslinking reactions in coatings applications[84] (with contributions from both the elimination-addition and addition-elimination mechanisms), the exploration of blocked isocyanates as a post-polymerization modification approach has scarcely been reported. A recent example by Bode et al.[85] demonstrated the use of blocked isocyanates for post-polymerization end-group modification of α,ω-telechelics (prepared by RAFT polymerization) via reaction of

the blocked NCO end-groups with small molecule amines and alcohols at elevated temperatures (130 °C). The addition-elimination scheme at ambient temperature has received minimal attention as a route to functional materials and surfaces. The few examples reported in the peer-reviewed literature have only focused on the reaction of primary amines with blocked NCOs under ambient conditions.[86-88] To our knowledge, the reaction of thiols directly with blocked NCOs under ambient conditions has not been reported and will be addressed in this dissertation. In the next section, emphasis will be shifted from solution polymers to PPM strategies for surface-tethered polymers.

1.4.3 PPM for Surface Modification

Despite recent advances in the SIP approach, there remains a large number of pendent functional groups that cannot be directly polymerized from the surface due to i) exorbitant cost of functional monomer synthesis and/or ii) intolerance of the functional moiety in the polymerization process (i.e. reactivity, steric bulk). A general depiction of PPM of polymer brush surfaces is shown in Scheme 1.7. This often necessitates the development of a modular approach to surface engineering in the form of PPM. The utility of the PPM strategy has been highlighted through several recent approaches implementing SIP. For example, Gao et al.[89] used a two-step process to immobilize an antimicrobial peptide to a poly(dimethylacrylamide-b-APMA) brush grafted from a titanium substrate via a thiol-ene "click" reaction. Song et al.[90] prepared poly(styene/divinylbenzene/glycidyl methacrylate) nanospheres by soap-free emulsion polymerization followed by thiol-epoxy "click" modification of the colloidal surface. Additionally, Schuh et al.[91] have studied the penetration of amine-terminated PEG into a polymer brush that contained pendent reactive esters. Similarly, Orski et al.[92, 93] and

Gelbrich et al.[94] carried out post-polymerization based on reactive esters. In a "grafting to" approach, Soto-Cantu et al.[95] prepared an alkyne functionalized surface by spin coating a substrate with an epoxy pendent polymer film followed by modification of using amine or acid-terminated alkyne and subsequent azide-alkyne click with an azide-terminated poly(dimethylazlactone). Recently, our group has developed a versatile method platform to post-polymerization modify surface initiated polymer brushes based on thiol-yne, thiol-isocyanate, thiol-epoxy and thiol-bromo reactions.[96, 97]

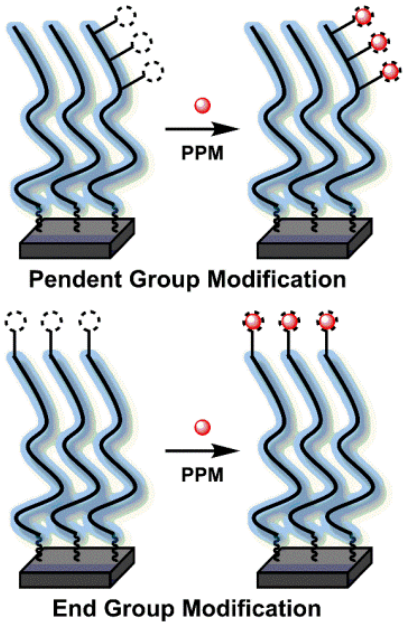

Scheme 1.7 PPM of polymer brush surface side chains and end-groups.

In this work, PPM of polymer brush surfaces synthesized via SI-ATRP will be investigated as a means to generate surfaces with dynamic covalent hydrazide moieties. Dynamic covalent chemistry, with special attention paid to hydrazide functional groups, is discussed below as a method to extend PPM as a route to generate RAFT and SIP scaffolds with dynamic, stimuli-responsive character.

1.5 Dynamic Covalent Polymer Scaffolds

As the demand for more sophisticated polymer architectures continues to grow, dynamic functionality is increasingly incorporated to achieve "smart"/responsive behavior such as triggered release, conformational switching, actuation, sensing, self-assembly, disassembly, and repair.[98-110] Non-covalent interactions (i.e. hydrogen bonding, coordination, π-π stacking, and hydrophobic interactions), have been widely used to control dynamic behavior in macromolecular and supramolecular architectures found in nature and obtained by synthetic design.[2, 111] The use of dynamic covalent chemistry (DCC), however, imparts significant advantages to the design of dynamic polymer scaffolds, such as chemical stability, when compared to weaker non-covalent interactions. As a result, interest in new methods to achieve DCC polymer scaffolds has increased significantly. DCC refers to a class of covalent bond formation that is reversible or exchangeable given the application of appropriate environmental stimuli (i.e. solvent, redox conditions, light, temperature, pH, etc.) (Scheme 1.8).

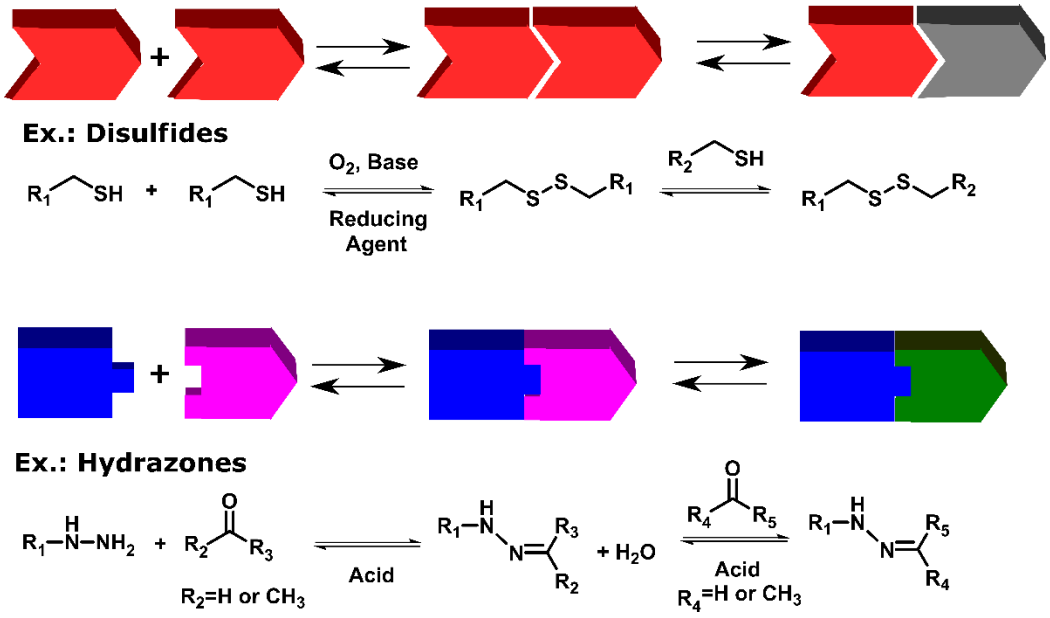

Scheme 1.8 General representation of self-complementary (top) and hetero-complementary (bottom) dynamic covalent bonds (adapted from ref. 110 with permission).

The dynamic nature of these covalent linkages is a result of bond formation controlled by a thermodynamic process rather than a kinetic process (Scheme 1.9).[111, 112] Thermodynamic product distributions are based on the relative stability of products formed whereas the product distribution in a kinetically controlled reaction is determined by the stability of the transition states. In thermodynamically-controlled reactions, the established equilibrium can be adjusted with external stimuli giving way to dynamic bond formation and exchange. Furthermore, catalysts are often required for these reactions to reach the thermodynamically-favored product in relevant time frames or to facilitate bond reversal/exchange. The need for a catalyst and/or additional stimulus whose presence can be withheld or delayed provides a means to turn formation/cleavage/exchange reactions "on" and "off".

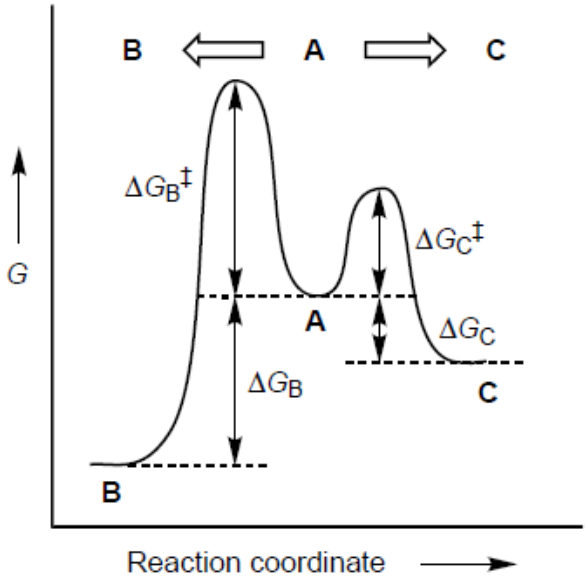

Scheme 1.9 Energy diagram for organic reactions under kinetic or thermodynamic control. Transition state stability determines product formation in kinetic systems, while product stability determines reaction products in thermodynamically-controlled reactions (i.e. dynamic covalent chemistries) (reproduced form ref. 111 with permission).

Mild conditions for stimuli response are especially important for many applications, particularly those with biological relevance.[113] Fortunately, DCC offers a great number of diverse reactions with wide range of available stimuli. Dynamic covalent linkages span many bond types including C-C bonds (Diels-Alder, olefin metathesis, etc.), C-N bonds (hydrazine, imine, oxime, etc.), C-O bonds (acetal exchange, alkoxyamine exchange, etc.), C-S bonds (thia-michael addition, thioacetal exchange, etc.), B-O bonds (boronic acid condensation), and S-S bonds (disulfide formation/exchange) and are covered extensively in multiple reviews.[111, 114] The next section of this introduction will focus on a particular class of C=N bonds, pH-responsive hydrazones, for the design and synthesis of dynamic, controlled polymer architectures.

1.5.1 Hydrazones

Hydrazones are C=N–N bonds that can be formed via the Japp-Klingemann reaction, aryl halide substitution, or reaction of a hydrazide with an aldehyde/ketone.[106] Hydrazone synthesis via condensation of an acyl or alkyl hydrazide and aldehyde/ketone is arguably the most common and the mechanism is shown in Scheme 1.10.[115] Once formed, hydrazones can revert back to the parent hydrazide and aldehyde/ketone under acidic conditions or participate in transimination reactions whereby one carbonyl moiety is exchanged for another. Imines and hydrazones are often grouped together in the same class since both are dynamic covalent C=N bonds, yet imines often suffer from issues with instability.[116] The versatility and robust nature of the hydrazone bond sets it apart from other pH-responsive DCC linkages.

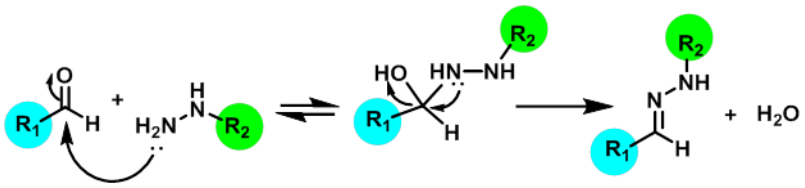

Scheme 1.10 Mechanism of hydrazone formation via reaction of a hydrazide with an aldehyde or ketone (reproduced from ref. 115 with permission).

The structural components of hydrazone bonds provide significant functional diversity (Scheme 1.11). The nucleophilic nitrogens of the hydrazide/hydrazone lead to rapid bond formation and cleavage without compromising bond stability. This feature is useful for anion and cation sensing as well as metal coordination. The nature of the C=N bonds results in configurational isomerism that can be switched between *E* and *Z* configurations for highly tunable photoswitch applications.[106, 107] Finally, acidic N-H protons provide hydrogen bonding, ion sensing, and metal coordination capabilities.[106]

Other applications of hydrazone bonds in materials include self-healing,[101] bioconjugation and controlled release,[98, 99, 102, 105, 117] actuation,[109] and dynamic nanoparticle and network strategies.[101, 104, 108, 118] In addition to solution or network polymer motifs, hydrazones have been used in functional surface applications like molecular recognition and cell-attachment motifs.[103, 119]

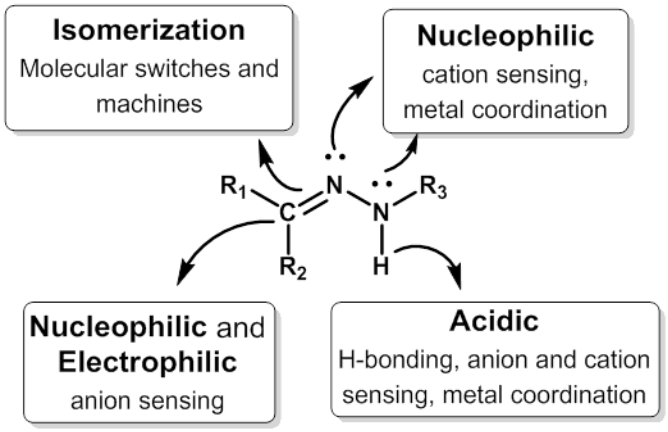

Scheme 1.11 Chemical features and related functions of the hydrazone bond (reproduced from ref. 106 with permission).

The structure of the hydrazide as well as the carbonyl moiety influences the rate of bond formation and cleavage and can be used to tune reaction kinetics, with electron-donating functional groups leading to faster hydrazone bond formation and increased bond stability.[115] Reaction rates are further controlled by the addition of aniline as a catalyst for hydrazone bond formation and exchange.[116, 120] Effort has been put forth to find alternatives to aniline that provide faster catalysis and/or are more biocompatible. 4-Aminophenylalanine has been shown to perform comparably to aniline and catalysts based on anthranilic acids and 3,5-diaminobenzoic acid significantly improve upon aniline catalysis.[121] The versatility of rate control and hydrazone reactions features make these linkages ideal for designing dynamic, controlled polymer architectures.

1.5.1.1 Installing Hydrazones on Controlled Polymer Architectures

1.5.1.1.1 Hydrazone Scaffolds via RDRP

Precisely placing hydrazone linkages in polymer scaffolds has been approached by (i) attaching an aldehyde or ketone to a linear or network polymer followed by reaction with hydrazide functional modifiers or (ii) installing hydrazide functionality in linear or network polymers and subsequent reaction with an active carbonyl moiety. This section will focus on approach (i) and (ii) from the perspective of synthesizing polymers via RDRP techniques to achieve dynamic, controlled polymer architectures. An additional approach (iii) involves attaching hydrazides/ aldehydes to polymer nanoparticles or surfaces as monolayers.

Aldehyde-functional polymer scaffolds have been achieved via direct controlled polymerization of aldehyde functional monomers[5, 118, 122, 123] and by attaching the aldehyde as an end-group.[124] These methods present viable options for installing hydrazone linkages on polymer scaffolds; however, there is a great deal of scaffold and modifier diversity left unexplored by the relatively few examples of acyl hydrazide-functional scaffolds.[104]

Acyl hydrazides are potent functional groups for C=N bond formation and exchange reactions with active carbonyl compounds and represent one of the most widely employed dynamic covalent chemical handles.[106, 110, 115, 120] However, fewer examples of controlled polymer architectures with pendent hydrazides exist (approach (ii)), due in part, to chemical attributes of acyl hydrazides (e.g. high nucleophilicity, low pK_a, and metal coordination propensity) that present synthetic obstacles, particularly with regard to RDRP techniques. Consequently, acyl hydrazides are most often installed on well-

defined polymer scaffolds by polymerization of protected monomers (e.g. BOC-protected)[105] or via PPM techniques (e.g. hydrazinolysis of ester pendent groups).[104] These synthetic approaches are broadly employed to achieve hydrazide-functionalized polymers but often require multistep PPM reactions and purifications, or the undesired use of hydrazine (anhydrous or hydrate form) as a chemical reagent. Alternatively, hydrazide-functionalized polymers have been obtained via conventional free radical polymerization of unprotected methacryloyl hydrazide (or similar derivatives);[98, 102, 117, 125] however, this approach does not provide access to hydrazide-functionalized polymer scaffolds with well-defined molecular weights and/or complex macromolecular architectures. Monomers containing unprotected acyl hydrazides exhibit pK_a values < 4. This attribute has precluded their polymerization by RDRP methods, until now. For RAFT polymerization, acyl hydrazide monomers require a polymerization medium with significantly lower pH (e.g. < 1) to ensure near quantitative protonation of the nucleophilic hydrazides. Low pH (pH = 0) aRAFT will be explored herein to achieve well-defined polymers via direct polymerization of an unprotected acyl hydrazide.

1.5.1.1.2 Hydrazone Scaffolds on Surfaces

Similarly to their solution counterparts, dynamic pH-responsive surfaces may be accessed via installing aldehyde or hydrazide functionality. Surfaces possessing aldehyde functionality have been demonstrated, but have focused mainly on imine formation rather than investigation of hydrazone chemistry for dynamic surface modification. Rozkiewicz et al.,[126] for example, demonstrates reversible patterning on gold and silicon oxide surfaces via SAMs with imine linkages, while Tauk and coworkers[127] demonstrate hierarchical functional gradients on surfaces via imine SAMs.

Singh et al.[128] modified mesoporous silica with aldehyde functionality to reversibly control pore size by imine formation. These examples highlight the sophisticated control of surface properties and functions when dynamic covalent imine-type bonds are employed. As mentioned above, however, hydrazones possess greater stability than imine linkages and are thus very interesting for the design of more robust dynamic covalent surfaces based on pH-responsive bonds.

As with hydrazide-functional solution polymers, fewer examples are found of hydrazide-functional surfaces. Yang et al.[129] attached short chains with hydrazide end-groups to inorganic beads for glycan analysis. Rao et al.[130] attached polystyrene and polyethylene glycol (PEG) polymer via a hydrazone-functional ATRP initiator and later cleaved the linkage to generate nanopores in thin films. Brinkhuis and coworkers also used hydrazide-functional PEG chains to install hydrazone functionality in polymersomes.[131] Zhi et al. fabricated oligosaccharide microarrays via SAMs of hydrazide functional oligomers on gold substrates.[119] Beyond these examples, hydrazone-functional surfaces have been underutilized as a means to achieve dynamic control of surface properties. Combining the advantages of SIP and hydrazone chemistry will further expand the ability of these dynamic linkages to influence surface behaviour. Additionally, hydrazide-functional surfaces for hydrazone formation are severely under-explored, especially as the hydrazide moiety offers a great deal of design versatility and attractive chemical attributes.

To date, there are no examples of direct, controlled polymerization of unprotected acyl hydrazides or hydrazide-functional polymer brush surfaces. The design and synthesis of these controlled polymer architectures featuring acyl hydrazides and

hydrazones will be addressed in this dissertation. Methods for low pH aqueous RAFT, introduced in a previous section, will be investigated and leveraged toward installing acyl hydrazides on polymer scaffolds by direct, controlled polymerization without the need for protecting groups. Dynamic control of surface properties is also investigated via hydrazone formation /exchange on hydrazide-functional polymer brush surfaces synthesized via SI-ATRP and PPM.

1.6 References

1. Koberstein, J. T. *Journal of Polymer Science Part B: Polymer Physics* **2004,** 42, (16), 2942-2956.

2. Lehn, J.-M. *Chemical Society Reviews* **2007,** 36, (2), 151-160.

3. Krishnamoorthy, M.; Hakobyan, S.; Ramstedt, M.; Gautrot, J. E. *Chemical Reviews* **2014,** 114, (21), 10976-11026.

4. Hill, M. R.; Carmean, R. N.; Sumerlin, B. S. *Macromolecules* **2015,** 48, (16), 5459-5469.

5. Gauthier, M. A.; Gibson, M. I.; Klok, H. A. *Angew. Chem. - Int. Ed.* **2009,** 48, (1), 48-58.

6. Hadjichristidis, N.; Iatrou, H.; Pitsikalis, M.; Mays, J. *Progress in Polymer Science* **2006,** 31, (12), 1068-1132.

7. Braunecker, W. A.; Matyjaszewski, K. *Progress in Polymer Science* **2007,** 32, (1), 93-146.

8. Lowe, A. B.; McCormick, C. L. *Progress in Polymer Science* **2007,** 32, (3), 283-351.

9. Moad, G.; Rizzardo, E.; Thang, S. H. *Accounts of Chemical Research* **2008,** 41, (9), 1133-1142.

10. Barbey, R.; Lavanant, L.; Paripovic, D.; Schüwer, N.; Sugnaux, C.; Tugulu, S.; Klok, H.-A. *Chemical Reviews* **2009,** 109, (11), 5437-5527.

11. Matyjaszewski, K., *Controlled/Living Radical Polymerization: Progress in RAFT, DT, NMP & OMRP*. American Chemical Society: 2009; Vol. 1024, p 415.

12. Moad, G.; Solomon, D. H., 9 - Living Radical Polymerization. In *The Chemistry of Radical Polymerization (Second Edition)*, Elsevier Science Ltd: Amsterdam, 2005; pp 451-585.

13. Matyjaszewski, K. *Israel Journal of Chemistry* **2012,** 52, (3-4), 206-220.

14. Khabibullin, A.; Mastan, E.; Matyjaszewski, K.; Zhu, S., Surface-Initiated Atom Transfer Radical Polymerization. In *Controlled Radical Polymerization at and from Solid Surfaces*, Vana, P., Ed. Springer International Publishing: Cham, 2016; pp 29-76.

15. Moad, G.; Rizzardo, E.; Thang, S. H. *Australian Journal of Chemistry* **2005,** 58, (6), 379-410.

16. Moad, G.; Rizzardo, E.; Thang, S. H. *Australian Journal of Chemistry* **2006,** 59, (10), 669-692.

17. Moad, G.; Rizzardo, E.; Thang, S. H. *Australian Journal of Chemistry* **2009,** 62, (11), 1402-1472.

18. Moad, G.; Rizzardo, E.; Thang, S. H. *Polymer International* **2011,** 60, (1), 9-25.

19. Willcock, H.; O'Reilly, R. K. *Polymer Chemistry* **2010,** 1, (2), 149-157.

20. Li, H.; Yu, B.; Matsushima, H.; Hoyle, C. E.; Lowe, A. B. *Macromolecules* **2009,** 42, (17), 6537-6542.

21. Qiu, X.-P.; Winnik, F. M. *Macromolecular Rapid Communications* **2006,** 27, (19), 1648-1653.

22. Moad, G.; Chong, Y. K.; Postma, A.; Rizzardo, E.; Thang, S. H. *Polymer* **2005,** 46, (19), 8458-8468.

23. Sinnwell, S.; Inglis, A. J.; Davis, T. P.; Stenzel, M. H.; Barner-Kowollik, C. *Chemical Communications* **2008**, (17), 2052-2054.

24. Li, Y.; Lokitz, B. S.; McCormick, C. L. *Angewandte Chemie* **2006,** 118, (35), 5924-5927.

25. Alidedeoglu, A. H.; York, A. W.; McCormick, C. L.; Morgan, S. E. *Journal of Polymer Science Part A: Polymer Chemistry* **2009,** 47, (20), 5405-5415.

26. He, L.; Read, E. S.; Armes, S. P.; Adams, D. J. *Macromolecules* **2007,** 40, (13), 4429-4438.

27. Xu, X.; Smith, A. E.; Kirkland, S. E.; McCormick, C. L. *Macromolecules* **2008,** 41, (22), 8429-8435.

28. Chong, Y. K.; Krstina, J.; Le, T. P. T.; Moad, G.; Postma, A.; Rizzardo, E.; Thang, S. H. *Macromolecules* **2003,** 36, (7), 2256-2272.

29. McLeary, J. B.; Calitz, F. M.; McKenzie, J. M.; Tonge, M. P.; Sanderson, R. D.; Klumperman, B. *Macromolecules* **2004,** 37, (7), 2383-2394.

30. McLeary, J. B.; McKenzie, J. M.; Tonge, M. P.; Sanderson, R. D.; Klumperman, B. *Chem. Commun.* **2004**, (17), 1950-1951.

31. Convertine, A. J.; Lokitz, B. S.; Lowe, A. B.; Scales, C. W.; Myrick, L. J.; McCormick, C. L. *Macromol. Rapid. Commun.* **2005,** 26, (10), 791-795.

32. Luo, J.; Li, M.; Xin, M.; Sun, W. *Macromol. Chem. Phys.* **2015,** 216, (15), 1646-1652.

33. Wang, A. R.; Zhu, S.; Kwak, Y.; Goto, A.; Fukuda, T.; Monteiro, M. S. *Journal of Polymer Science Part A: Polymer Chemistry* **2003,** 41, (18), 2833-2839.

34. Thomas, D. B.; Convertine, A. J.; Hester, R. D.; Lowe, A. B.; McCormick, C. L. *Macromolecules* **2004,** 37, (5), 1735-1741.

35. York, A. W.; Kirkland, S. E.; McCormick, C. L. *Advanced Drug Delivery Reviews* **2008,** 60, (9), 1018-1036.

36. Abel, B. A.; Sims, M. B.; McCormick, C. L. *Macromolecules* **2015,** 48, (16), 5487-5495.

37. Flores, J. D.; Shin, J.; Hoyle, C. E.; McCormick, C. L. *Polymer Chemistry* **2010,** 1, (2), 213-220.

38. Thomas, D. B.; Convertine, A. J.; Myrick, L. J.; Scales, C. W.; Smith, A. E.; Lowe, A. B.; Vasilieva, Y. A.; Ayres, N.; McCormick, C. L. *Macromolecules* **2004,** 37, (24), 8941-8950.

39. McCormick, C. L.; Lowe, A. B. *Accounts of Chemical Research* **2004,** 37, (5), 312-325.

40. Baussard, J.-F.; Habib-Jiwan, J.-L.; Laschewsky, A.; Mertoglu, M.; Storsberg, J. *Polymer* **2004,** 45, (11), 3615-3626.

41. Thomas, D. B.; Convertine, A. J.; Hester, R. D.; Lowe, A. B.; McCormick, C. L. *Macromolecules* **2004,** 37, (5), 1735-1741.

42. Levesque, G.; Arsène, P.; Fanneau-Bellenger, V.; Pham, T.-N. *Biomacromolecules* **2000,** 1, (3), 400-406.

43. Convertine, A. J.; Lokitz, B. S.; Lowe, A. B.; Scales, C. W.; Myrick, L. J.; McCormick, C. L. *Macromolecular Rapid Communications* **2005,** 26, (10), 791-795.

44. Ferguson, C. J.; Hughes, R. J.; Nguyen, D.; Pham, B. T. T.; Gilbert, R. G.; Serelis, A. K.; Such, C. H.; Hawkett, B. S. *Macromolecules* **2005,** 38, (6), 2191-2204.

45. Thomas, D. B.; Sumerlin, B. S.; Lowe, A. B.; McCormick, C. L. *Macromolecules* **2003,** 36, (5), 1436-1439.

46. Allen, M. H.; Hemp, S. T.; Smith, A. E.; Long, T. E. *Macromolecules* **2012,** 45, (9), 3669-3676.

47. Prucker, O.; Ruhe, J. *Langmuir* **1998,** 14, (24), 6893-6898.

48. Milner, S. T. *Science* **1991,** 251, (4996), 905-914.

49. Murata, H.; Prucker, O.; Ruhe, J. *Macromolecules* **2007,** 40, (15), 5497-5503.

50. Senaratne, W.; Andruzzi, L.; Ober, C. K. *Biomacromolecules* **2005,** 6, (5), 2427-2448.

51. Edmondson, S.; Osborne, V. L.; Huck, W. T. S. *Chemical Society Reviews* **2004,** 33, (1), 14-22.

52. Orski, S. V.; Fries, K. H.; Sontag, S. K.; Locklin, J. *Journal of Materials Chemistry* **2011,** 21, (37), 14135-14149.

53. Gauthier, M. A.; Gibson, M. I.; Klok, H. A. *Angew. Chem. Int. Ed.* **2009,** 48, (1), 48-58.

54. Boaen, N. K.; Hillmyer, M. A. *Chem. Soc. Rev.* **2005,** 34, (3), 267-275.

55. Mansfeld, U.; Pietsch, C.; Hoogenboom, R.; Becer, C. R.; Schubert, U. S. *Polym. Chem.* **2010,** 1, (10), 1560-1598.

56. Arnold, R. M.; Patton, D. L.; Popik, V. V.; Locklin, J. *Acc. Chem. Res.* **2014,** 47, (10), 2999-3008.

57. Arnold, R. M.; Huddleston, N. E.; Locklin, J. *J. Mater. Chem.* **2012,** 22, (37), 19357-19365.

58. Iha, R. K.; Wooley, K. L.; Nyström, A. M.; Burke, D. J.; Kade, M. J.; Hawker, C. J. *Chem. Rev.* **2009,** 109, (11), 5620-5686.

59. Kakuchi, R.; Theato, P. *Polym. Chem.* **2014,** 5, (7), 2320-2325.

60. Moldenhauer, F.; Theato, P., Sequential Reactions for Post-polymerization Modifications. In *Multi-Component and Sequential Reactions in Polymer Synthesis*, Theato, P., Ed. Springer-Verlag: Berlin, 2015; Vol. 269, pp 133-162.

61. Malkoch, M.; Thibault, R. J.; Drockenmuller, E.; Messerschmidt, M.; Voit, B.; Russell, T. P.; Hawker, C. J. *J. Am. Chem. Soc.* **2005,** 127, (42), 14942-14949.

62. Gauthier, M. A.; Gibson, M. I.; Klok, H.-A. *Angewandte Chemie International Edition* **2009,** 48, (1), 48-58.

63. Iha, R. K.; Wooley, K. L.; Nyström, A. M.; Burke, D. J.; Kade, M. J.; Hawker, C. J. *Chemical Reviews* **2009,** 109, (11), 5620-5686.

64. Günay, K. A.; Theato, P.; Klok, H.-A. *Journal of Polymer Science Part A: Polymer Chemistry* **2013,** 51, (1), 1-28.

65. Xu, J.; Tao, L.; Boyer, C.; Lowe, A.; Davis, T. *Macromolecules* **2010,** 43, (1), 20-24.

66. Rosen, B. M.; Lligadas, G.; Hahn, C.; Percec, V. *J. Polym. Sci. A: Polym. Chem.* **2009,** 47, (15), 3931-3939.

67. Rosen, B. M.; Lligadas, G.; Hahn, C.; Percec, V. *J. Polym. Sci. A: Polym. Chem.* **2009,** 47, (15), 3940-3948.

68. Hoyle, C. E.; Lowe, A. B.; Bowman, C. N. *Chem. Soc. Rev.* **2010,** 39, (4), 1355 - 1387.

69. Sparks, B. J.; Ray, J. G.; Savin, D. A.; Stafford, C. M.; Patton, D. L. *Chem. Commun.* **2011,** 47, (22), 6245-6247.

70. Cai, T.; Wang, R.; Neoh, K. G.; Kang, E. T. *Polym. Chem.* **2011,** 2, (8), 1849-1858.

71. Jonkheijm, P.; Weinrich, D.; Koehn, M.; Engelkamp, H.; Christianen, P.; Kuhlmann, J.; Maan, J.; Nuesse, D.; Schroeder, H.; Wacker, R.; Breinbauer, R.; Niemeyer, C.; Waldmann, H. *Angew. Chem. Int. Ed.* **2008,** 47, (23), 4421.

72. Wendeln, C.; Rinnen, S.; Schulz, C.; Arlinghaus, H. F.; Ravoo, B. J. *Langmuir* **2010,** 26, (20), 15966-15971.

73. Li, M.; De, P.; Li, H.; Sumerlin, B. S. *Polym. Chem.* **2010,** 1, (6), 854-859.

74. Hensarling, R. M.; Doughty, V. A.; Chan, J. W.; Patton, D. L. *J. Am. Chem. Soc.* **2009,** 131, (41), 14673-14675.

75. Wang, C.; Ren, P. F.; Huang, X. J.; Wu, J.; Xu, Z. K. *Chem. Commun.* **2011,** 47, (13), 3930-3932.

76. Huang, Y.; Zeng, Y.; Yang, J.; Zeng, Z.; Zhu, F.; Chen, X. *Chem. Commun.* **2011,** 47, (26), 7509-7511.

77. Konkolewicz, D.; Gaillard, S.; West, A. G.; Cheng, Y. Y.; Gray-Weale, A.; Schmidt, T. W.; Nolan, S. P.; Perrier, S. *Organometallics* **2011,** 30, (6), 1315-1318.

78. Naik, S. S.; Chan, J. W.; Comer, C.; Hoyle, C. E.; Savin, D. A. *Polym. Chem.* **2011,** 2, (2), 303-305.

79. Hensarling, R. M.; Rahane, S. B.; LeBlanc, A. P.; Sparks, B. J.; White, E. M.; Locklin, J.; Patton, D. L. *Polym. Chem.* **2011,** 2, (1), 88-90.

80. Li, H.; Yu, B.; Matsushima, H.; Hoyle, C. E.; Lowe, A. B. *Macromolecules* **2009,** 42, (17), 6537-6542.

81. Nasar, A. S.; Subramani, S.; Radhakrishnan, G. *Polymer International* **1999,** 48, (7), 614-620.

82. Muhlebach, A. *Journal of Polymer Science Part a-Polymer Chemistry* **1994,** 32, (4), 753-765.

83. Wicks, D. A.; Wicks Jr, Z. W. *Progress in Organic Coatings* **1999,** 36, (3), 148-172.

84. Wicks, D. A.; Wicks Jr, Z. W. *Progress in Organic Coatings* **2001,** 41, (1–3), 1-83.

85. Bode, S.; Enke, M.; Gorls, H.; Hoeppener, S.; Weberskirch, R.; Hager, M. D.; Schubert, U. S. *Polymer Chemistry* **2014,** 5, (7), 2574-2582.

86. Viganò, M.; Levi, M.; Turri, S.; Chiari, M.; Damin, F. *Polymer* **2007,** 48, (14), 4055-4062.

87. Petrak, S.; Shadurka, V.; Binder, W. H. *Progress in Organic Coatings* **2009,** 66, (3), 296-305.

88. Vigano, M.; Suriano, R.; Levi, M.; Turri, S.; Chiari, M.; Damin, F. *Surface Science* **2007,** 601, (5), 1365-1370.

89. Gao, G.; Yu, K.; Kindrachuk, J.; Brooks, D. E.; Hancock, R. E. W.; Kizhakkedathu, J. N. *Biomacromolecules* **2011,** 12, (10), 3715-3727.

90. Song, X.-J.; Hu, J.; Wang, C.-C. *Colloids and Surfaces A: Physicochem. Eng. Aspects* **2011,** 380, 250-256.

91. Schuh, C.; Rühe, J. *Macromolecules* **2011,** 44, (9), 3502-3510.

92. Orski, S. V.; Fries, K. H.; R., S. G.; Locklin, J. *Langmuir* **2010,** 26, (3), 2136-2143.

93. Orski, S. V.; Poloukhtine, A. A.; Arumugam, S.; Mao, L.; Popik, V. V.; Locklin, J. *J. Am. Chem. Soc.* **2010,** 132, (32), 11024-11026.

94. Gelbrich, T.; Reinartz, M.; Schmidt, A. M. *Biomacromolecules* **2010,** 11, (3), 635-642.

95. Soto-Cantu, E.; Lokitz, B. S.; Hinestrosa, J. P.; Deodhar, C.; Messman, J. M.; Ankner, J. F.; Kilbey II, S. M. *Langmuir* **2011,** 27, (10), 5986-5996.

96. Hensarling, R. M.; Doughty, V. A.; Chan, J. W.; Patton, D. L. *J. Am. Chem. Soc.* **2009,** 131, (41), 14673-14675.

97. Hensarling, R. M.; Rahane, S. B.; LeBlanc, A. P.; Sparks, B. J.; White, E. M.; Locklin, J.; Patton, D. L. *Polym. Chem.* **2011,** 2, (1), 88-90.

98. Ballard, N.; Bon, S. A. F. *Polymer Chemistry* **2014,** 5, (23), 6789-6796.

99. Binauld, S.; Stenzel, M. H. *Chemical Communications* **2013,** 49, (21), 2082-2102.

100. Daigle, J.-C.; Arnold, A. A.; Piche, L.; Claverie, J. P. *Polymer Chemistry* **2013,** 4, (3), 449-452.

101. Deng, G.; Li, F.; Yu, H.; Liu, F.; Liu, C.; Sun, W.; Jiang, H.; Chen, Y. *ACS Macro Letters* **2012,** 1, (2), 275-279.

102. Iwasaki, Y.; Maie, H.; Akiyoshi, K. *Biomacromolecules* **2007,** 8, (10), 3162-3168.

103. Iwasaki, Y.; Tabata, E.; Kurita, K.; Akiyoshi, K. *Bioconjugate Chemistry* **2005,** 16, (3), 567-575.

104. Kumar, A.; Ujjwal, R. R.; Mittal, A.; Bansal, A.; Ojha, U. *ACS Applied Materials & Interfaces* **2014,** 6, (3), 1855-1865.

105. Lane, D. D.; Chiu, D. Y.; Su, F. Y.; Srinivasan, S.; Kern, H. B.; Press, O. W.; Stayton, P. S.; Convertine, A. J. *Polymer Chemistry* **2015,** 6, (8), 1286-1299.

106. Su, X.; Aprahamian, I. *Chemical Society Reviews* **2014,** 43, (6), 1963-1981.

107. van Dijken, D. J.; Kovaříček, P.; Ihrig, S. P.; Hecht, S. *Journal of the American Chemical Society* **2015,** 137, (47), 14982-14991.

108. Vetrík, M.; Přádný, M.; Hrubý, M.; Michálek, J. *Polymer Degradation and Stability* **2011,** 96, (5), 756-759.

109. von Delius, M.; Geertsema, E. M.; Leigh, D. A.; Tang, D.-T. D. *Journal of the American Chemical Society* **2010,** 132, (45), 16134-16145.

110. Wojtecki, R. J.; Meador, M. A.; Rowan, S. J. *Nat Mater* **2011,** 10, (1), 14-27.

111. Rowan, S. J.; Cantrill, S. J.; Cousins, G. R. L.; Sanders, J. K. M.; Stoddart, J. F. *Angewandte Chemie International Edition* **2002,** 41, (6), 898-952.

112. Gasparini, G.; Dal Molin, M.; Lovato, A.; Prins, L. J., Dynamic Covalent Chemistry. In *Supramolecular Chemistry*, John Wiley & Sons, Ltd: 2012.

113. Fleige, E.; Quadir, M. A.; Haag, R. *Advanced Drug Delivery Reviews* **2012,** 64, (9), 866-884.

114. Jin, Y.; Yu, C.; Denman, R. J.; Zhang, W. *Chemical Society Reviews* **2013,** 42, (16), 6634-6654.

115. Kool, E. T.; Park, D.-H.; Crisalli, P. *Journal of the American Chemical Society* **2013,** 135, (47), 17663-17666.

116. Bhat, V. T.; Caniard, A. M.; Luksch, T.; Brenk, R.; Campopiano, D. J.; Greaney, M. F. *Nat Chem* **2010,** 2, (6), 490-497.

117. Etrych, T.; Mrkvan, T.; Chytil, P.; Koňák, Č.; Říhová, B.; Ulbrich, K. *Journal of Applied Polymer Science* **2008,** 109, (5), 3050-3061.

118. Murray, B. S.; Fulton, D. A. *Macromolecules* **2011,** 44, (18), 7242-7252.

119. Zhi, Z.-l.; Powell, A. K.; Turnbull, J. E. *Analytical Chemistry* **2006,** 78, (14), 4786-4793.

120. Dirksen, A.; Dirksen, S.; Hackeng, T. M.; Dawson, P. E. *Journal of the American Chemical Society* **2006,** 128, (49), 15602-15603.

121. Crisalli, P.; Kool, E. T. *The Journal of Organic Chemistry* **2013,** 78, (3), 1184-1189.

122. Liu, J.; Li, R. C.; Sand, G. J.; Bulmus, V.; Davis, T. P.; Maynard, H. D. *Macromolecules* **2013,** 46, (1), 8-14.

123. Alconcel, S. N. S.; Kim, S. H.; Tao, L.; Maynard, H. D. *Macromolecular Rapid Communications* **2013,** 34, (12), 983-989.

124. Tao, L.; Mantovani, G.; Lecolley, F.; Haddleton, D. M. *Journal of the American Chemical Society* **2004,** 126, (41), 13220-13221.

125. Hruby, M.; Kucka, J.; Lebeda, O.; Mackova, H.; Babic, M.; Konak, C.; Studenovsky, M.; Sikora, A.; Kozempel, J.; Ulbrich, K. *Journal of Controlled Release* **2007,** 119, (1), 25-33.

126. Rozkiewicz, D. I.; Ravoo, B. J.; Reinhoudt, D. N. *Langmuir* **2005,** 21, (14), 6337-6343.

127. Tauk, L.; Schröder, A. P.; Decher, G.; Giuseppone, N. *Nat Chem* **2009,** 1, (8), 649-656.

128. Singh, D. K.; Pavan Kumar, B. V. V. S.; Eswaramoorthy, M. *Nanoscale* **2015,** 7, (32), 13358-13362.

129. Yang, S. J.; Zhang, H. *Analytical Chemistry* **2012,** 84, (5), 2232-2238.

130. Rao, J.; Khan, A. *Polymer Chemistry* **2013,** 4, (9), 2691-2695.

131. Brinkhuis, R. P.; de Graaf, F.; Hansen, M. B.; Visser, T. R.; Rutjes, F. P. J. T.; van Hest, J. C. M. *Polymer Chemistry* **2013,** 4, (5), 1345-1350.

CHAPTER II – RESEARCH OBJECTIVES

The development of methods to precisely control polymer architecture enables the synthesis of materials for sophisticated applications where polymer function closely follows polymer structure. Reversible-deactivation radical polymerizations (RDRP) have enabled the synthesis of a host of functional and controlled polymer architectures; however, some functional groups like acyl hydrazides (i.e. monomers with low pK_a values and nucleophilic functional groups) remain inaccessible or difficult to polymerize with control. Post-polymerization modification further enhances RDRP routes to achieve multifunctional materials. Isocyanate reactions possess many of the characteristics (e.g. efficient, versatile, readily available reactants, etc.) found in the most ideal chemistries for PPM, yet are under-explored as a PPM strategy due to hydrolytic instability. Blocked isocyanates that are reactive under mild conditions have the potential to improve the robustness of isocyanate PPM strategies in order to take full advantage of isocyanate chemistry for the synthesis of multifunctional materials. Surface-initiated polymerizations, especially when combined with RDRP and PPM, also afford a versatile and powerful technique to install multifunctional materials on surfaces for control of surface properties and interfaces. Imines and hydrazones have been successfully used as chemical handles for dynamic, pH-responsive surface modification, but most reports focus on imine formation and are limited to self-assembled monolayers (SAMs). As a result, few examples exist of robust, densely functional pH-responsive modification strategies and would benefit from the combination of hydrazone linkages and surface-initiated polymerization (SIP).

The work described herein addresses the design and synthesis of polymer scaffolds in solution and on surfaces with reactive functional groups for robust, sequential post-polymerization modification (PPM) or dynamic covalent chemistry (DCC) in order to develop multifunctional and stimuli-responsive polymers. This dissertation is divided into three sections. In the first section, RAFT polymerization of blocked isocyanato methacrylates, post-polymerization modification of blocked isocyanate homopolymers at ambient temperature with thiols, and sequential modification of blocked isocyanate copolymers are described. In the second section, controlled polymerization of unprotected monomers with nucleophilic functional groups and low pK_a values (i.e. acyl hydrazide methacrylamides and 4-vinylimidazole) was achieved under low pH (pH = 0) aqueous RAFT conditions. Finally, in the last section, hydrazide-functional surfaces are synthesized to develop a dynamic, hydrazone-based surface modification platform. The specific objectives of this research are as follows:

1. Synthesize blocked isocyanato methacrylates and small molecule blocked isocyanato model compounds with azole blocking agents of various deblocking reactivity.
2. Investigate deblocking conditions at room temperature in the presence of thiols and amine and the hydrolytic stability of blocked isocyanato methacrylates and model compounds.
3. Investigate room temperature RAFT polymerization and post-polymerization modification of blocked isocyanato methacrylates with thiols and amines.

4. Develop sequential modification platform based on copolymerization and modification of blocked isocyanato methacrylates possessing blocking agents with different reactivities.
5. Synthesize acyl hydrazide methacrylamides and 4-vinyl imidazole in order to study the polymerization of monomers with low pK_a, nucleophilic functional groups via aqueous RAFT polymerization.
6. Synthesize novel RAFT agent that is hydrolytically stable at low pH values (< 1) to facilitate low pH aqueous RAFT polymerization.
7. Develop low pH (pH < 1) aqueous RAFT polymerization methods to achieve direct, controlled polymerization of acyl hydrazide methacrylamides and 4-vinylimidazole in water.
8. Synthesize hydrazide-functional polymer brush surfaces in order to study hydrazone, cleavage, and exchange reactions on brush surfaces.
9. Employ hydrazone exchange reaction on brush surfaces to dynamically control surface properties.

CHAPTER III – RAFT POLYMERIZATION OF "SPLITTERS" AND "CRYPTOS": EXPLOITING AZOLE-*N*-CARBOXAMIDES AS BLOCKED ISOCYANATES FOR AMBIENT TEMPERATURE POST-POLYMERIZATION MODIFICATION

3.1 Introduction

Engineering modular macromolecules via post-polymerization modification (PPM) of reactive polymer scaffolds – an approach with origins dating back to the late 1800s – has emerged as a powerful, contemporary method to access soft materials with complex architectures and multifunctional compositions.[1-5] PPM strategies provide access to a library of functional polymers from a single scaffold upon chemical transformation of reactive moieties incorporated in the polymer backbone, at the chain-ends, or as pendent groups using an array of modifying derivatives.[6, 7] Synthetic routes to modular polymer scaffolds have rapidly advanced via a powerful synergism between click chemistry[8] and reversible-deactivation radical polymerization (RDRP) techniques – such as reversible addition-fragmentation chain transfer (RAFT) polymerization and atom-transfer radical polymerization (ATRP).[3] RDRP methods enable the polymerization of monomers with chemoselective pendent groups that are inert during the polymerization, but activated under specific post-polymerization conditions to provide a set of modified polymers with well-defined molecular weight characteristics and controlled architectures. Click reactions are most commonly used for PPM because these transformations are rapid, high-yielding, and proceed under mild conditions. Advancements in synthetic protocols have extended PPM strategies to polymer scaffolds containing two or more reactive moieties enabling the synthesis of multifunctional materials using orthogonal,[9] sequential,[10, 11] or cascade transformations.[12]

Reactions of isocyanates with various nucleophiles (e.g. alcohols, amines, and thiols) have been widely used to crosslink or chain extend polymers, and have underpinned common technologies such as polyurethane/polythiourethane coatings, foams, and thermoplastic elastomers for more than 70 years.[13, 14] However, these isocyanate chemistries have been scarcely employed in PPM strategies despite the fact that the nucleophilic addition of amines and thiols to isocyanates proceeds with hallmark characteristics of a click reaction. Recent efforts by our group,[15-17] and others,[18-20] have demonstrated the synthesis of isocyanate functionalized polymer scaffolds and subsequent PPM of these scaffolds using various X-NCO (X = OH, NH_2, SH) addition reactions as routes to multifunctional polymers and surfaces. While the isocyanate functionality is stable towards radical-mediated chemistries, including RAFT polymerization,[21, 22] isocyanates are highly reactive and inherently sensitive to water, making NCO-functional polymers difficult to handle and store prior to modification. An approach that exploits the versatility of X-NCO chemistry while mitigating the inherent instability of the isocyanate would be advantageous in PPM strategies.

In this direction, we were inspired by the reversibility of urea and urethane bonds. The dynamic nature of these linkages has recently been exploited for the design of reversible and self-healing polymers (using sterically hindered ureas),[23, 24] and historically for the design of latent isocyanates in coating formulations.[25, 26] Latent isocyanates, also known as "splitters", "cryptos" and "blocked" isocyanates, are adducts containing a relatively weak bond formed by the reaction of isocyanates and active hydrogen compounds, such as oximes, phenols, and N-based compounds (e.g. amides, imides, and azoles).[27-29] According to the elimination-addition mechanism shown in

Scheme 3.1a, the blocked isocyanate adduct dissociates at elevated temperature to regenerate the parent isocyanate, which then reacts with nucleophilic substrates to yield more thermally stable urethanes, ureas, and thiourethanes. The elimination-addition process has been used in coatings applications for shelf-stable 1K formulations that can be activated at elevated temperatures; however, relatively high temperatures (100 – 200 °C) are often necessary to facilitate the deblocking reaction. For this reason, blocked isocyanates have received little attention for contemporary post-polymerization modification processes. Several examples have been reported that employed bisulfite-blocked and oxime-blocked NCOs as monolayers[30] or polymer thin films[31] for DNA microarrays;[30, 31] however, these surfaces required deblocking at 180 °C under vacuum prior to postmodification with amines. Postmodification of a caprolactam-blocked hyperbranched polymer surface with polyethyleneimine was reported by Asri *et al*.[32] – a process that required immobilization reactions at 125 °C for up to 52 h. Bode et al.[33] recently reported the synthesis of α,ω-carboxy-terminated telechelics via RAFT polymerization and subsequent conversion of these end-groups to 3,5-dimethyl pyrazole-blocked isocyanates. The pyrazole-blocked telechelics were then reacted with amines and alcohols at 130 °C to achieve postmodification of the chain-ends. Although multiple synthetic steps, high temperatures, and lengthy reaction times were required to effect the PPM process, Bode's work demonstrates the potential synergism between controlled radical polymerization and blocked NCOs to access functional polymer materials.

If appropriately designed, blocked NCOs may also undergo direct displacement reactions with good nucleophiles at ambient temperatures – a process known as chemical deblocking that typically proceeds via an addition-elimination mechanism (Scheme 3.1b).

In one of the few examples of ambient temperature chemical deblocking of isocyanates for polymer postmodification, Penelle *et al.*[34] demonstrated the synthesis of a water-soluble ionic poly(methacrylate) containing pendent isocyanates blocked with sodium 4-hydroxybenzenesulfonate. The electron-withdrawing sulfonate group on the phenol served to activate the blocked adduct towards displacement by an amine; however the modification reaction was slow (requiring 72 h) and the polymer product exhibited poor solubility. With interest in fully exploiting ambient temperature deblocking for PPM processes, we turned our attention to azole-*N*-carboxamides – blocked isocyanate analogues that have been used extensively as acyl transfer reagents.[35-37] Azole-*N*-carboxamides offer a wide spectrum of reactivity in nucleophilic reactions, where reactivity depends on the number and location of nitrogen atom in the azole ring.[38] Imidazole-*N*-carboxamides, and the more reactive 1,2,4-triazole-*N*-carboxamides, are particularly activated towards nucleophilic reactions with amines and thiols to give ureas and thiocarbamates, respectively, in high yield at ambient temperatures.[37, 39-41] These characteristics make azole-*N*-carboxamides ideal candidates as blocked isocyanates for the development of a modular PPM platform under mild conditions.

In this work, we aim to significantly broaden the utility of blocked isocyanate chemistry for postmodification processes by employing azole-*N*-carboxamides as polymer pendent groups. This strategy will reduce the temperature range required to facilitate the isocyanate deblocking process in the presence of nucleophilic modifiers. Herein, we report the synthesis of well-defined *N*-heterocycle-blocked isocyanate polymer scaffolds via room temperature RAFT polymerization and successfully demonstrate post-polymerization modification of these scaffolds with thiols and amines

at *ambient* temperatures. *N*-heterocyclic blocking agents – including 3,5-dimethyl pyrazole, imidazole, and 1,2,4-triazole, incorporated as pendent moieties along the polymer backbone, were chemically deblocked with thiols using 1,8-diazabicyclo[5.4.0]undec-7-ene (DBU) as a catalyst. We further exploit differences in reactivity of pyrazole- and triazole-blocked adducts in a copolymer as a facile route to multifunctional polymers via sequential post-polymerization modification reactions. Notably, the current work brings blocked isocyanate chemistry into an enabling temperature range for efficient polymer modification strategies.

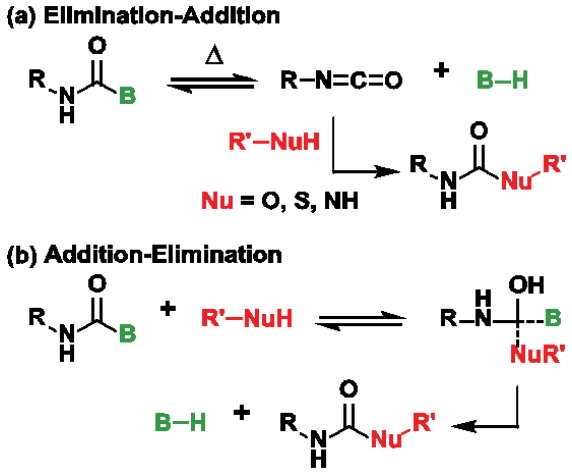

Scheme 3.1 (a) Elimination-addition and (b) addition-elimination mechanisms for deblocking blocked isocyanates.

3.2 Results and Discussion

3.2.1 Monomer and Model Blocked NCOs: Synthesis and Stability

In order to investigate polymer pendent blocked isocyanates as scaffolds for ambient temperature post-polymerization modification with thiols, three isocyanatoethyl methacrylate monomers blocked with a series of *N*-heterocycles were synthesized (Scheme 3.2a) including NCOP (pyrazole blocked), NCOI (imidazole blocked), and NCOT (triazole blocked). NCOP was commercially available. The one-step monomer

reactions were carried out in diethyl ether or a 2:1 (v:v) mixture of diethyl ether-THF at room temperature for 1-3 h. Both imidazole and 1,2,4-triazole monomers precipitated readily as stable crystalline solids, and were easily isolated in high yields (76-96%) by isolation via vacuum filtration.

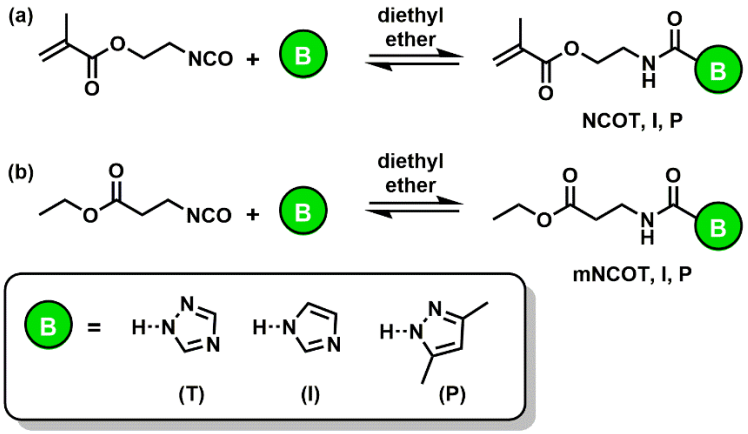

Scheme 3.2 Synthetic routes to (a) blocked NCO monomers and (b) model blocked NCO analogues.

A primary advantage of employing blocked NCO monomers for synthesis of functional polymer scaffolds as compared to free isocyanate analogues lies in the significant enhancement in hydrolytic stability of blocked NCOs. Figure 3.1 shows the hydrolytic degradation kinetics for NCOP, NCOI, NCOT, and the unprotected isocyanatoethyl methacrylate (IEM) in DMSO-d_6 containing 1% D_2O at 20 °C. NCOP showed the highest hydrolytic stability with less than 3% hydrolysis observed after 120 h. NCOI and NCOT were also quite stable and showed < 5% and ~13% hydrolysis at 12 and 120 h, respectively. In stark contrast, the unblocked IEM underwent ~20% hydrolysis after 1 h, and approached 90% hydrolysis at 12 h.

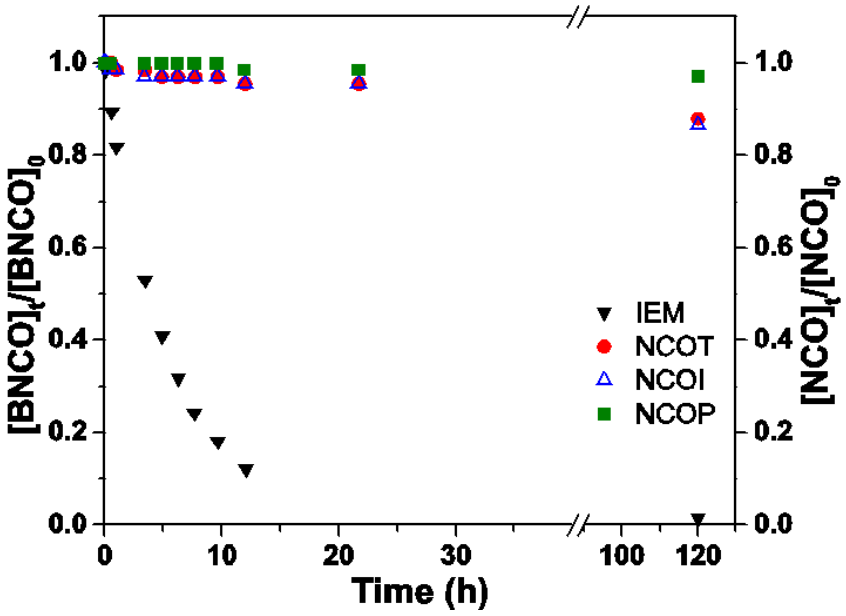

Figure 3.1 Hydrolytic stability plots for NCOP, NCOI, NCOT, and IEM in DMSO-d_6 containing 1% D_2O at 20 °C. The reactions were followed using ^1H NMR.

Because thiols undergo Michael addition reactions with methacrylates,[42] model blocked NCO analogues without the methacrylate group were used to investigate the relative rates of chemical deblocking with thiols under various conditions. Model blocked NCO analogues were synthesized from ethyl-3-isocyanatopropionate, as shown in Scheme 3.2b. The model compounds are denoted mNCOP, mNCOI, and mNCOT for 3,5-dimethyl pyrazole-, imidazole-, and 1,2,4-triazole-blocked 2-isocyanatoethyl propionates, respectively. The *N*-heterocycle blocking agents investigated in this work were chosen based on previous reports of a good balance between latency and reactivity of the respective blocked isocyanates at relatively lower temperatures as compared to more common blocking agents such as phenols and amides.[43, 44] More importantly, 3,5-dimethylpyrazole, imidazole, and 1,2,4-triazole provide a range of leaving group pK_a values (DMSO) (pyrazole, 19.8 > imidazole, 14.4 > 1,2,4-triazole, 10.3) allowing study of room temperature deblocking with nucleophiles. As the pK_a of the *N*-heterocycle

decreases (i.e. becomes a better leaving group), the extent of room temperature deblocking via the addition-elimination pathway is expected to increase.

3.2.2 Chemical Deblocking *N*-Heterocyle Blocked Isocyanates with Thiols: Model Reactions.

To our knowledge, there are no previous reports detailing the reaction of thiols with blocked isocyanates for polymer modification. In the first stage of this study, real-time ^{1}H NMR analysis was utilized to study the influence of blocking group, catalyst concentration, and reaction temperature on the kinetics and selectivity of reacting 1-hexanethiol with model blocked isocyanates (mNCOP, mNCOI, and mNCOT). From these experiments, optimal conditions for polymer modification were determined.

In a typical model reaction, a blocked isocyanate analogue was reacted with 1.1 equiv. of 1-hexanethiol in the presence of DBU at room temperature. Traditionally, DBU was considered a non-nucleophilic base, but has recently been shown to function as a strong nucleophilic catalyst in numerous reactions.[45, 46] In the case of chemical deblocking of isocyanates with thiols, DBU likely functions as both a base catalyst by generating the nucleophilic thiolate species while also acting as a nucleophilic catalyst via transient displacement of the *N*-heterocycle blocking agent to afford the more reactive zwitterionic amidine–isocyanate adduct.[47, 48] Although detailed kinetic analysis (i.e. determination of reaction order and rate constants) for these reactions will require additional focus beyond the scope of this paper, the data shown here establish conditions applicable for rapid and efficient post-polymerization modifications.

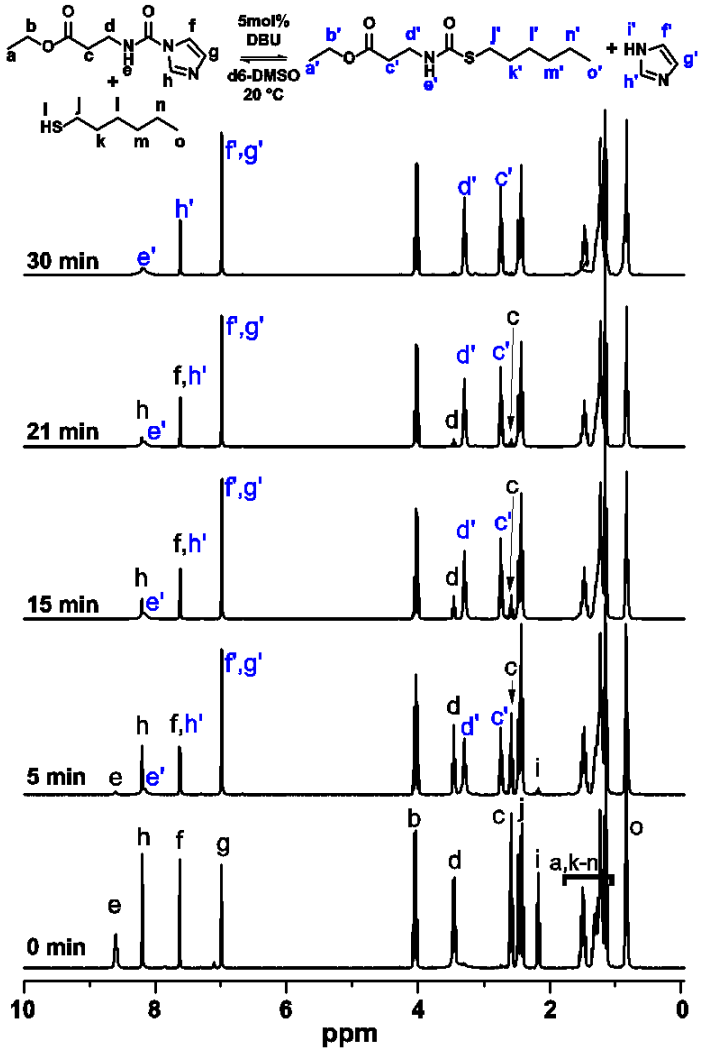

Figure 3.2 ^{1}H NMR spectra for the reaction of mNCOI with 1-hexanethiol in the presence of 5 mol% DBU (scheme pictured above spectra) at room temperature as the reaction proceeds. Peaks are labeled according to the structure above.

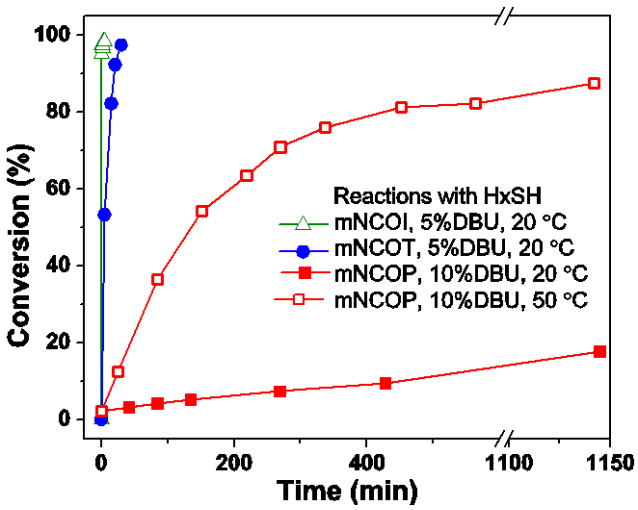

Figure 3.3 Conversion versus time plots for the following reactions (■) mNCOP + 1-hexanethiol + 10 mol% DBU at 20ºC, (□) mNCOP + 1-hexanethiol + 10 mol% DBU at 50ºC, (●) mNCOI + 1-hexanethiol + 5 mol% DBU at 20ºC, and (Δ) mNCOT + 1-hexanethiol + 5 mol% DBU at 20ºC.

A representative sequence of real-time ^{1}H NMR spectra for the DBU-catalyzed room temperature reaction of 1-hexanethiol with mNCOI is shown in Figure 3.2. Conversion was measured via integration of the protons beta to the urea (peak c), relative to the unchanging methylene protons alpha to the ester at 4.04 ppm (peak b). Figure 3.3 shows the blocked isocyanate conversion plots for the DBU-catalyzed reaction of 1-hexanethiol with the series of model *N*-heterocycle-blocked isocyanates. The reaction of 1-hexanethiol with mNCOP with 10 mol% DBU at 20 °C yielded only 18% conversion after 19 h – a result that points to the relative stability of the 3,5-dimethylpyrazole blocked isocyanate which typically requires temperatures around 130 °C for quantitative reaction with amines and alcohols.[33] Conducting the same mNCOP chemical deblocking reaction with thiol at 50 °C provided a significant increase in the rate of the reaction, with 88% conversion achieved after 19 h. By contrast, the reactions of 1-hexanethiol with mNCOI and mNCOT proceeded rapidly at 20 °C using lower DBU concentrations (5

mol%). The chemical deblocking of mNCOI with 1-hexanethiol in the presence of 5 mol% DBU at room temperature was nearly quantitative after 30 min. The significant increase in reactivity of mNCOI is not unexpected; imidazole is more activating than 3,5-dimethyl pyrazole.[38] Staab and coauthors also showed that imidazole-*N*-carboxamides readily dissociate into isocyanate and imidazole in a rapid equilibrium at room temperature (e.g. 16% dissociation at 20 °C in chloroform).[37, 49] The reaction of 1-hexanethiol with mNCOT under the same conditions was quite rapid, reaching 95% conversion within 30 s, and then almost quantitative conversion within 5 min (Figure 3.3). The higher reactivity of mNCOT (due to activating effect of an additional nitrogen atom in the azole ring)[38] also allowed for reducing the DBU concentration to 1 mol% while still providing quantitative thiourethane conversion within 30 min at 20 °C (Figure A.1, Appendix A). It is worth noting that triethylamine was also explored as a catalyst; however, high catalyst loading (> 30 mol% TEA) was required to achieve kinetic profiles comparable to those with low DBU concentrations (Figure A.2, Appendix A). The N-heterocycle blocking agents follow the expected trend of 1,2,4-triazole > imidazole > 3,5-dimethyl pyrazole in terms of leaving group ability based on their pK_a values. The kinetic profiles for the reaction of thiols with mNCOI and mNCOT indicate that imidazole and 1,2,4-triazole may be the ideal blocking agents as polymer pendent scaffolds for post-polymerization modification. Importantly, the full series of N-heterocycle blocking agents provides a range of reactivity that may be exploited for sequential modification via appropriate choice of reaction conditions.

3.2.3 Polymer Synthesis

After determination of optimal deblocking conditions with thiols, the N-heterocycle blocked NCO methacrylate monomers were polymerized by RAFT using 2-cyano-2-propyl-4-cyanobenzodithioate (CPCB) as the chain transfer agent (Scheme 3.3). Dithiobenzoates with electron withdrawing Z-group substituents, such as CPCB, have been shown to provide good control and low dispersities for methacrylates.[50] DMSO was chosen as the polymerization solvent since NCOP, NCOI, and NCOT are readily soluble in this solvent at room temperature.

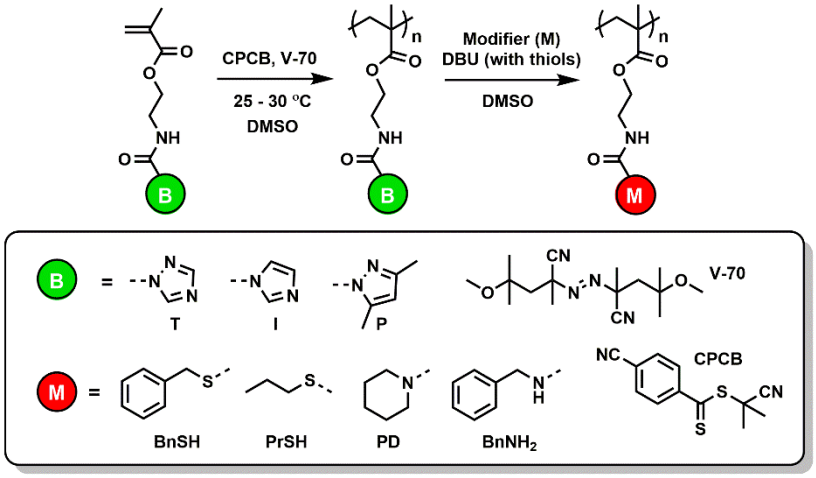

Scheme 3.3 RAFT polymerization and postmodification of blocked NCO polymers with thiols or amines.

The temperature sensitivity of the pendent N-heterocycle blocked isocyanate moieties present a challenge for controlled polymerizations under standard conditions. Initial RAFT polymerizations conducted at 60 – 70 °C led to broad dispersities, particularly for mNCOI and mNCOT. Despite reported deblocking temperatures greater than 100 °C for pyrazole-, imidazole-, and triazole-blocked isocyanate derivatives, thermal deblocking and subsequent side reactions occur over a range of temperatures. Side reactions ensue when amines generated by the hydrolysis of deblocked isocyanates

react to form crosslinks. To avoid complications associated with thermal deblocking during polymer synthesis, polymerizations were conducted at either 25 or 30 °C using V-70 – an azo initiator with a 10 hour half-life decomposition temperature of 30 ºC. Conversion, molecular weight, and dispersity data obtained from exploratory polymerizations of each monomer at 25 or 30 °C and $[M]_o$:$[CTA]_o$:$[I]_o$ = 300:1:0.2 are shown in Table A.1; these data were used to select experimental conditions for polymerization kinetics discussed below. Temperature sensitivity and solubility of the blocked NCOI and NCOT polymers also present a challenge for characterization since size-exclusion chromatography (SEC) analysis was conducted in DMF (0.2M LiBr) at 65 °C. pNCOI and pNCOT samples were postmodified with 1-propanethiol, using DBU as a catalyst, prior to SEC analysis to avoid issues with thermal deblocking during analysis. Thus, all polymer molecular weight and dispersity data for NCOI and NCOT reflect the characteristics of the modified polymers. pNCOP was sufficiently stable to enable SEC analysis in the heterocycle blocked state.

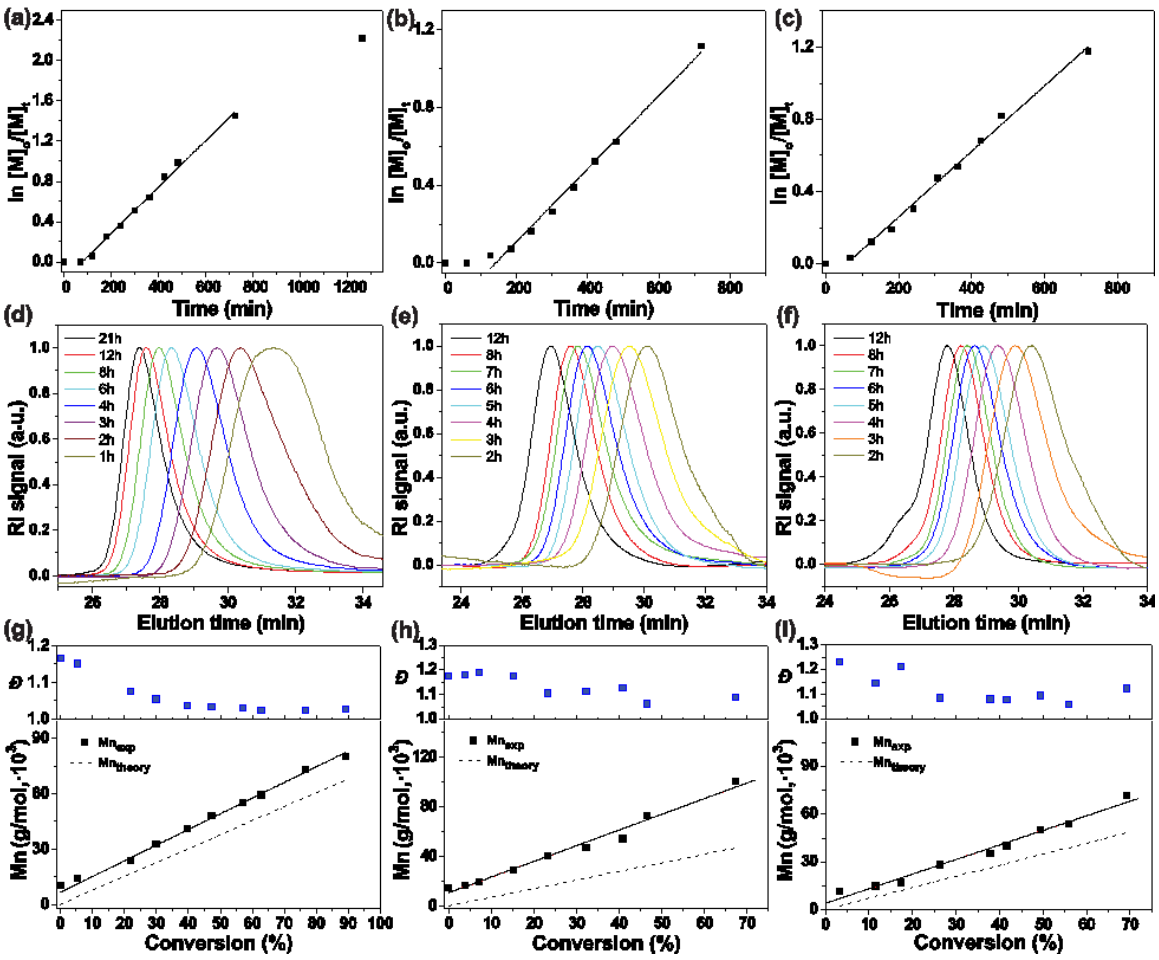

Figure 3.4 Kinetic plots for CPCD-mediated RAFT polymerization of (a) NCOP at 30 °C, (b) NCOI at 30 °C, and (c) NCOT at 25 °C in DMSO. SEC traces for RAFT polymerization of (d) NCOP (e) NCOI, (f) NCOT. Molecular weight and dispersity versus conversion plots for (g) NCOP, (h) NCOI, and (i) NCOT. SEC for NCOP was performed in the blocked form, whereas NCOI and NCOP were modified with propanethiol prior to analysis.

Figure 3.4a shows the kinetic plot for the polymerization of NCOP at 30 °C. Following a 60 min induction period, linear pseudo-first-order kinetic behavior was observed up to 720 min. The induction period may be attributed to an initialization time required for consumption of the CTA, as described by Klumperman et al.,[51, 52] or slow fragmentation of the intermediate radical – effects often observed in ambient temperature RAFT polymerizations.[53, 54] At longer reaction times (1260 min), deviation from

linearity is observed, likely due to a decrease in radical flux associated with half-life of the V-70 initiator ($t_{1/2}$ = 600 min at 30 °C). The SEC chromatograms shown in Figure 3.4d are symmetrical and shift to lower elution volumes with increasing polymerization time. Additional evidence of a well-controlled polymerization for NCOP is indicated by the linear progression of M_n vs monomer conversion and the narrow molecular weight distributions ($Đ \leq 1.10$ above 20% conversion), as shown in Figure 3.4g. The experimentally determined molecular weight ($M_{n,exp}$) values are higher than values predicted based upon conversion ($M_{n,theory}$) for a 300:1 $[M]_0$:$[CTA]_0$ ratio. The discrepancy in $M_{n,exp}$ determined by SEC-MALLS and $M_{n,theory}$ may be attributed to irreversible coupling of CTA intermediate radicals or incomplete CTA consumption during the initialization stage.[51] Nonetheless, control for NCOP could be maintained up to high conversions (> 90%) to yield relatively high molecular weight polymer (M_n > 80k g/mol).

RAFT polymerization of NCOI was first attempted at 25 °C; however, an extensive initialization period provided low monomer conversion (~ 9%) after 300 min (Table A.1). At 30 ºC, the polymerization of NCOI exhibited an initialization period of approximately 60 min, followed by linear pseudo-first-order behavior up to 700 min indicating good control beyond the initialization period (Figure 3.4b). The SEC chromatograms shown in Figure 3.4e are unimodal and shift to lower elution times with increasing reaction time – an observation that translates into a linear relationship between $M_{n,exp}$ vs monomer conversion (Figure 3.4e). Again, the observed $M_{n,exp}$ values are consistently higher than $M_{n,theory}$ values (Figure 3.4h). Given the observation of a stable concentration of radicals and the absence of polymer chain coupling (e.g. no observations

of high MW shoulders by SEC), the discrepancy is likely, as mentioned previously, attributed to irreversible coupling of CTA intermediate radicals or incomplete CTA consumption during the initialization stage. It is also worth noting that a color change was observed upon addition of the CTA to the NCOI monomer solution (Figure A.3). We attribute the color change to partial degradation of the CTA via aminolysis with imidazole (approximately 4% CTA degradation in 60 min as indicated by NMR, Figure A.3) – a process that would contribute to overshooting the theoretical molecular weight values.[55] The behavior of NCOI in solution, in terms of freely dissociating to give imidazole, is not entirely surprising. As mentioned previously, Staab showed that imidiazole-*N*-carboxamides readily dissociate to imidazole and isocyanates even at room temperature (up to 16% dissociation at 20 °C by FTIR).[35, 37]

NCOT was polymerized at 25ºC to evaluate polymerization kinetics. As with the other monomers in this series, RAFT polymerization of NCOT shows linear pseudo-first-order behavior up to 700 min following a 60 min initialization period (Figure 3.4c). The SEC chromatograms shown in Figure 3.4h shift to lower elution times and are symmetrical up to the 8h aliquot. At 12h, a high molecular weight shoulder is observed that is approximately double the molecular weight of the main polymer peak and can be attributed to radical-radical coupling. Increasing the polymerization temperature to 30 °C shifted the observation of the high molecular weight shoulder to lower conversions (Figure A.4). Analysis of the SEC chromatograms showed dispersities above 1.2 at conversions less than 20% that gradually decreased ($Đ < 1.1$) with increasing monomer conversion (Figure 3.4f). Chain coupling above 50% conversion resulted in a small increase in dispersity. A well-controlled polymerization of NCOT was also indicated by

a linear increase in $M_{n,exp}$ with conversion (Figure 3.4i). As with NCOP and NCOI, the $M_{n,exp}$ values were higher than the targeted $M_{n,theo}$; however, due to a shorter initialization period (e.g. minimal CTA side reactions), the expected and actual M_n values for NCOT are in better agreement than those for NCOI. The polymerization kinetics reported in this paper demonstrate that this series of n-heterocyclic blocked NCO methacrylates can be polymerized to yield controlled molecular weights and dispersities, even when polymers were modified by thiols prior to characterization.

3.2.4 Post-Polymerization Modification

After establishing conditions for controlled polymerization of NCOP, NCOI, and NCOT, the resulting polymers were exploited as scaffolds for post-polymerization modification. For simple proof of concept, two thiols, 1-propanethiol (PrSH) and benzyl mercaptan (BnSH), and two amines, piperidine (PD) and benzyl amine ($BnNH_2$), were chosen to demonstrate postmodification of the blocked NCO polymers. The results obtained from reactions of thiols with small molecule analogs, as described previously, were used to guide the choice of reaction conditions for the polymer modifications described herein. Polymers blocked with 3,5-dimethyl pyrazole were isolated via precipitation prior to postmodification, and subsequently modified with PrSH and BnSH at 50 °C with DBU as a catalyst, or PD and $BnNH_2$ at 50 °C without DBU. However, the high reactivity of the pNCOI and pNCOT scaffolds presented a challenge to standard isolation, e.g. precipitation resulted in high molecular weight tailing observed in the isolated SEC traces likely due to instability of the blocked pendent groups. Thus, polymers blocked with imidazole and triazole were efficiently postmodified in crude form at 25 °C to avoid adventitious side reactions. Figure A.5 shows the SEC traces for

isolated, unmodified pNCOP and pNCOP modified with BnSH. A shift to lower elution time occurs after modification of pNCOP, which is consistent with the increase in molecular weight expected by displacing 3,5-dimethyl pyrazole (96.13 g/mol) with BnSH (124.2 g/mol). Table 2.1 provides a summary of the polymer molecular weights and dispersities following postmodification of pNCOP, pNCOI, and pNCOT with PrSH, BnSH, and PD. As shown, molecular weights greater that 40 kg/mol and low dispersities ($Đ \leq 1.21$) were obtained for all postmodified polymer scaffolds.

Table 3.1

Molecular weights and dispersities for thiol and amine modified blocked NCO polymers.

Entry	**Polymer**	**Temp (°C)[a]**	**Time[b] (h)**	**PPM $M_{n,exp}$[c] (kg/mol)**	**PPM $Đ_M$[c]**
1a	pNCOP-PrSH	50	48	38.3	1.21
1b	pNCOP-BnSH			42.2	1.10
1c	pNCOP-PD			40.1	1.03
1d	pNCOP-$BnNH_2$			29.5[d]	1.04
2a	pNCOT-PrSH	25	12	41.8	1.08
2b	pNCOT-BnSH			51.0	1.07
2c	pNCOT-PD			45.8	1.06
2d	pNCOT-$BnNH_2$			43.3[d]	1.05
3a	pNCOI-PrSH	25	12	74.4	1.08
3b	pNCOI-BnSH			87.4	1.18
3c	pNCOI-PD			73.3	1.11

[a]PPM temperature; [b]PPM time; [c]As determined by SEC-MALLS (DMF with 20 mM LiBr). [d] MW determined on a different column set than all other polymers in the table due to instrumentation issues during the revision process.

Typical ^{1}H NMR spectra for the postmodified polymer scaffolds based on pNCOI are shown in Figure 3.5. The absence of peaks at 6.99 ppm, 7.61 ppm, and 8.18 ppm in the NMR spectra indicates quantitative chemical deblocking of the imidazole moieties

with BnSH (Figure 3.5a), PrSH (Figure 3.5b), PD (Figure 3.5c), and $BnNH_2$ (Figure 3.5d). The carbamide proton peak of the asymmetrical urea is located at 8.63 ppm prior to modification and shifts to 6.5 ppm or 6.0 ppm upon formation of the new thiocarbamate or urea, respectively. The presence of peak f, representative of each modifier, in each spectrum in Figure 3.5 also suggests the successful modification of blocked NCO polymers.

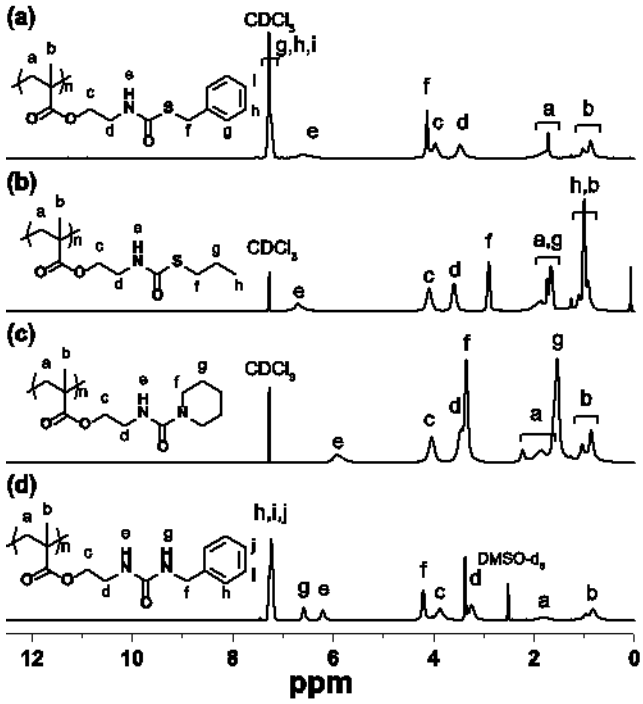

Figure 3.5 ^{1}H NMR spectra of imidazole-blocked NCO polymers modified at room temperature with (a) benzyl mercaptan, (b) 1-propanethiol, (c) piperidine or (d) benzyl amine after purification.

3.2.5 Sequential Polymer Modification

Sequential postmodification reactions offer a direct route to multifunctional polymers and find the most utility in scaffolds containing independently addressable reactive moieties. Sequential modifications are typically achieved by either exploiting inherently orthogonal chemical transformations or inducing selective reactivity through

judicious choice of reaction conditions. In this section, we describe how the differences in reactivity of 1,2,4-triazole blocked NCOs and 3,5-dimethyl pyrazole blocked NCOs can be leveraged to achieve sequential polymer modification. Recalling the results from our small molecule model reactions, we observed that reactions of a nucleophile with 3,5-dimethyl pyrazole blocked NCOs were slow or unreactive at room temperature, but could be driven towards higher conversion at elevated temperatures (e.g. 50 °C). Conversely, nucleophiles were found to react rapidly with 1,2,4-triazole blocked NCOs at 25 °C.

To exploit the "staggered" reactivity of pyrazole and triazole derivatives for sequential polymer modifications, copolymers were synthesized by RAFT polymerization at 25 ºC using a 50:50 molar ratio of NCOT and NCOP monomers. Figure 3.6a shows the synthetic route used to sequentially modify p(NCOT-*co*-NCOP) copolymers. Figure 3.6b shows the ^{1}H NMR spectrum of the crude copolymer prior to postmodification. The copolymerization of NCOT and NCOP was stopped after 5 h and the crude polymerization mixture was added to a solution of piperidine at 20 °C to displace the triazole blocking agent. Figure 3.6b shows the ^{1}H NMR spectrum of the copolymer after piperidine modification and purification by precipitation. The formation of a new carbamide with the amine modifier was confirmed by the presence of PD peaks, labeled f" (3.27 ppm) and g" (1.46 ppm) in Figure 3.6c, and the absence of 1,2,4-triazole peaks located at 8.27 and 9.16 ppm. Notably, the 3,5-dimethyl pyrazole blocking agents in the copolymer were still present following the initial modification, as indicated by the presence of protons assigned f', h', and g' in Figure 3.6c. To gauge the selectivity of the initial modification, a pNCOP homopolymer was modified with PD under identical conditions (12 h, 20 °C) and integration showed less than 3% of the pyrazole blocking

agents were displaced by PD (Figure A.6). Returning to the copolymer, integration of ^{1}H NMR spectrum (Figure A.7a) after piperidine modification indicated the composition of the pendent groups was approximately 50:50 (mol%) piperidine to 3,5-dimethylpyrazole. The piperidine modified copolymer was then sequentially modified with benzyl mercaptan in anhydrous DMSO with DBU at 50 °C to displace the 3,5-dimethyl pyrazole blocking agents. The ^{1}H NMR spectrum of the copolymer sequentially modified with PD and BnSH is shown in Figure 3.6d. The disappearance of the pyrazole peaks at 2.12 ppm (f'), 2.46 ppm (h'), and 5.85 ppm (g'), and the appearance of BnSH peaks at 4.07 ppm (f''') and 7.22 ppm (g''', h''', and i'''), shown in Figure 3.6d, indicate that the modification with benzyl mercaptan proceeded to high conversion. Furthermore, the peaks attributed to the PD functionalized units (f'' and g'') from the initial modification remain unchanged, where integration (Figure A.7b) indicated the composition of the pendent groups was approximately 50:50 (mol%) piperidine to triazole. These results demonstrate the sequential nature of the post-modifications, and while not perfectly selective, point to the utility of using the large difference in reactivity of various blocking agents to design multifunctional polymers in a modular fashion. SEC-RI traces, shown in Figure A.8, also support the sequential nature of the postmodification reactions. After modification with piperidine, the molecular weight of p(NCOT-PD-*co*-NCOP) was 43.4 kg/mol with a dispersity of 1.05 and, after the second modification with BnSH, the molecular weight increased to 52.7 kg/mol with a dispersity of 1.24 for p(NCOT-PD-*co*-NCOP-BnSH). The shift to higher molecular weight from the first modification to the second was expected to be relatively small based on the small increase in molecular weight going from 3,5-dimethyl pyrazole to BnSH. The increase in dispersity during modification with

BnSH may be attributed to various intermolecular side chain reactions that may occur at temperatures as low as 50 °C (e.g. allophanate formation) or in the presence of trace amounts of water (e.g. urea and biuret formation).[56] We are currently exploring other blocking agents that eliminate these unwanted side reactions. The results from ^{1}H NMR and SEC show that with judicious choice of blocking agents and PPM conditions, it is possible to design and synthesize dually modifiable copolymer scaffolds with low dispersities and controlled molecular weights. Furthermore, this strategy has the potential for additional versatility by selecting from a variety of thiols, amines, and alcohols available to react with the blocked NCOs.

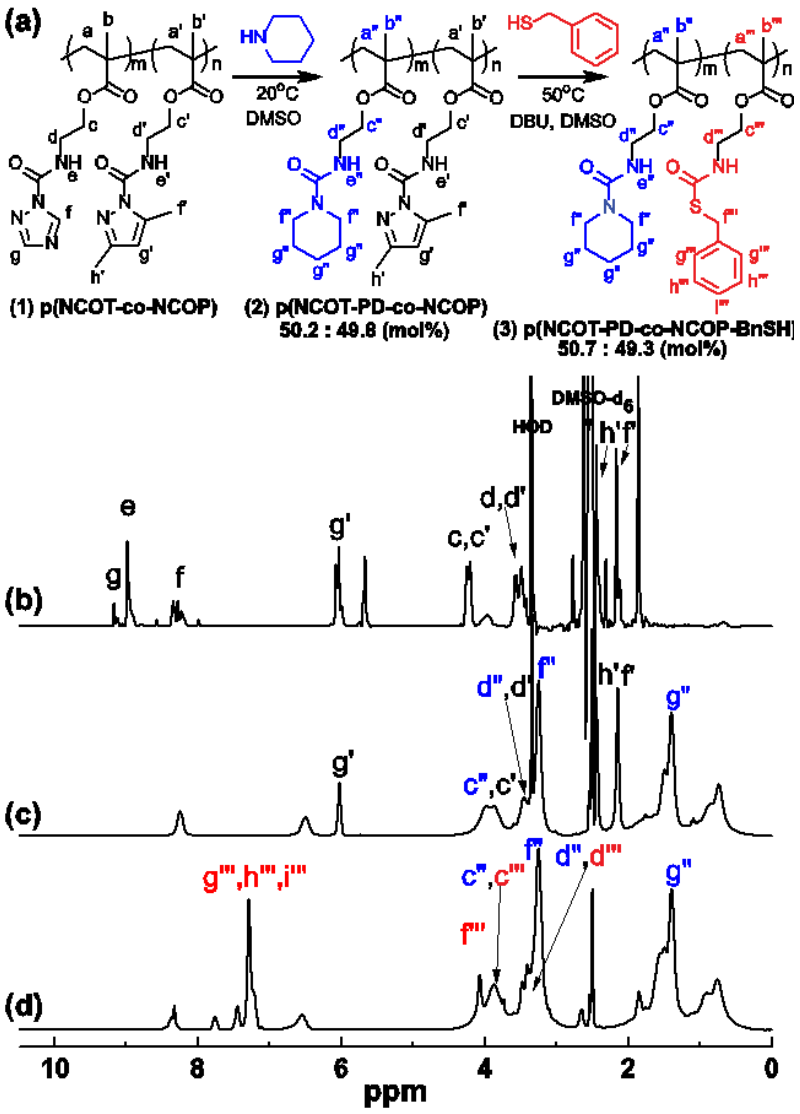

Figure 3.6 (a) Synthetic route to sequentially modified blocked NCO copolymers. ^{1}H NMR spectra of (b) crude pNCOT-*co*-NCOP (c) after the first modification with piperidine and (d) after the second modification with benzyl mercaptan. All NMR spectra were collected in DMSO-d_6.

3.3 Conclusions

In summary, we report the synthesis of well-defined polymethacrylate scaffolds containing pendent N-heterocycle-blocked isocyanates via low temperature RAFT polymerization. Judicious choice of N-heterocycle blocking agents enabled rapid and efficient post-polymerization modification with thiols and amines at ambient temperature

via chemical deblocking. Sequential modification reactions on copolymer scaffolds were demonstrated by exploiting differences in the latent reactivity of pendent triazole and pyrazole blocked isocyanates. Triazole-blocked NCO moieties were initially deblocked with an amine at ambient temperature; subsequently, the NCOP units were deblocked with a thiol at 50 ºC enabling the synthesis of multifunctional polymer scaffolds. We expect the azole-*N*-carboxamide derivatives employed here as blocked isocyanates for post-polymerization modification will find broad use in other polymer synthetic strategies where balanced latency and reactivity under mild conditions are necessary to engineer functional macromolecular materials.

3.4 Experimental

3.4.1 Materials

Karenz MOI-BP (3,5-dimethyl pyrazole blocked isocyanate methacrylate) was obtained from Showa Denko and passed through a neutral alumina plug to remove inhibitor prior to use. Ethyl 3-isocyanatopropionate (Aldrich, 98%), 2, 2'-Azobis(4-methoxy-2-4-dimethyl valeronitrile) (V-70) (Wako, 96%), 2-isocyanatoethyl methacrylate (TCI, > 98%), 1,8-diazabicyclo[5.4.0]undec-7-ene (DBU) (Acros, 98%), 2-cyano-2-propyl 4-cyanobenzodithioate (CPCB) (Aldrich, 98%,), imidazole (Aldrich, ≥ 99%), 1,2,4-triazole (Acros, 99.5%), 3,5-dimethyl pyrazole (Aldrich, 99%), 1-propanethiol (Aldrich, 99%), benzyl mercaptan (Fluka, ≥ 99%), piperidine (Aldrich, redistilled, 99.5+%), tetrahydrofuran (THF) (Aldrich, anhydrous, inhibitor free, ≥ 99.9%) and dimethyl sulfoxide (DMSO) (Aldrich, anhydrous, 99.9%) were used as received.

3.4.2 Characterization

NMR studies were conducted using a Varian INOVA 300 MHz NMR spectrometer in DMSO-d_6 or $CDCl_3$ at 25 °C. Model reactions requiring reaction temperatures at 50 °C were acquired on a Bruker Ascend™ 600 MHz spectrometer using DMSO-d_6, whereas reactions requiring ambient temperatures were acquired on the Varian INOVA 300 MHz NMR. Number-average molecular weight (M_n) and dispersities ($Đ$) were determined using a size-exclusion chromatography (SEC) system consisting of a Waters Alliance 2695 separation module, online multi-angle laser light scattering (MALLS) detector fitted with a gallium arsenide laser (20 mW power) operating at 690 nm (MiniDAWN Wyatt Technology Inc.), an interferometric refractometer (Optilab DSP, Wyatt Technology Inc.), and two Polymer Laboratories mixed C columns (5 μm beadsize) connected in series. The eluent used was HPLC grade dimethyl formamide (DMF) (0.02 M LiBr) at a flow rate of 0.5 mL/minute at 65 °C. The refractive index increment (d*n*/d*c*) of each polymer was determined in DMF (0.02 M LiBr).

3.4.3 Synthesis of 2-(1H-1,2,4-Triazole-1-Carboxamido)Ethyl Methacrylate (NCOT)

2-Isocyanatoethyl methacrylate (13.84 g, 89.2 mmol) was added dropwise over 15 minutes at room temperature to a stirred solution of 1,2,4-triazole (6.16 g, 89.2 mmol) in a 4:5 (v:v) mixture of THF (80 mL) and diethyl ether (100 mL). The reaction was stirred for an additional 3 h after which the product precipitated as a white solid. The solid precipitate was isolated by vacuum filtration, rinsed with THF (20 mL), and dried *in-vacuo* to give the desired product as a white solid (15.16 g, 76%). Mp: 100-103 °C. ^{1}H NMR (300 MHz, DMSO-d_6): δ 9.16 (s, 1H), 8.90 (t, J = 5.6 Hz, 1H), 8.27 (s, 1H), 6.02

(s, 1H), 5.65 (s, 1H), 4.23 (t, *J* = 5.4 Hz, 2H), 3.55 (q, *J* = 5.5 Hz, 2H), 1.83 (s, 3H). ^{13}C NMR (75 MHz, DMSO-d_6): δ 166.51, 152.60, 148.02, 144.39, 135.89, 126.05, 62.72, 39.04, 17.99. Elemental analysis calculated for $C_9H_{12}N_4O_3$: C, 48.21; H, 5.39; N, 24.99; O, 21.41. Found: C, 48.22; H, 5.38; N, 24.76; O, 21.69.

3.4.4 Synthesis of 2-(1H-Imidazole-1-Carboxamido)Ethyl Methacrylate (NCOI)

2-Isocyanatoethyl methacrylate (7.59 g, 48.9 mmol) was added dropwise over 15 minutes at room temperature to a stirred solution of imidazole (3.33 g, 48.9 mmol) in diethyl ether (100 mL). The reaction was stirred for 1 h after which the product precipitated as a white solid. The solid precipitate was isolated by vacuum filtration, rinsed with diethyl ether (20 mL), and dried *invacuo* to give the desired product as a white solid (10.47 g, 96%). Mp: 75-80 ºC. ^{1}H NMR (300 MHz, DMSO-d_6): δ 8.64 (t, *J* = 5.2 Hz, 1H), 8.20 (s, 1H), 7.63 (s, 1H), 7.01 (s, 1H), 6.03 (s, 1H), 5.69 – 5.59 (m, 1H), 4.23 (t, *J* = 5.5 Hz, 2H), 3.53 (q, *J* = 5.5 Hz, 2H), 1.84 (s, 3H). ^{13}C NMR (75 MHz, $CDCl_3$): δ 167.93, 149.31, 135.98, 129.76, 126.70, 116.70, 63.03, 40.47, 18.30. Elemental analysis calculated for $C_{10}H_{13}N_3O_3$: C, 53.80; H, 5.87; N, 18.82; O, 21.50. Found: C, 53.89; H, 6.00; N, 18.78; O, 21.70.

3.4.5 Synthesis of 3-(1H-1,2,4-Triazole-1-Carboxamido)Propanoate (mNCOT)

Ethyl-3-isocyanatopropionate (1.89, 13.2 mmol) was added dropwise over 5 minutes to a stirred solution of 1,2,4-triazole (0.91 g, 13.2 mmol) in a 1:2 (v:v) mixture of THF (15 mL) and diethyl ether (30 mL). The reaction was stirred for 2 h, while the product precipitated as a white solid. The solid precipitate was isolated by vacuum filtration, rinsed with THF (20 mL), and dried *in-vacuo* to give 1.62 g (58% yield) of product as a white solid. Mp: 81-85 ºC. ^{1}H NMR (300 MHz, DMSO-d_6): δ 8.95 (s, 2H),

8.89 (t, J = 5.0 Hz, 1H), 4.12 – 3.96 (m, 2H), 3.46 (dd, J = 12.2, 6.7 Hz, 2H), 2.59 (t, J = 6.8 Hz, 2H), 1.20 – 1.05 (m, 3H). ^{13}C NMR (75 MHz, DMSO-d_6): δ 171.40, 147.12, 140.88, 60.65, 36.81, 33.63, 14.44. Elemental analysis calculated for $C_8H_{12}N_4O_3$: C, 45.28; H, 5.70; N, 26.40; O, 22.62. Found: C, 45.27; H, 5.63; N, 19.97; O, 22.82.

3.4.6 Synthesis of Ethyl 3-(1H-Imidazole-1-Carboxamido)Propanoate (mNCOI)

Ethyl-3-isocyanatopropionate (1.93 g, 13.5 mmol) was added dropwise over 5 minutes to a stirred solution of imidazole (0.917 g, 13.5 mmol) in diethyl ether (50 mL) over 10 minutes. The reaction was stirred for 1 h at room temperature, while a white precipitate formed. The solid precipitate was isolated by vacuum filtration, rinsed with diethyl ether, and dried *in-vacuo* to give 2.58 g (91% yield) of product as a white solid. Mp: 80-84 ºC. ^{1}H NMR (300 MHz, $CDCl_3$): δ 8.16 (s, 1H), 7.37 (s, 1H), 7.09 (s, 1H), 7.08 – 7.02 (m, 1H), 4.18 (q, *J* = 7.1 Hz, 2H), 3.69 (dd, *J* = 11.8, 5.9 Hz, 2H), 2.67 (t, *J* = 5.9 Hz, 2H), 1.28 (t, *J* = 7.2 Hz, 3H). ^{13}C NMR (75 MHz, $CDCl_3$): δ 172.20, 149.07, 136.11, 129.74, 116.38, 60.92, 36.49, 33.63, 14.09. Elemental analysis calculated for $C_9H_{13}N_3O_3$: C, 51.18; H, 6.20; N, 19.89; O, 22.72. Found: C, 51.21; H, 6.32; N, 19.87; O, 22.80.

3.4.7 Synthesis of Ethyl 3-(3,5-Dimethyl-1H-Pyrazole-1-Carboxamido)Propanoate (mNCOP)

Ethyl-3-isocyanatopropionate (1.49 g, 10.4 mmol) was added dropwise over 15 minutes to a stirred solution of pyrazole (1.00 g, 10.4 mmol) diethyl ether (50 mL). The reaction was stirred for 1 h before the product was isolated from diethyl ether by rotary evaporation and dissolved in CH_2Cl_2. The product was then transferred to a separatory funnel and washed with water (150 mL) and with brine solution (150 mL). The organic

layer was dried over $MgSO_4$ and the filtrate collected. Solvent was then removed by rotary evaporation and dried *invacuo* to give a colorless oil (2.05 g, 82.4% yield). ^1H NMR (300 MHz, $CDCl_3$): δ 7.68 – 7.50 (m, 1H), 5.81 (s, 1H), 4.09 (qd, *J* = 7.1, 1.1 Hz, 2H), 3.63 – 3.46 (m, 2H), 2.56 (t, *J* = 6.3 Hz, 2H), 2.46 (s, 3H), 2.10 (s, *J* = 1.0 Hz, 3H), 1.19 (td, *J* = 7.1, 1.2 Hz, 3H). ^{13}C NMR (75 MHz, $CDCl_3$): δ 172.03, 151.42, 150.18, 143.46, 109.72, 60.80, 35.56, 34.38, 14.20, 13.98, 13.62. Elemental analysis calculated for $C_{11}H_{17}N_3O_3$: C, 55.22; H, 7.16; N, 17.56; O, 20.06. Found: C, 55.24; H, 7.37; N, 17.52; O, 18.31.

3.4.8 General Procedure for RAFT (Co)Polymerization of Blocked Isocyano Methacrylates.

Blocked NCO functional monomer (8.0×10^{-3} mol), or a mixture of blocked NCO monomer and co-monomer (total 8.0×10^{-3} mol), was added to a vial and dissolved in anhydrous DMSO (6.5 mL). RAFT agent (2-cyano-2-propyl 4-cyanobenzodithioate, CPCB) (2.6×10^{-5} mol), initiator (V-70) (5.2×10^{-6} mol), and *p*-xylene (NCOP and NCOT, 100 μL, ^1H NMR internal standard) or 1,3,5-trioxane (NCOI, 70 mg, ^1H NMR internal standard) were then combined in the vial with monomer and solvent. The final volume was adjusted by adding anhydrous DMSO to achieve a final solution volume of 8 mL ($[M]_0$= 1 M). V-70 was added under the above polymerization conditions as a solution in anhydrous THF (1.6 mg/100 μL) and CPCB was added as a solution in anhydrous DMSO (6.5 mg/100 μL). The polymerization solution was capped with a rubber septum and purged with N_2 for 30 minutes. Polymerizations were conducted at either 25 ºC or 30 ºC. An initial aliquot (200 μL) was taken after purging, but prior to placing the vial in a preheated oil bath. After placing the reaction vessel in the oil bath,

aliquots for kinetic measurements were taken at timed intervals. Each aliquot was exposed to oxygen and quenched in liquid N_2. After warming to room temperature, a portion of each aliquot (50 μL) was analyzed by ^{1}H NMR (DMSO-d_6) to determine monomer conversion and the remaining portion (150 μL, 1.5 x 10^{-4} mol blocked NCO) was modified immediately with 1-propanethiol (2 mmol) and 10 mol% DBU (2 x 10^{-4} mol) for analysis by SEC-MALLS. pNCOP was analyzed by SEC-MALLS without prior modification. pNCOP was purified by precipitation in 10-fold excess diethyl ether-ethyl acetate (9:1) (2x) and finally in diethyl ether (1x). Unmodified pNCOT and pNCOI were not isolated. The modification of blocked NCOT and NCOI polymers with thiols and their subsequent purification is described in detail in a later section.

3.4.9 Model Reaction Kinetics of Thiol-Modification of Blocked Isocyanates.

For a typical thiol modification model reaction, model blocked NCO (2 mmol) was dissolved in DMSO-d_6 (1 mL, $[mNCO]_0$= 0.2 M) and a thiol (0.2 mmol) was added. The solution was transferred to an NMR tube for ^{1}H NMR analysis. An initial ^{1}H NMR spectrum was obtained of the thiol plus model blocked NCO and then the catalyst (DBU or TEA) (0.01, 0.05, 0.1, or 0.3 equiv) was added. Subsequent ^{1}H NMR experiments were collected at timed intervals to determine conversion of blocked NCO to thiocarbamate by comparing the relative integral areas of the alpha hydrogens of the ethyl ester (4.04 ppm, 2H) to the beta hydrogens (2.60 ppm, 2H) of the nitrogen in the NCO functional group. For model reactions at elevated temperatures, the NMR tube was placed in an oil bath at 50 ºC in between ^{1}H NMR collection at timed intervals or heated to 50 ºC during scan collection in the NMR instrument as described in the characterization section. In the case of model reactions with amines, an initial ^{1}H NMR

experiment was collected for the model blocked NCO in DMSO-d_6 and an amine was added to the NMR tube (2.2 mmol). Additional ^{1}H NMR experiments were collected at timed intervals to determine the conversion of blocked NCO to a new carbamide by comparing the same relative integrals areas described above.

3.4.10 General Procedure for Post-Polymerization Modification of Blocked NCO Polymers with Thiols.

3.4.10.1 Procedure for Rooms Temperature Modification of 1,2,4-Triazole and Imidazole Blocked NCO Polymers

Synthesis of polymers for post-polymerization modification was conducted according to the general RAFT procedure provided and stopped after 5 h by exposing to oxygen and quenching with liquid N_2. After quenching, polymers were allowed to warm to room temperature and modified as a crude polymerization solution. In a model modification reaction with a thiol, the crude polymerization solution (8 mmol) was added dropwise to a solution of thiol (80 mmol) and DBU (0.8 mmol) and stirred for 12-18 h at room temperature. Thiol-modified polymers were isolated by precipitation first into a 9:1 (v:v) mixture of methanol and water (9:1) from DMSO and then into diethyl ether (2x) from THF. In an exemplary modification reaction with an amine, the crude polymerization solution (4 mmol) was added dropwise to a vial containing an amine (40 mmol) and stirred for 12-18 h at room temperature. Amine-modified polymers were precipitated in 10-fold excess diethyl ether-ethyl acetate (9:1) (2x) and diethyl ether (1x). Polymers were redissolved in methanol in between precipitations.

3.4.10.2 Procedure for Modification of 3,5-Dimethyl Pyrazole Blocked NCO Homopolymers at 50°C.

Synthesis of polymers for post-polymerization modification of pNCOP were conducted according to the general RAFT procedure provided in the experimental section and stopped after 5 h. NCOP homopolymers were isolated prior to modification as described previously. In a model reaction with a thiol, purified pNCOP (1 mmol of blocked NCO) was dissolved in anhydrous DMSO (2 mL) and added to a solution of thiol (10 mmol) and DBU (1 mmol). In the case of modification with an amine, pNCOP in DMSO was added dropwise to a vial containing the amine (10 mmol). The reaction flask was then placed in a pre-heated oil bath set at 50 ºC and stirred for 48 h. The modified polymer was isolated by precipitation into a 10-fold excess diethyl ether-ethyl acetate (9:1) (2x) and finally in diethyl ether (1x). Polymers were redissolved in THF in between precipitations.

3.4.10.3 Procedure for Sequential Thiol-Modification of Blocked NCO Copolymers.

Copolymerizations of NCOT and NCOP were conducted according to the general RAFT procedure provided and stopped after 5 h. In a typical sequential blocked NCO modification, the NCOT units of the copolymer were modified first by adding the crude polymerization solution (8 mmol (NCOP + NCOT)) dropwise to a solution of amine (X) (80 mmol). The reaction was stirred at room temperature for 12 h. The amine modified copolymer with unreacted NCOP units was isolated by precipitation first in diethyl ether-ethyl acetate (9:1) (2x) and then diethyl ether (1x). For modification of the second blocked NCO unit, p(NCOT-X- *r*-NCOP) (0.75 mmol of NCOP) was dissolved in anhydrous DMSO (1.5 mL) and added to a solution of thiol (Y) (7.5 mmol) and DBU

(0.75 mmol). The modification reaction was then stirred at 50 ºC for 24 h and the resulting polymer, p(NCOT-X-*co*-NCOP-Y), was isolated by precipitation into a 10-fold excess diethyl ether-ethyl acetate (9:1) (2x) and finally in diethyl ether (1x).

This chapter and the related appendix were adapted with permission from Hoff, E. A.; Abel, B. A.; Tretbar, C. A.; McCormick, C. L.; Patton, D. L. RAFT Polymerization of "Splitters" and "Cryptos": Exploiting Azole-N-carboxamides As Blocked Isocyanates for Ambient Temperature Postpolymerization Modification. *Macromolecules* **2016,** 49, (2), 554-563. Copyright (2016) American Chemical Society.

3.5 References

1. Gauthier, M. A.; Gibson, M. I.; Klok, H. A. *Angew. Chem. Int. Ed.* **2009,** 48, (1), 48-58.

2. Boaen, N. K.; Hillmyer, M. A. *Chem. Soc. Rev.* **2005,** 34, (3), 267-275.

3. Mansfeld, U.; Pietsch, C.; Hoogenboom, R.; Becer, C. R.; Schubert, U. S. *Polym. Chem.* **2010,** 1, (10), 1560-1598.

4. Arnold, R. M.; Patton, D. L.; Popik, V. V.; Locklin, J. *Acc. Chem. Res.* **2014,** 47, (10), 2999-3008.

5. Arnold, R. M.; Huddleston, N. E.; Locklin, J. *J. Mater. Chem.* **2012,** 22, (37), 19357-19365.

6. Sumerlin, B. S.; Vogt, A. P. *Macromolecules* **2010,** 43, (1), 1-13.

7. Lutz, J.-F.; Schlaad, H. *Polymer* **2008,** 49, (4), 817-824.

8. Hartmuth, C.; Finn, M.; Sharpless, B. *Angew. Chem. Int. Ed.* **2001,** 40, (11), 2004-2021.

9. Iha, R. K.; Wooley, K. L.; Nyström, A. M.; Burke, D. J.; Kade, M. J.; Hawker, C. J. *Chem. Rev.* **2009,** 109, (11), 5620-5686.

10. Kakuchi, R.; Theato, P. *Polym. Chem.* **2014,** 5, (7), 2320-2325.

11. Moldenhauer, F.; Theato, P., Sequential Reactions for Post-polymerization Modifications. In *Multi-Component and Sequential Reactions in Polymer Synthesis*, Theato, P., Ed. Springer-Verlag: Berlin, 2015; Vol. 269, pp 133-162.

12. Malkoch, M.; Thibault, R. J.; Drockenmuller, E.; Messerschmidt, M.; Voit, B.; Russell, T. P.; Hawker, C. J. *J. Am. Chem. Soc.* **2005,** 127, (42), 14942-14949.

13. Saunders, J. H.; Slocombe, R. J. *Chem. Rev.* **1948,** 43, (2), 203-218.

14. Król, P. *Prog. Mater. Sci.* **2007,** 52, (6), 915-1015.

15. Hensarling, R. M.; Hoff, E. A.; LeBlanc, A. P.; Guo, W.; Rahane, S. B.; Patton, D. L. *J. Polym. Sci. A Polym. Chem.* **2013,** 51, (5), 1079-1090.

16. Hensarling, R. M.; Rahane, S. B.; LeBlanc, A. P.; Sparks, B. J.; White, E. M.; Locklin, J.; Patton, D. L. *Polym. Chem.* **2011,** 2, (1), 88-90.

17. Rahane, S. B.; Hensarling, R. M.; Sparks, B. J.; Stafford, C. M.; Patton, D. L. *J. Mater. Chem.* **2012,** 22, (3), 932-943.

18. Li, H.; Yu, B.; Matsushima, H.; Hoyle, C. E.; Lowe, A. B. *Macromolecules* **2009,** 42, (17), 6537-6542.

19. Gody, G.; Rossner, C.; Moraes, J.; Vana, P.; Maschmeyer, T.; Perrier, S. *J. Am. Chem. Soc.* **2012,** 134, (30), 12596-12603.

20. Beck, J. B.; Killops, K. L.; Kang, T.; Sivanandan, K.; Bayles, A.; Mackay, M. E.; Wooley, K. L.; Hawker, C. J. *Macromolecules* **2009,** 42, (15), 5629-5635.

21. Flores, J. D.; Shin, J.; Hoyle, C. E.; McCormick, C. L. *Polym. Chem.* **2010,** 1, (2), 213-220.

22. Flores, J. D.; Treat, N. J.; York, A. W.; McCormick, C. L. *Polym. Chem.* **2011,** 2, (9), 1976-1985.

23. Ying, H.; Zhang, Y.; Cheng, J. *Nat. Commun.* **2014,** 5.

24. Ying, H.; Cheng, J. *J. Am. Chem. Soc.* **2014,** 136, (49), 16974-16977.

25. Petersen, S. *Ann. Chem. Liebigs* **1949,** 562, 205.

26. Wicks Jr, Z. W. *Prog. Org. Coat.* **1975,** 3, (1), 73-99.

27. Delebecq, E.; Pascault, J.-P.; Boutevin, B.; Ganachaud, F. *Chem. Rev.* **2013,** 113, (1), 80-118.

28. Wicks, D. A.; Wicks Jr, Z. W. *Prog. Org. Coat.* **1999,** 36, (3), 148-172.

29. Wicks, D. A.; Wicks Jr, Z. W. *Prog. Org. Coat.* **2001,** 41, (1–3), 1-83.

30. Viganò, M.; Suriano, R.; Levi, M.; Turri, S.; Chiari, M.; Damin, F. *Surface Science* **2007,** 601, (5), 1365-1370.

31. Viganò, M.; Levi, M.; Turri, S.; Chiari, M.; Damin, F. *Polymer* **2007,** 48, (14), 4055-4062.

32. Asri, L. A. T. W.; Crismaru, M.; Roest, S.; Chen, Y.; Ivashenko, O.; Rudolf, P.; Tiller, J. C.; van der Mei, H. C.; Loontjens, T. J. A.; Busscher, H. J. *Adv. Func. Mater.* **2014,** 24, (3), 346-355.

33. Bode, S.; Enke, M.; Gorls, H.; Hoeppener, S.; Weberskirch, R.; Hager, M. D.; Schubert, U. S. *Polym. Chem.* **2014,** 5, (7), 2574-2582.

34. Barruet, J.; Molle, R.; Babinot, J.; Penelle, J. *Polymer* **2009,** 50, (11), 2335-2340.

35. Staab, H. A. *Liebigs Ann. Chem.* **1957,** 609, (1), 83-88.

36. Staab, H. A. *Liebigs Ann. Chem.* **1957,** 609, (1), 75-83.

37. Staab, H. A. *Angew. Chem. Int. Ed.* **1962,** 1, (7), 351-367.

38. Staab, H. A.; Bauer, H.; Schneider, K. M., Reactivity of Azolides. In *Azolides in Organic Synthesis and Biochemistry*, Wiley-VCH Verlag: 2003; pp 1-12.

39. Duspara, P. A.; Islam, M. S.; Lough, A. J.; Batey, R. A. *J. Org. Chem.* **2012,** 77, (22), 10362-10368.

40. Batey, R. A.; Yoshina-Ishii, C.; Taylor, S. D.; Santhakumar, V. *Tetrahedron Lett.* **1999,** 40, (14), 2669-2672.

41. Batey, R. A.; Santhakumar, V.; Yoshina-Ishii, C.; Taylor, S. D. *Tetrahedron Lett.* **1998,** 39, (35), 6267-6270.

42. Li, G.-Z.; Randev, R. K.; Soeriyadi, A. H.; Rees, G.; Boyer, C.; Tong, Z.; Davis, T. P.; Becer, C. R.; Haddleton, D. M. *Polym. Chem.* **2010,** 1, (8), 1196-1204.

43. Muhlebach, A. *J. Polym. Sci. A Polym. Chem.* **1994,** 32, (4), 753-765.

44. Nasar, A. S.; Subramani, S.; Radhakrishnan, G. *Polym. Int.* **1999,** 48, (7), 614-620.

45. Chan, J. W.; Hoyle, C. E.; Lowe, A. B.; Bowman, M. *Macromolecules* **2010,** 43, (15), 6381-6388.

46. Baidya, M.; Mayr, H. *Chem. Commun.* **2008**, (15), 1792-1794.

47. Polenz, I.; Laue, A.; Uhrin, T.; Ruffer, T.; Lang, H.; Schmidt, F. G.; Spange, S. *Polym. Chem.* **2014,** 5, (23), 6678-6686.

48. Larrivée-Aboussafy, C.; Jones, B. P.; Price, K. E.; Hardink, M. A.; McLaughlin, R. W.; Lillie, B. M.; Hawkins, J. M.; Vaidyanathan, R. *Org. Lett.* **2010,** 12, (2), 324-327.

49. Staab, H. A.; Bauer, H.; Schneider, K. M., Syntheses of Amides and Analogous Compounds with CONR Functions (Part 1). In *Azolides in Organic Synthesis and Biochemistry*, Wiley-VCH Verlag: 2003; pp 129-186.

50. Benaglia, M.; Rizzardo, E.; Alberti, A.; Guerra, M. *Macromolecules* **2005,** 38, (8), 3129-3140.

51. McLeary, J. B.; Calitz, F. M.; McKenzie, J. M.; Tonge, M. P.; Sanderson, R. D.; Klumperman, B. *Macromolecules* **2004,** 37, (7), 2383-2394.

52. McLeary, J. B.; McKenzie, J. M.; Tonge, M. P.; Sanderson, R. D.; Klumperman, B. *Chem. Commun.* **2004**, (17), 1950-1951.

53. Convertine, A. J.; Lokitz, B. S.; Lowe, A. B.; Scales, C. W.; Myrick, L. J.; McCormick, C. L. *Macromol. Rapid. Commun.* **2005,** 26, (10), 791-795.

54. Luo, J.; Li, M.; Xin, M.; Sun, W. *Macromol. Chem. Phys.* **2015,** 216, (15), 1646-1652.

55. Thomas, D. B.; Convertine, A. J.; Hester, R. D.; Lowe, A. B.; McCormick, C. L. *Macromolecules* **2004,** 37, (5), 1735-1741.

56. Schwetlick, K.; Noack, R. *J. Chem. Soc., Perkin Trans. 2* **1995**, (2), 395-402.

CHAPTER IV – LOW pH AQUEOUS RAFT: CONTROLLED POLYMERIZATION OF ACYL HYYDRAZIDES METHACRLAMIDES AND 4-VINYLIMIDAZOLE

4.1 Introduction

Acyl hydrazides are potent dynamic covalent functional groups and efforts have recently increased to precisely install these functional groups in polymer scaffolds for applications such as bioconjugation/controlled release,[1-5] supramolecular and coordination motifs,[6] dynamic nanoparticles,[7] and stimuli-responsive actuation[8] and network formation[9-11]. Acyl hydrazides form pH-responsive, reversible hydrazone bonds with active carbonyl moieties (Scheme 4.1a) that a host of useful reactions are based upon.[6] This class of dynamic covalent chemistry offers attractive features such as stability combined with rapid bond formation/cleavage, a high degree of tunability in substrate (i.e. parent hydrazide and aldehyde/ketone), and the ability to undergo transimination reactions.[12-14] Acyl hydrazides have been installed in polymer scaffolds via uncontrolled free radical polymerization of hydrazide functional monomers[1, 2] and dispersion polymerization of methacryloyl hydrazide to form microgels[4]. Kumar et al. used post-polymerization modification (PPM) to synthesize poly(acryloyl hydrazide) and generated hydrogels, crosslinked networks, and probe and dye labeled polymers via modification of the hydrazide groups.[11] In recent work, Convertine and cowokers employed reversible addition-fragmentation chain transfer (RAFT) polymerization to synthesize controlled brushed-brush polymers that included a protected acyl hydrazide comonomer for subsequent release of the therapeutic, doxorubicin.[5] These examples highlight the utility of acyl hydrazide-functionalized polymer scaffolds, but lack precision (i.e. uncontrolled free radical polymerizations) or simplicity (i.e. require

protecting groups or multistep PPM). Synthesizing acyl hydrazide-containing polymers would benefit greatly from direct, controlled polymerization to impart precision monomer placement and control over polymer architecture.

Reversible addition-fragmentation chain transfer (RAFT) polymerization has made possible the synthesis of advanced functional polymers owing to a powerful combination of functional group tolerance and control over polymer architecture (i.e. molecular weight, dispersity, topology, side-chain and chain-end identity).[15-18] A variety of functional vinyl monomers have been readily polymerized under aqueous, organic, or heterogenous RAFT conditions including those with nucleophilic functional groups such as primary amines.[19] Despite the versatility of RAFT polymerization, acyl hydrazides have not been successfully polymerized without the use of protecting groups due to the nucleophilic nature of these functional groups that also exhibit uniquely low pK_a values ($pk_a < 4$)[20]. This deficiency precludes not only the controlled polymerization of acyl hydrazides, but also valuable functional monomers with atypical amine architectures such as 4-vinylimidazole (4VIM), which has a pK_a value < 7 and is of interest for biological and ionic liquid applications.[21, 22] Aqueous RAFT (aRAFT) polymerization has overcome issues associated with controlled polymerization of reactive nucleophiles incompatible with organic RAFT polymerizations by the use of mildly acidic aqueous polymerization media. In acidic media, nucleophiles are protonated and inactive toward side reactions with the chain transfer agent (CTA) responsible for polymerization control.

Many reports, starting with the controlled polymerization of acrylamide in water, have demonstrated that using an acetate buffer at pH = 5 is ideal for aRAFT polymerization of a variety of amide- or amine-containing monomers.[23] N-(3-

aminopropyl)methacrylamide, for example, contains a primary amine with a pK_a value of ~ 9 and is polymerized readily with excellent control under typical aRAFT conditions.[24] For monomers with functional groups with pK_a values < 7, however, aqueous media with pH values < 5 are necessary to protonate the nucleophilic sites (i.e. amine or hydrazide). Previous attempts to achieve controlled polymerization of 4VIM in organic or aqueous (acetate buffer with pH = 5) RAFT polymerizations were met with limited success due to aminolysis of CTA by the imidazole ring in an unprotonated state.[25] Inspiration for a strategy to overcome issues with aRAFT polymerization of low pK_a monomers, such as acyl hydrazides and 4VIM, was derived from work by Allen et al.[25] in which they synthesized 4VIM polymers via RAFT polymerization in glacial acetic acid. Controlled polymerization of 4VIM in glacial acetic was achieved because the acidity of the media was sufficiently low to protonate the imidazole rings and eliminate CTA aminolysis. While this is the only strategy employed thus far to address the controlled polymerization of low pK_a monomers, it is not sufficient to protonate monomers with pK_a values as low as acyl hydrazides and cannot be applied over a range of low pH values in aqueous media. Lowering the pH of aRAFT polymerizations offers a versatile solution to achieving controlled polymerization of monomers with low pKa.

Adjusting the pH of aRAFT polymerization solvents requires consideration of CTA stability at low pH. Thomas and McCormick have shown that decreasing the pH of the aRAFT polymerization media prevents CTA hydrolysis and aminolysis.[26] Investigations of CTA stability at values as low as pH=2 showed no observable hydrolysis provided the CTA is soluble.[26, 27] Common CTAs for aRAFT polymerizations that rely on carboxylic acid groups to dissolve in water, exhibit poor solubility at low pH

values. However, CTAs with an R-group possessing a charged functional group at low pH promote water solubility.[27] An example of a charged R-group used in this work is shown in Scheme 4.1b. Beyond stability and solubility at low pH, CTA selection can also be further tailored by class (i.e. dithiobenzoate or trithiocarbonate). Trithiocarbonates are known to have high fragmentation rates that lead to increased polymerization conversions and improved hydrolytic stability in most cases when compared to dithiobenzoates.[28, 29] Despite evidence suggesting CTA compatibility few examples exist of RAFT polymerizations performed at pH values in the low pH range. Developing routes to low pH RAFT polymerization will allow for the controlled polymerization of nucleophilic monomers with low pK_a values directly without the need for protecting groups.

In this work, we aim to directly polymerize nucleophilic monomers with low pK_a values via aqueous RAFT polymerization in order to access advanced hydrazone and imidazole polymer scaffolds. In this direction, we report the low pH (< 1) aqueous RAFT polymerization of acyl hydrazide-containing monomers and 4VIM (Scheme 4.1c) possessing pK_a values below the range that can typically be polymerized by aRAFT. A CTA containing an imidazolium group to promote solubility at low pH was synthesized that imparted excellent polymerization control at pH < 1. In addition to methacryloyl hydrazide, an acyl-hydrazide containing monomer with an ethyl spacer was synthesized. The spacer proved important to maintain polymerization control. 4VIM has been successfully polymerized in glacial acidic acid in previous reports, but has now been shown to polymerize readily and in a controlled fashion in water at low pH. Additionally, conditions for size-exclusion chromatography (SEC) of the polymers

synthesized herein are investigated and hydrazones are formed from acyl hydrazide polymers. This work is the first example of the controlled polymerization of an unprotected hydrazide-containing monomer and is expected to provide a significant contribution to dynamic covalent polymer scaffolds as well as open a route for polymerization of previously intractable monomer types.

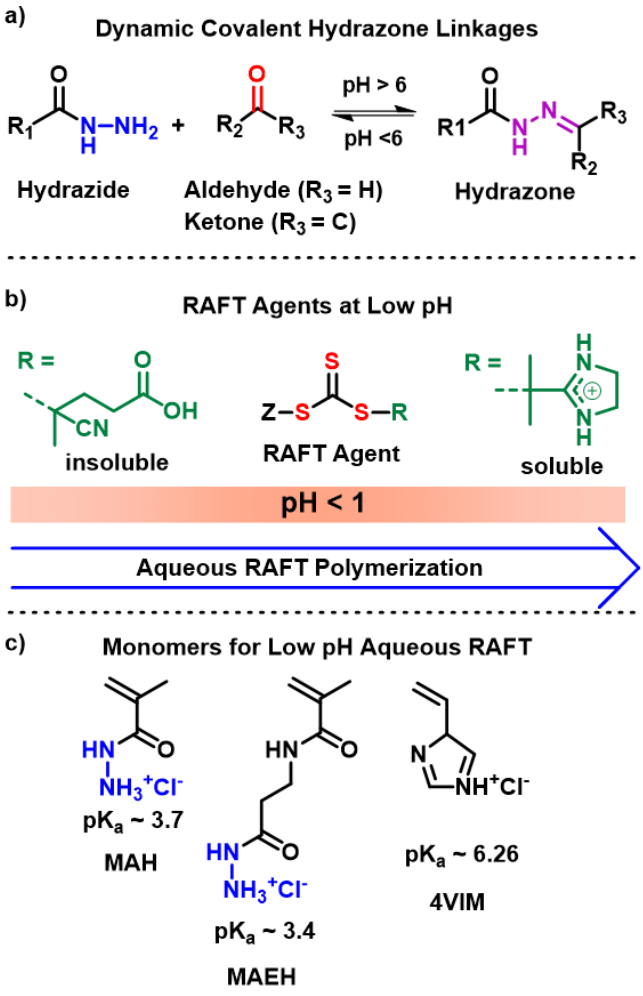

Scheme 4.1 (a) Dynamic covalent hydrazone equilibrium, (b) general chain transfer agent structure and R-groups at low pH, and (c) monomers with low pK_a values investigated for low pH RAFT polymerization.

4.2 Results and Discussion

4.2.1 Monomers and Low pH RAFT Agent: Design and Synthesis

We first synthesized methacryloyl hydrazide hydrochloride (MAH) and 4-vinylimidazole (4VIM) to begin our investigation of the low pH aqueous RAFT (aRAFT) polymerization of nucleophilic monomers with low pK_a values. The pK_a values of MAH and 4VIM were measured by potentiometric titration to be 3.70 and 6.26 respectively (Table S1). These values are substantially lower than the pK_a values for primary amine-containing monomers ($pk_a \approx 9$) that have been polymerized previously by aRAFT in pH = 5.0 acetate buffer.[15, 24] Polymerizing monomers with nucleophilic functional groups and low pK_a values, such as MAH and 4VIM, requires more acidic polymerization media to keep the nucleophile protonated to prevent CTA aminolysis. Therefore, aqueous HCl solutions were investigated as polymerization solvents in order to lower the polymerization pH and broaden the scope of low pK_a monomers that can be polymerized. Based on the Henderson-Hasselbach equation, we can hypothesize that for ~99.9% protonation of MAH during polymerization an aqueous solution with a pH < 0.7 was required as the solvent. After a pH range was selected for the proposed low pH RAFT polymerization, a suitable CTA for low pH aqueous RAFT polymerization was synthesized.

One of the barriers to low pH RAFT polymerizations is the necessity for the CTA to be soluble at low pH values (pH < 1) and stable towards hydrolysis. With this in mind, we designed the trithiocarbonate, 2-(ethylthiocarbonothioylthio) 2-(2-imidazolin-2-yl)propane hydrochloride (ImET), containing an imidazolium R-group to provide

solubility at low pH. ImET was synthesized in relatively high yields according to the route shown in Scheme 4.2.

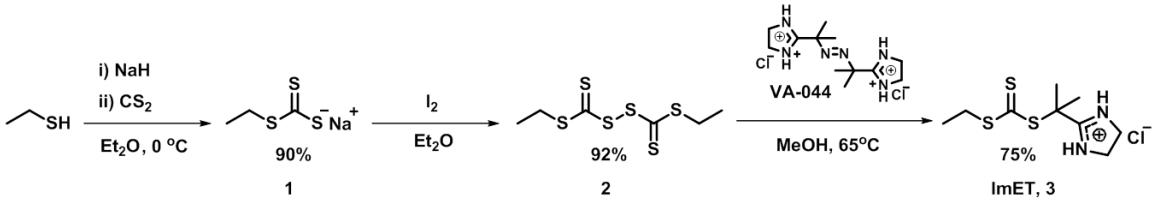

Scheme 4.2 Synthetic route for 2-(ethylthiocarbonothioylthio) 2-(2-imidazolin-2-yl)propane hydrochloride (ImET).

When compared to dithiobenzoate CTAs, trithiocarbonates exhibit slower rates of hydrolysis[30] and promote higher polymerization conversions while maintaining polymerization control[28]. Baussard and coworkers examined the stability and solubility of different CTAs over a range of pH values and showed that in water at pH = 1 or 2 CTAs with sulfonate-containing R-groups (i.e. functional groups that possess a charge at low pH) were stable while CTAs with a carboxylic acid R-group were not soluble.[27] The imidiazolium R-group for ImET was chosen, instead of another charged group like the sulfonate in the above example, based on ease of synthesis and the resemblance of the R-group to 4VIM. Synthesis of ImET was achieved with a high overall yield of 62% after recrystallization.

4.2.2 Low pH aRAFT Polymerization of Methacryloyl Hydrazide HCl (MAH)

MAH was polymerized in 1 M HCl using ImET as the CTA and the low decomposition temperature initiator VA-044 (Figure 4.1a, inset). In 1 M HCl, the pH of the polymerization solution should be zero, well below the hypothesized pH (0.7) for protonating ~99.9% the monomer and successfully controlling aRAFT polymerization of MAH. The SEC traces and dispersity data for MAH polymerization kinetics with the

above conditions and at $[M]_0$:$[CTA]_0$:$[I]_0$ = 250:1:0.25 are shown in Figure 4.1b and 4.1c, respectively.

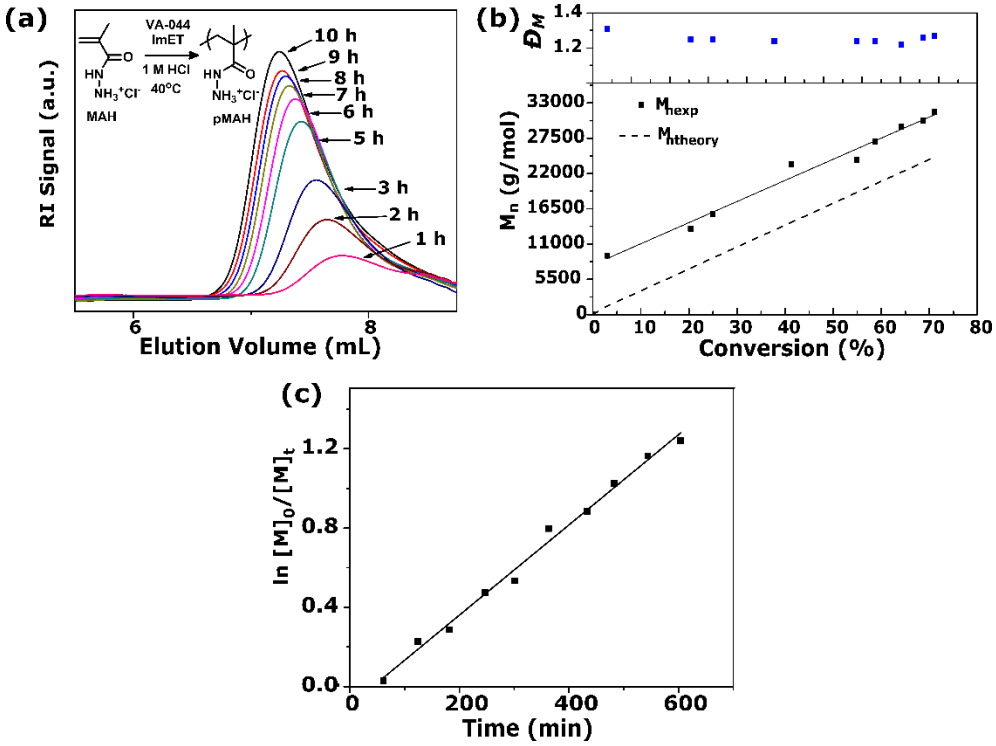

Figure 4.1 (a) SEC traces for polymerization kinetics of MAH and inset scheme of low pH aRAFT polymerization of MAH, (b) dispersities and M_n vs. conversion plot, and (c) pseudo-first order kinetic plot for aRAFT polymerization of MAH in 1 M HCl with VA-044 and ImET at 40ºC.

From Figure 4.1b and 4.1c, it is apparent that ImET-mediated aRAFT polymerization of MAH in 1 M HCl affords broad SEC traces with low molecular weight tailing (Figure 4.1a). While the high molecular weight sides of the SEC curves shift to lower elution volumes with polymerization time, the relatively large dispersities (ĐM = 1.22-1.31) in Figure 4.1b and low molecular weight tailing are indicative of significant chain-end termination occurring during the aRAFT polymerization of MAH in 1M HCl. It is also worth noting that after an initialization period of ~60 min, linear pseudo-first-order kinetic behavior is observed up to 600 min, indicating that the radical concentration

remains constant (Figure 4.1c). Furthermore, while Figure 4.1b shows a linear increase in $M_{n,exp}$ vs. monomer conversion as determined by ASEC-MALLS, the $M_{n,exp}$ values are higher than theoretically predicted based upon monomer conversion and a 250 : 1 $[M]_0$: $[CTA]_0$ ratio. A loss in yellow color was also observed after prolonged reaction times and is suggestive of trithiocarbonate degradation via hydrolysis or aminolysis during MAH polymerization in 1 M HCl – a process that would yield low MW tailing resulting from a reduced number of "living" chain ends.[26] This result was surprising since the amount of unprotonated hydrazide groups capable of aminloysis should be insignificant at pH ≈ 0. Consequently, we next sought to elucidate the exact cause of trithiocarbonate chain-end degradation during the ImET-mediated polymerization of MAH in 1M HCl.

4.2.3 Trithiocarbonate Degradation during ImET-Mediated Polymerization of MAH.

Suspecting that trithiocarbonate chain-end degradation was responsible for poor molecular weight control during the polymerization of MAH, studies were conducted using UV-Vis spectroscopy to investigate the individual and combined influences of solvent, monomer, and initiator on the occurrence and extent of ImET degradation under the conditions representative of those used for the polymerization of MAH. A systematic approach was adopted where ImET degradation was investigated in the presence of the following components: 1 M HCl, VA-044 plus 1 M HCl, MAH plus 1 M HCl, and VA-044, MAH, and 1 M HCl at 40ºC under an argon atmosphere. Fractional change in trithiocarbonate concentration $[TTC]/[TTC]_0$ vs. time for the above experiments with MAH is shown in Figure 4.2.

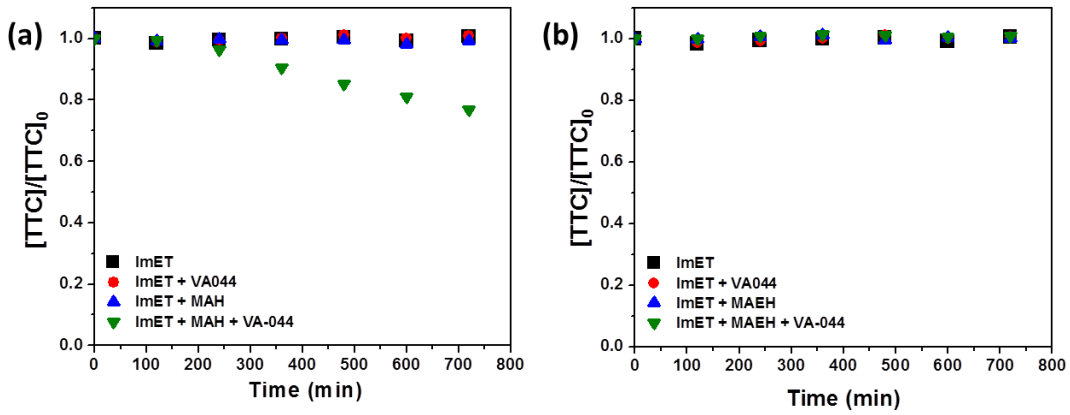

Figure 4.2 (a) Degradation kinetics of ImET in 1M HCl (black ■) and in the presence of initiator (red ●), MAH (blue ▲), and initiator plus MAH (green ▼) at $[M]_0$:$[ImET]_0$:$[VA\text{-}044]_0$ = 10:1:0.2 and 40º C under argon. (b) Degradation kinetics of ImET in 1M HCl (black ■) and in the presence of initiator (red ●), MAEH (blue ▲), and initiator plus MAEH (green ▼) at $[M]_0$:$[ImET]_0$:$[VA\text{-}044]_0$ = 10:1:0.2 and 40º C under argon.

Figure 4.2a reveals no measurable influences of 1 M HCl (black ■), VA-044 (red ●), or MAH (blue ▲) independently on the concentration of ImET at 40 °C. This result suggests that ImET is stable towards hydrolysis at low pH and that the hydrazide functional groups are indeed protonated sufficiently to avoid intermolecular aminolysis of the CTA. However, when ImET, MAH, and VA-044 were combined at 40 °C in 1M HCl such that polymerization could take place, (Figure 4.2a, green ▼), a 25% decrease in $[TTC]/[TTC]_0$ is observed after 720 min. This result confirms that trithiocarbonate chain-end degradation is responsible for the poor molecular weight control observed during the ImET-mediated polymerization of MAH in 1M HCl. The ImET degradation plots in Figure 4.2 show that trithiocarbonate degradation only occurs during the polymerization of MAH. This indicates that intramolecular attack of the trithiocarbonate by the hydrazide group of the terminal monomer unit is responsible for the observed

degradation of ImET during polymerization of MAH at 40 °C as illustrated in Scheme 4.3b. At low pH, the acid equilibrium (Scheme Xa) is shifted in favor of protonated hydrazides, however, when deprotonation of the terminal hydrazide does occur, it can adopt a favorable conformation to react with the thiocarbonyl of the CTA six atoms away with a high collision frequency (Scheme 4.3b). In fact, Abel and coworkers recently reported a similar result in the RAFT polymerization of *N*-arylmethacrylamides.[31] To combat the issue of trithiocarbonate chain-end degradation, we next synthesized MAEH, an analogue of MAH that positions the acyl hydrazide further from the methacrylamide backbone (Scheme 4.3d). As shown in Scheme 4.3c, intramolecular nucleophilic attack of the trithiocarbonate chain-end by the hydrazide group of the terminal MAEH monomer is unlikely due to the unfavorable formation of a 10-atom cyclic product.

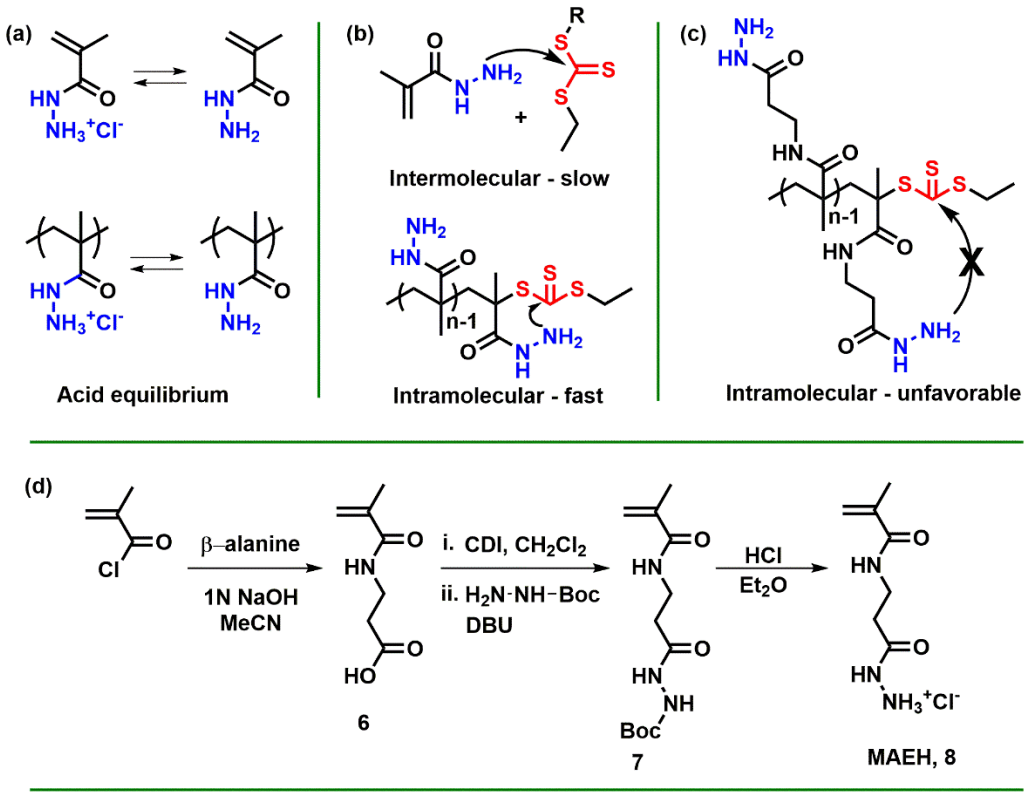

Scheme 4.3 (a) Acid equilibrium of MAH monomer and polymer, (b) proposed mechanisms for inter- and intramolecular monomer-induced trithiocarbonate chain-end degradation, (c) unfavorable intramolecular aminolysis via MAEH, and (d) synthetic route to MAEH.

The influence of MAEH on trithiocarbonate degradation was again investigated using UV-Vis spectroscopy. A plot of the $[TTC]/[TTC]_0$ vs. time for ImET at 40° C in the presence of 1 M HCl with VA-044, MAEH, and finally ImET plus MAEH and VA-044 is shown in Figure 4.2b. When MAEH is substituted as the monomer, no trithiocarbonate degradation is observed under the conditions representative of a polymerization (Figure 4.2b, green ▼) unlike the case with MAH. This result supports our hypothesis that trithiocarbonate chain-end degradation during the polymerization of MAH is due to intramolecular attack of the trithiocarbonate by the hydrazide group of the terminal monomer unit and that adding an ethyl spacer between methacrylamide and acyl

hydrazide functional groups places the terminal hydrazide group in an unfavorable position to react with CTA.

4.2.4 Low pH aRAFT Polymerization of MAEH

In contrast to aRAFT polymerization of MAH, controlled polymerization behavior was achieved in the ImET-mediated low pH aRAFT polymerization of MAEH. MAEH was polymerized at 40º C in 1 M HCl with VA-044 as the initiator (Figure Xa, inset). A $[CTA]_0:[I]_0 = 1:0.25$ was originally used for MAEH, but SEC traces were slightly narrower at $[CTA]_0:[I]_0 = 1:0.20$ and this ratio was subsequently used instead in aRAFT polymerizations of MAEH.

The SEC RI traces in Figure 4.3a are narrow, symmetrical, and shift to lower elution volumes with polymerization time without low molecular weight tailing. These results contrast with those obtained for the ImET-mediated polymerization of MAH (Figure 4.3a) indicating the absence of trithiocarbonate chain-end degradation. Dispersities, shown in Figure 4.3b, also remain low ($Đ_M < 1.08$) throughout the polymerization of MAEH demonstrating improved "living" chain-end retention. The SEC traces and dispersity data agree with the results in the previous section that suggest the CTA is stable during low pH aRAFT polymerization of MAEH. The pseudo-first-order kinetic plot in Figure 4.3c and the M_n vs. conversion plot (Figure 4.3b) are both linear as expected.

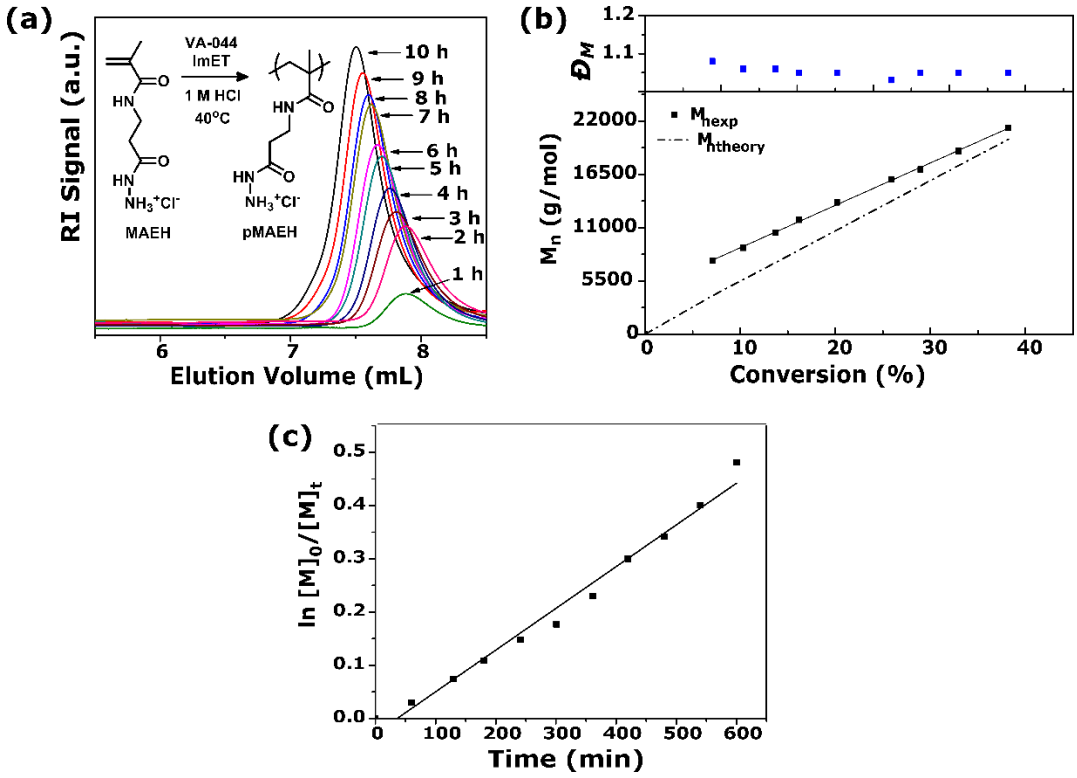

Figure 4.3 (a) SEC traces for polymerization kinetics of MAEH and inset scheme of low pH aRAFT polymerization of MAEH, (b) dispersities and M_n vs. conversion plot, and (c) pseudo-first order kinetic plot for aRAFT polymerization of MAEH in 1 M HCl with VA-044 and ImET at 40ºC.

The conversion, molecular weight, and dispersity data for aRAFT polymerization of MAH and MAEH are summarized in Table 4.1. $M_{n,exp}$ values measured for polymerization of MAEH (entry 2a-2c) are in better agreement with $M_{n,theory}$ values as compared to the greater discrepancy in $M_{n,exp}$ and $M_{n,theory}$ values obtained during the aRAFT polymerization of MAH (entry1a-1c).

Table 4.1

Conversion, molecular weight, and dispersity data for the aRAFT polymerization of MAH and MAEH in 1 M HCl at 40°C.[a]

Entry	Monomer	*t* (min)	Conv[b] (%)	$[M]_0$ (mol/L)	$M_{n,theory}$ (g/mol)	$M_{n,exp}$[c] (g/mol)	$Đ_M$[c]
1a	MAH	180	24.9	1	8800	15 700	1.25
1b	MAH	360	55.0		19 000	24 100	1.24
1c	MAH	600	71.1		24 600	31 600	1.27
2a	MAEH	180	10.3	1	5600	8900	1.06
2b	MAEH	360	20.2		10 800	13 600	1.05
2c	MAEH	600	38.2		20 100	21 300	1.05

[a] MAH and MAEH were polymerized at 40° C in 1 M HCl ($[M]_0$:$[CTA]_0$:$[I]_0$ = 250:1:0.2 for MAH or $[M]_0$:$[CTA]_0$:$[I]_0$ = 1:0.20 for MAEH) using VA-044 as the initiator. [b]Conversions were determined by ^{1}H NMR spectroscopy. [c]As determined by SEC-MALLS (0.4% (v/v) TFA and 0.1M $NaNO_3$ in water).

MAEH polymers were also chain-extended to confirm chain-end fidelity. Retention of RAFT chain-ends is important for block copolymer applications and also signifies that the CTA is not degraded during the polymerization. A MAEH macro-CTA was synthesized and chain-extended with additional MAEH monomer. The SEC traces of pMAEH before and after chain extension are shown in Figure 4.4.

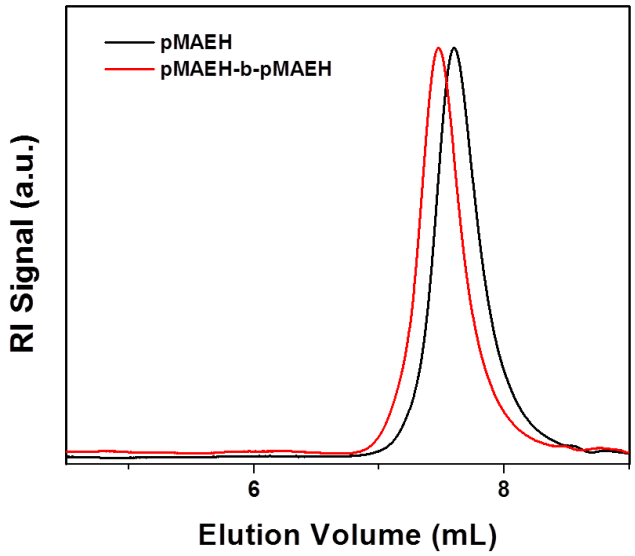

Figure 4.4 SEC traces for pMAEH before (Mn = 17,600 g/mol, $Đ_M$= 1.06) (black) and after (Mn = 22,600 g/mol, $Đ_M$ = 1.04) (red) chain extension.

The SEC trace for the macro-CTA was narrow and symmetrical with a molecular weight of 17,600 g/mol and $Đ_M$ = 1.06. After chain-extension the SEC trace shifts to a lower elution volume with a molecular weight of 22,600 g/mol and $Đ_M$ = 1.04. The SEC trace of the chain extension remains narrow with no low molecular weight tailing that points to a low amount of dead chains throughout polymerization and purification. It should be noted that purification of the macro-CTA was achieved by precipitating in isopropanol two times, redissolving in 1M HCl between precipitations, and then lyophilizing from 1M HCl. The 1M HCl prevented hydrolysis of the CTA. The controlled polymerization of MAEH by ImET-mediated, low pH aRAFT polymerization demonstrated herein is significant as is it is, to our knowledge, the first example of successful RDRP of unprotected acyl-hydrazide containing monomer and the first example of aqueous RAFT polymerization at pH ≈ 0.

4.2.5 Low pH aRAFT Polymerization of 4-Vinylimidazole.

In this section, we discuss the low pH aRAFT polymerization of 4VIM with ImET and VA-044 shown in Figure 4.5a, inset. Because 4VIM is not protonated prior to polymerization, HCl is required both to generate the hydrochloride salt of the imidazole groups and lower the pH sufficiently to maintain protonation. Two different concentrations of HCl, 1.25 M and 2 M, were investigated as the polymerization solvent. When the kinetics of the low pH aRAFT polymerization in 2 M HCl indicated excellent polymerization control (Figure B.2), 1.25 M HCl was investigated as a polymerization solvent to reduce the amount of acid required for controlled aqueous polymerization of 4VIM (Figure 4.5). Conversion, molecular weight, and dispersity data for 4VIM aRAFT polymerization kinetics in both 2 M and 1.25 M HCl at $[M]_0$:$[CTA]_0$:$[I]_0$ = 250:1:0.2 are summarized in Table 4.2.

Table 4.2

Conversion, molecular weight, and dispersity data for aRAFT polymerization of 4VIM at 40°C in 2 M and 1.25 M HCl.[a]

Entry	Solvent	*t* (min)	Conv[b] (%)	$[M]_0$ (mol/L)	$M_{n,theory}$ (g/mol)	$M_{n,exp}$[c] (g/mol)	$Đ_M$[c]
1a	2 M HCl	180	51.4	1	12 400	14 700	1.02
1b		360	72.4		17 300	21 400	1.02
1c		600	90.2		21 500	25 600	1.10
2a	1.25 M HCl	180	30.4	1	7400	10 500	1.04
2b		360	58.8		14 100	16 700	1.07
2c		600	75.2		18 000	19 800	1.09

[a]4VIM monomers were polymerized at 40° C in 1.25 or 2 M HCl ($[M]_0$:$[CTA]_0$:$[I]_0$ = 250:1:0.2) using VA-044 as the initiator. [b]Conversions were determined by ^{1}H NMR spectroscopy. [c]As determined by SEC-MALLS (0.2% (v/v) TFA and 0.2 M NaCl in water).

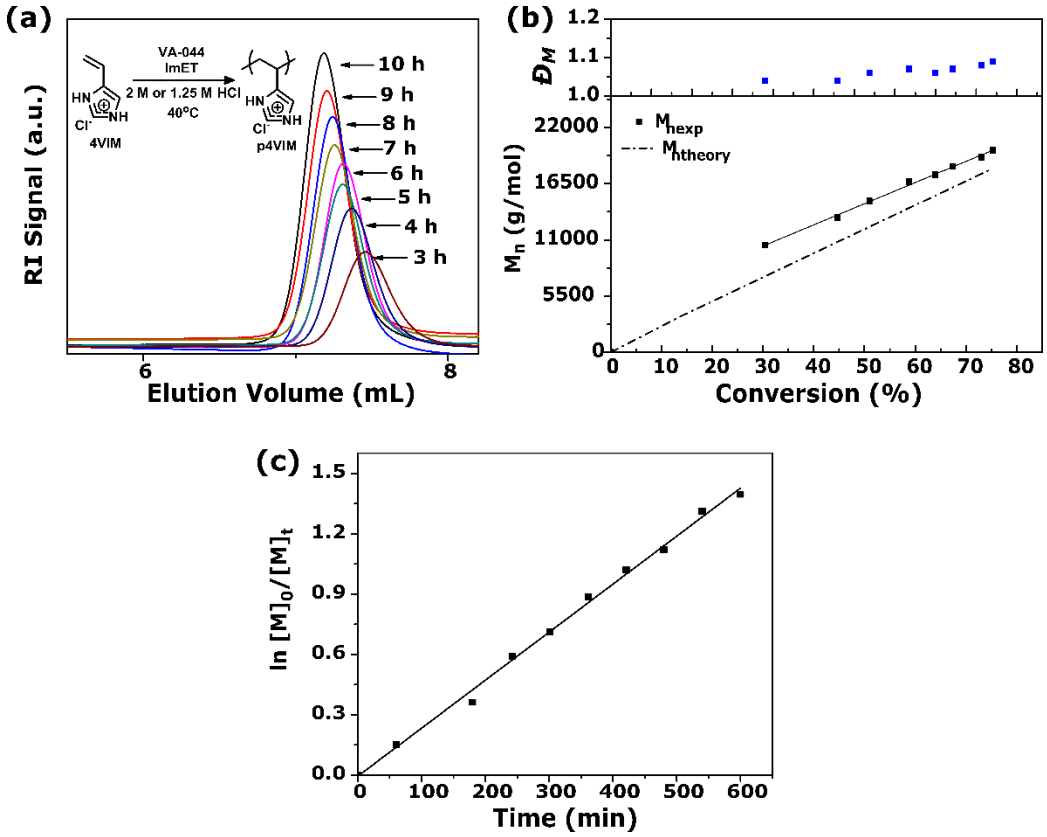

Figure 4.5 (a) SEC traces for polymerization kinetics of 4VIM and inset scheme of low pH aRAFT polymerization of 4VIM, (b) dispersities and M_n vs. conversion plot, and (c) pseudo-first order kinetic plot for aRAFT polymerization of 4VIM in 1.25 M HCl with VA-044 and ImET at 40°C.

A linear M_n vs. conversion plot and pseudo-first-order kinetic plot were obtained for the aRAFT polymerizations of 4VIM in 1.25 M HCl as shown in Figure 4.5b and 4.5c, respectively. Polymerization of 4VIM in 2 M HCl (Table 2, entry 1a-1c) affords polymers of low dispersities ($Đ_M$ < 1.03) for the majority of the polymerization and only reaches $Đ_M$ = 1.1 at 90% conversion. The increased $Đ_M$ at high (90%) conversion is likely due to a substantial decrease in the rate of propagation relative to the rate of termination (Table 4.2, entry 1c). While the polymerization of 4VIM in 1.25 M HCl reaches lower conversions than in 2 M HCl, polymerizations under both conditions obtain reasonable molecular weights determined by SEC-MALLS that agree well with

the theoretical molecular weights calculated based upon conversion. Shown in Table 4.2, entry 2a-2c, polymerization of 4VIM in 1.25 M HCl also maintains low dispersities ($Đ_M$ < 1.09) throughout the polymerization. Figure 4.5a shows the SEC chromatogram overlays for the ImET-mediated polymerization of 4VIM in 1.25 M HCl. The symmetrical peak shapes that shift to lower elution volumes as the polymerization time increases without low molecular weight tailing are indicative of high thiocarbonylthio chain-end retention. It is also worth noting that the terminal monomer unit in growing p4VIM chains has the potential, as with MAH, to react intramolecularly with the CTA to cause aminolysis due to a favorable orientation of the ultimate heterocyclic 4VIM nitrogen relative to the thiocarbonyl of the CTA. However, the linear M_n vs. conversion plots, low dispersities, and narrow and symmetric SEC chromatograms indicate that there is no significant CTA degradation due to intramolecular aminolysis.

Additional evidence of high "living" chain-end retention was provided by chain-extending a p4VIM macro-CTA using low pH aRAFT conditions (Figure 4.6). A p4VIM macro-CTA was chain-extended to demonstrate high polymer chain-end fidelity when using low pH aRAFT polymerization and its applicability towards block copolymer formation. The SEC traces for the parent polymer and chain-extended polymer are shown in Figure 4.6.

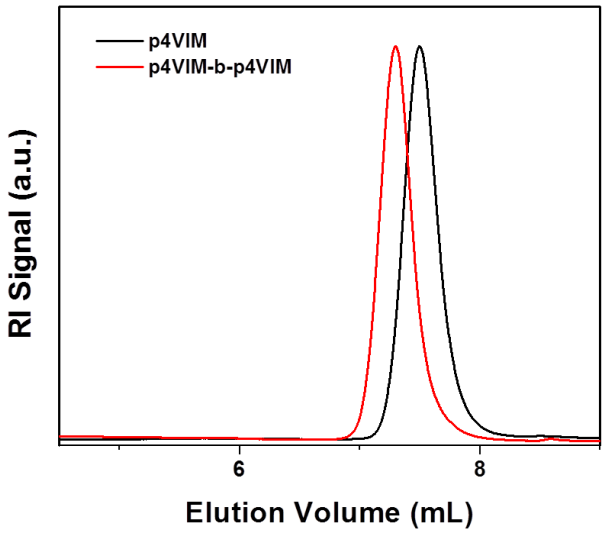

Figure 4.6 SEC traces for poly(4-vinlimidazole) before (M_n = 12,000 g/mol, $Đ_M$ = 1.09) (black) and after (M_n = 22,300 g/mol, $Đ_M$ = 1.09) (red) chain extension.

The SEC trace of the chain extended p4VIM macro-CTA is narrow, symmetric, and shifts from a molecular weight of 12,000 g/mol and $Đ_M$ = 1.09 to a lower elution volume with a molecular weight of 22,300 g/mol and $Đ_M$ = 1.09. The lack of low molecular weight tailing in the chain-extended SEC trace indicates that the ImET chain-ends were retained throughout the polymerization of both blocks. In this work, the well-controlled RAFT polymerization of 4-vinylimidazole has been demonstrated in aqueous media at low pH in the presence of a CTA designed for highly acidic environments.

4.3 Conclusions

In summary, the first example of controlled radical polymerization of monomers containing unprotected acyl hydrazide pendent groups was demonstrated using aqueous RAFT polymerization under acidic conditions. This approach eliminates the need for multistep protection/deprotection and postpolymerization procedures to access well-defined acyl hydrazide- and 4-vinylimidazole-functionalized polymer scaffolds. A new

imidazolium-based trithiocarbonate CTA was synthesized that exhibited excellent solubility and stability under acidic conditions and facilitated controlled polymerizations of MAH, MAEH, and 4VIM. The low pK_a of the monomers required a pH ≈ 0 (1 M HCl) polymerization medium to sufficiently protonate the hydrazide and imidazole groups and avoid degradation of the CTA. The incorporation of an ethyl spacer between the backbone and the acyl hydrazide in MAEH proved important to avoid intramolecular aminolysis of the trithiocarbonyl end-group by the terminal monomer unit. High chain-end fidelity was demonstrated via chain extension experiments, highlighting the ability to access block copolymer architectures. aRAFT at pH 0 not only enables the facile synthesis of well-defined hydrazide polymer scaffolds, but also provides a vantage point to expand aRAFT polymerization to a broader library of monomers containing low pK_a functional groups.

4.4 Experimental

4.4.1 Materials

Methacryloyl chloride (Aldrich, 97%) was distilled under vacuum and stored under N_2 prior to use. VA-044 (Wako) was recrystallized from MeOH and stored at -10 °C. Dichloromethane (Fisher, ≥ 99.5%) was dried over $CaCl_2$ and distilled prior to use in reactions. Ethanethiol (Aldich, 97%), hydrochloric acid solution (1 N and 2 N, Fisher), aminopropionic acid (Aldrich, 99%), *tert*-butyl carbazate (Aldrich, 98%), 1,1'-carbonyldiimidazole (Aldrich, ≥ 90%), 1,8-diazabicyclo[5.4.0]undec-7-ene (DBU) (Acros, 98%), 4-imidazoleacrylic acid (Aldrich, 99%), carbon disulfide (Aldrich, ≥ 99.9%), sodium hydride (Aldrich, 95%), anhydrous THF (inhibitor free, Aldrich, ≥ 99.9%), iodine (Aldrich, 99.8%), potassium iodide (Aldrich, ≥ 99%), anhydrous

methanol (Aldrich, 99.8%), triethylamine (Aldrich, ≥ 99.5%), and hydrogen chloride solution (2 M in diethyl ether, Aldrich) were used as received.

4.4.2 Characterization

NMR studies were conducted using a Varian INOVA 300 MHz NMR spectrometer. Polymer molecular weights and dispersities ($Đ_M$) were determined by aqueous size-exclusion chromatography (ASEC) with an eluent of 0.4% (v/v) trifluoroacetic acid and 0.1 M $NaNO_3$ (aq) (for analysis of pMAH and pMAEH polymers) or 0.2% (v/v) trifluoroacetic acid and 0.2 M NaCl (aq) (for analysis of p4VIM polymers) at a flow rate of 0.25 mL/min, Eprogen Inc. CATSEC columns (100, 300, and 1000 Å) connected in series with a Wyatt Optilab DSP interferometric refractometer (λ = 690 nm) and Wyatt DAWN EOS multiangle laser light scattering (MALLS) detector (λ = 633 nm). Absolute molecular weights and $Đ_M$ were calculated using a Wyatt ASTRA SEC/LS software package. d*n*/d*c* values were determined offline utilizing a Wyatt Optilab DSP interferometric refractometer (λ = 690 nm) at 25 °C and Wyatt ASTRA d*n*/d*c* software.

4.4.3 Synthesis of Sodium Ethyl Trithiocarbonate

A suspension of NaH (2.11 g, 83.5 mmol) in anhydrous diethyl ether (150 mL) was cooled to 0 °C using an ice bath, upon which ethanethiol (5.73 g, 92.3 mmol) was added over 15 min accompanied by vigorous evolution of hydrogen gas. The reaction was stirred for an additional 15 min at 0 °C followed by dropwise addition of CS_2 (7.03g, 92.3 mmol) over 5 min and the reaction stirred for an additional 60 min at room temperature. The reaction was diluted with pentane (100 mL) and the yellow precipitate isolated by vacuum filtration before drying *invacuo* yielding **1** (12.07 g, 90%) as a

hygroscopic yellow powder. ^{1}H NMR (300 MHz, D_2O) δ 3.16 (q, *J* = 7.4 Hz, 2H), 1.27 (t, *J* = 7.4 Hz, 3H).

4.4.4 Synthesis of Bis(ethylsulfanylthiocarbonyl) Disulfide.

Solid I_2 (8.63g, 34.0 mmol) was added to a suspension of sodium ethyl trithiocarbonate (9.89g, 61.7 mmol) in diethyl ether (200 mL) at room temperature over 5 min. The reaction was stirred for 60 min at room temperature and the precipitated NaI salts removed by vacuum filtration and washed with 50 mL diethyl ether. The filtrate was transferred to a separatory funnel and washed with 5% $Na_2S_2O_4$ (2 x 150 mL), H_2O (1 x 150 mL), and brine (1 x 150 mL) before drying over $MgSO_4$. The solvent was removed via rotary evaporation followed by drying *in-vacuo* to yield **2** (8.13 g, 96%) as a yellow oil. ^{1}H NMR (300 MHz, $CDCl_3$) δ 3.30 (q, *J* = 7.4 Hz, 4H), 1.35 (t, *J* = 7.4 Hz, 6H).

4.4.5 Synthesis of 2-(Ethylthiocarbonothioylthio) 2-(2-Imidazolin-2yl)propane Hydrochloride (ImET).

Bis(ethylsulfanylthiocarbonyl) disulfide (3.00 g, 11.0 mmol) and VA-044 (5.30 g, 16.3 mmol) were combined in anhydrous MeOH (250 mL) and heated at 65 °C for 18 h. The reaction was quenched by cooling to room temperature and exposing to air followed by removal of the solvent via rotary evaporation. CH_2Cl_2 (75 mL) was added to the crude solid, inducing precipitation of residual VA-044, which was then removed via vacuum filtration. The filtrate was isolated and the solvent removed by rotary evaporation and the crude product dissolved in acetonitrile (35-40 °C) followed by recrystallization at 0 °C to give **3** (ImET) (4.65 g, 75%) as orange needle-like crystals. ^{1}H NMR (300 MHz, D2O) δ 3.38 (s, 1H), 2.77 (q, *J* = 7.3 Hz, 1H), 1.25 (s, 6H), 0.75 (t, *J*

= 7.3 Hz, 3H). ^{13}C NMR (75 MHz, D_2O) δ 221.09, 173.63, 49.18, 44.78, 31.73, 24.94, 12.21.

4.4.6 Synthesis of *tert*-Butyl Methacryloylhydrazinecarboxylate.

tert-Butyl carbazate (8.72g, 66.0 mmol) and triethylamine (6.68g, 66.0 mmol) were dissolved in CH_2Cl_2 (100 mL) and cooled to 0 ºC in an ice bath. Methacryloyl chloride (6.27g, 60.0 mmol) was added to the solution dropwise over 15 min and the reaction was allowed to warm to room temperature. The reaction was stirred for 2 h under N_2 and then washed with 0.5 M HCl in 50% brine (3 x 100 mL), saturated $NaHCO_3$ (1 x 100 mL), and brine (1 x 100 mL). The organic layer was dried over Na_2SO_4 before the solvent was removed via rotary evaporation to yield **4** (9.04g, 75%) as a white crystalline solid. ^{1}H NMR (300 MHz, CDCl3) δ 8.69 (s, 1H), 7.08 (s, 1H), 5.80 (s, 1H), 5.34 (s, 1H), 1.90 (s, 3H), 1.39 (s, 9H). ^{13}C NMR (75 MHz, $CDCl_3$) δ 167.96, 156.06, 137.48, 121.61, 81.57, 28.11, 18.39.

4.4.7 Synthesis of Methacryloyl Hydrazide Hydrochloride (MAH)

tert-Butyl 2-methacryloylhydrazinecarboxylate (7.97g, 39.8 mmol) was dissolved in anhydrous THF (10 mL) under a N_2 atmosphere. To this solution, 2M HCl in diethyl ether (200 mL, 0.4 mol HCl) was transferred via cannula and stirred at room temperature for 24 h. The precipitate was isolated by vacuum filtration, rinsed with diethyl ether, and dried *invacuo* to give **5** (4.31g, 79%) as a white solid. ^{1}H NMR (300 MHz, D_2O) δ 5.79 (s, 1H), 5.59 (s, 1H), 1.88 (s, 3H). ^{13}C NMR (75 MHz, D_2O) δ 169.33, 135.49, 124.16, 16.96.

4.4.8 Synthesis of Carboxyethyl Methacrylamide.

Methacryloyl chloride (9.39 g, 90 mmol) in acetonitrile (30 mL) was added dropwise over 30 min to a solution of β-alanine (8.00 g, 90 mmol) and BHT (100 mg, inhibitor) in 1 N NaOH (180 mL) and acetonitrile (80 mL) at 0 °C. The reaction was then stirred for 60 min at room temperature upon which NaCl (25 g) was added to the reaction mixture followed removal of acetonitrile by rotary evaporation. The aqueous solution was then cooled using an ice bath and the solution acidified to pH = 2 using 12 N HCl. The acidified solution was transferred to a separatory funnel and extracted with EtOAc (4 x 100 mL) followed by washing the combined EtOAc extracts with brine (1 x 200 mL). The organic layer was isolated, dried over Na_2SO_4, and the solvent removed by rotary evaporation to yield **6** (11.94 g, 85%) as a colorless solid. ^{1}H NMR (300 MHz, $CDCl_3$) δ 10.42 (s, 1H), 6.81 (s, 1H), 5.67 (s, 1H), 5.29 (s, 1H), 3.53 (q, *J* = 3.5 Hz, 2H), 2.56 (t, *J* = 5.1 Hz, 2H), 1.87 (s, 3H). ^{13}C NMR (75 MHz, $CDCl_3$) δ 176.27, 169.12, 139.08, 120.81, 35.14, 33.55, 18.43.

4.4.9 Synthesis of *tert*-Butyl 2-(3-Methacrylamidopropanoyl)Hydrazinecarboxylate.

A solution of carboxyethyl methacrylamide (11.73 g, 75 mmol) and BHT (100 mg, inhibitor) in anhydrous CH_2Cl_2 (300 mL) was added via cannula over 15 min to a suspension of 1,1'-carbonyldiimidazole (12.10 g, 75 mmol) in anhydrous CH_2Cl_2 (250 mL) and the resulting homogenous solution stirred at room temperature for an additional 90 min. *tert*-Butyl carbazate (10.85 g, 82 mmol) was then added as a solid followed by DBU (0.52 mL, 3.5 mmol) and the reaction stirred at room temperature for 4 h. The reaction mixture was then filtered of any solids and the filtrate transferred to a separatory funnel and washed with a 4:1 (v:v) mixture of brine and 4 M HCl (2 x 200 mL), brine (1

x 200 mL), and dried over Na_2SO_4 before removing the solvent via rotary evaporation to yield **7** (17.03g, 84%) as a colorless solid. ^{1}H NMR (300 MHz, $CDCl_3$) δ 8.34 (s, 1H), 6.92 (s, 1H), 6.70 (d, *J* = 2.3 Hz, 1H), 5.75 (s, 1H), 5.30 (s, 1H), 3.67 – 3.54 (m, 2H), 2.47 (t, *J* = 5.8 Hz, 2H), 1.92 (s, 3H), 1.44 (s, 9H). ^{13}C NMR (75 MHz, $CDCl_3$) δ 172.12, 168.79, 155.63, 139.30, 120.40, 81.62, 35.87, 33.56, 28.10, 18.46.

4.4.10 Synthesis of (2-Methacrylamidoethyl) Carbohydrazide Hydrochloride (MAEH).

A suspension of *tert*-butyl 2-(3-methacrylamidopropanoyl)hydrazinecarboxylate (10.00 g, 37 mmol) in anhydrous diethyl ether (150 mL) was cooled to 0 °C followed by the addition 2.0 M HCl in diethyl ether (130 mL, 260 mmol) via cannula over 30 min. The reaction was stirred overnight (18 h) at room temperature upon which the precipitated product was briefly isolated by vacuum filtration. The hygroscopic white solid was then triturated with a 1:1 (v:v) mixture of anhydrous diethyl ether and cyclohexane (3 x 50 mL) followed by trituration with cyclohexane (1 x 50 mL) and dried overnight *in-vacuo* to yield **8** (7.65 g, 82%) as a hygroscopic solid that was stored under nitrogen at -10 °C. ^{1}H NMR (300 MHz, D_2O) δ 5.62 (s, 1H), 5.39 (s, 1H), 3.50 (t, *J* = 6.3 Hz, 2H), 2.54 (t, *J* = 6.3 Hz, 2H), 1.85 (s, 3H). ^{13}C NMR (75 MHz, D_2O) δ 171.83, 171.73, 138.72, 121.14, 35.23, 32.78, 17.48.

4.4.11 Synthesis of 4-Vinylimidazole (4VIM).

4-Vinylimidazole was synthesized according to a modified literature procedure.[25] Anhydrous urocanic acid (4.99 g, 36.1 mmol) was heated to 230-240 °C under vacuum in a short path distillation apparatus. Upon melting, the urocanic acid decomposed and 4-vinylimidazole distilled as a colorless, viscous oil that readily crystallized at room

temperature. The off-white solid sublimed at 60 °C under vacuum yielding **12** (1.90 g, 56%) as a colorless crystalline solid. ^{1}H NMR (300 MHz, $CDCl_3$) δ 13.23 (s, 1H), 7.67 (s, 1H), 7.08 (s, 1H), 6.66 (dd, *J* = 17.6, 11.1 Hz, 1H), 5.70 (d, *J* = 17.6 Hz, 1H), 5.14 (d, *J* = 11.2 Hz, 1H). ^{13}C NMR (75 MHz, $CDCl_3$) δ 135.88, 135.59, 126.63, 120.05, 112.13.

4.4.12 Monomer Titrations.

Monomer stock solutions of MAH or MAEH (1 mM) were first prepared by weighing each monomer (0.1 mmol) into separate 100 mL volumetric flasks, followed by the addition of 2.00 mL of 0.05 N HCl (0.1 mmol) to each flask. 4VIM stock solutions were prepared by weighing monomer (0.1 mmol) into a 100 mL volumentric flask, followed by the addition of 4.00 mL of 0.05 N HCl (0.2 mmol). Once the monomers were completely dissolved, DI H_2O (18.2 MΩ) was added to each volumetric flask to achieve a final volume of 100 mL. Twenty-five mL of each stock solution was transferred to a 100 mL beaker containing a stir bar and titrated against 0.05 N NaOH in volume increments of 5 μL at 25 °C using a Metrohm 848 Titrino Plus autotitrator. All titrations were performed in triplicate. Monomer pK_a values were determined using eq 1, where $pH_{EP1/2}$ is the pH corresponding to the half equivalence point ($EP_{1/2}$) of the titration curve. The volume of NaOH titrant required to reach $EP_{1/2}$ ($Vol_{EP1/2}$) was determined by eq 2, where Vol_{EP} is the volume of NaOH titrant required to reach the equivalence of the titration curve, [monomer] is the concentration of monomer being titrated, [NaOH] is the concentration of titrant used, and Vol_{sol} is the initial volume of the monomer solution being titrated. Figure B.1 of the supporting information shows the positions of EP and $EP_{1/2}$ on the titration curve obtained for MAEH.

$$pK_a = pH_{EP_{1/2}} \quad (1)$$

$$Vol_{EP_{1/2}} = Vol_{EP} - \frac{1}{2}\frac{[monomer]}{[NaOH]}Vol_{sol} \quad (2)$$

4.4.13 Trithiocarbonate Degradation Analysis by UV-Vis.

Reactions (final volume = 2500 μL) were performed using $[ImET]_0 = 5 \times 10^{-3}$ M and $[M]_0$:$[ImET]_0$:$[VA\text{-}044]_0$ = 10:1:0.2 in 1 N HCl. A typical procedure was as follows: MAEH (250 μL of an 103.8 mg/mL stock solution in 1 N HCl, 10 equiv), ImET (250 μL of a 14.2 mg/mL stock soln. in 1 N HCl, 1 equiv), VA-044 (25 μL of a 32.3 mg/mL stock solution in 1 N HCl, 0.2 equiv), and 1 N HCl (1975 μL) were combined in a 4 mL test tube equipped with magnetic stir bar and rubber septum. The reaction was then degassed via three freeze-pump-thaw cycles and backfilled with argon. An initial aliquot (50 μL) was taken using an argon-purged gastight syringe and subsequently diluted into a quartz cuvette containing 2500 μL of DI water (18.2 M) before measuring the absorbance at λ = 315 nm using a Lambda 35 UV-vis spectrometer. Subsequent aliquots (50 μL) were taken and analyzed in the same manner.

4.4.14 General Procedure for aRAFT Polymerization of Acyl Hydrazide-Containing Monomers and 4-Vinylimidazole.

An acyl hydrazide-containing monomer or 4VIM (4.8×10^{-3} mol) was added to a vial containing a magnetic stir bar and dissolved in a solution of RAFT agent, 2-(ethylthiocarbonothioylthio) 2-(2-imidazolin-2-yl)propane hydrochloride (ImET) (1.93×10^{-5} mol), in 1.0 M HCl (MAH, MAEH) or 2.0 M HCl (4VIM). Initiator (VA-044) (4.8×10^{-6} mol) and benzene sulfonic acid (70 mg, ^{1}H NMR internal standard) were then combined in the vial with monomer and RAFT agent and 1.0 M HCl was added to achieve a final solution volume of 4.8 mL ($[M]_0$= 1 M). The vial containing

polymerization solution was then capped with a rubber septum and purged with argon for 40 min. before placing the reaction vessel in an oil bath preheated to 40 ºC. To monitor polymerization kinetics, an initial aliquot (200 μL) was taken after degassing, but prior to placing reaction vessel in an oil bath. After initiating the polymerization, additional aliquots for kinetic measurements were taken at timed intervals. Aliquots were analyzed by ^{1}H NMR (D_2O) to determine monomer conversion and SEC-MALLS to determine molecular weights and dispersities. Polymers derived from monomers MAH, MAEH, or 4VIM are denoted pMAH, pMAEH, or p4VIM, respectively, and were purified via precipitation in 10-fold excess isopropanol and followed by lyophilization from 1.0 M HCl.

Portions of this chapter and the related appendix were adapted from Hoff, E.; Abel, B.; Tretbar, C.; McCormick, C.; Patton, D. Aqueous RAFT at pH zero: Enabling controlled polymerization of unprotected acyl hydrazide methacrylamides. *Polymer* Chemistry, **2016**, DOI: 10.1039/c6py01563h with permission from the Royal Society of Chemistry.

4.5 References

1. Iwasaki, Y.; Maie, H.; Akiyoshi, K. *Biomacromolecules* **2007,** 8, (10), 3162-3168.

2. Etrych, T.; Mrkvan, T.; Chytil, P.; Koňák, Č.; Říhová, B.; Ulbrich, K. *Journal of Applied Polymer Science* **2008,** 109, (5), 3050-3061.

3. Binauld, S.; Stenzel, M. H. *Chemical Communications* **2013,** 49, (21), 2082-2102.

4. Ballard, N.; Bon, S. A. F. *Polymer Chemistry* **2014,** 5, (23), 6789-6796.

5. Lane, D. D.; Chiu, D. Y.; Su, F. Y.; Srinivasan, S.; Kern, H. B.; Press, O. W.; Stayton, P. S.; Convertine, A. J. *Polymer Chemistry* **2015,** 6, (8), 1286-1299.

6. Su, X.; Aprahamian, I. *Chemical Society Reviews* **2014,** 43, (6), 1963-1981.

7. Murray, B. S.; Fulton, D. A. *Macromolecules* **2011,** 44, (18), 7242-7252.

8. von Delius, M.; Geertsema, E. M.; Leigh, D. A.; Tang, D.-T. D. *Journal of the American Chemical Society* **2010,** 132, (45), 16134-16145.

9. Vetrík, M.; Přádný, M.; Hrubý, M.; Michálek, J. *Polymer Degradation and Stability* **2011,** 96, (5), 756-759.

10. Deng, G.; Li, F.; Yu, H.; Liu, F.; Liu, C.; Sun, W.; Jiang, H.; Chen, Y. *ACS Macro Letters* **2012,** 1, (2), 275-279.

11. Kumar, A.; Ujjwal, R. R.; Mittal, A.; Bansal, A.; Ojha, U. *ACS Applied Materials & Interfaces* **2014,** 6, (3), 1855-1865.

12. Kool, E. T.; Park, D.-H.; Crisalli, P. *Journal of the American Chemical Society* **2013,** 135, (47), 17663-17666.

13. Dirksen, A.; Dirksen, S.; Hackeng, T. M.; Dawson, P. E. *Journal of the American Chemical Society* **2006,** 128, (49), 15602-15603.

14. Wojtecki, R. J.; Meador, M. A.; Rowan, S. J. *Nat Mater* **2011,** 10, (1), 14-27.

15. McCormick, C. L.; Lowe, A. B. *Accounts of Chemical Research* **2004,** 37, (5), 312-325.

16. Hill, M. R.; Carmean, R. N.; Sumerlin, B. S. *Macromolecules* **2015,** 48, (16), 5459-5469.

17. Moad, G.; Chong, Y. K.; Postma, A.; Rizzardo, E.; Thang, S. H. *Polymer* **2005,** 46, (19), 8458-8468.

18. Lowe, A. B.; McCormick, C. L. *Progress in Polymer Science* **2007,** 32, (3), 283-351.

19. York, A. W.; Kirkland, S. E.; McCormick, C. L. *Advanced Drug Delivery Reviews* **2008,** 60, (9), 1018-1036.

20. Lindegren, C. R.; Niemann, C. *Journal of the American Chemical Society* **1949,** 71, (4), 1504-1504.

21. Kirby, A. H. M.; Neuberger, A. *Biochemical Journal* **1938,** 32, (7), 1146-1151.

22. Anderson, E. B.; Long, T. E. *Polymer* **2010,** 51, (12), 2447-2454.

23. Thomas, D. B.; Sumerlin, B. S.; Lowe, A. B.; McCormick, C. L. *Macromolecules* **2003,** 36, (5), 1436-1439.

24. Li, Y.; Lokitz, B. S.; McCormick, C. L. *Angewandte Chemie* **2006,** 118, (35), 5924-5927.

25. Allen, M. H.; Hemp, S. T.; Smith, A. E.; Long, T. E. *Macromolecules* **2012,** 45, (9), 3669-3676.

26. Thomas, D. B.; Convertine, A. J.; Hester, R. D.; Lowe, A. B.; McCormick, C. L. *Macromolecules* **2004,** 37, (5), 1735-1741.

27. Baussard, J.-F.; Habib-Jiwan, J.-L.; Laschewsky, A.; Mertoglu, M.; Storsberg, J. *Polymer* **2004,** 45, (11), 3615-3626.

28. Mayadunne, R. T. A.; Rizzardo, E.; Chiefari, J.; Krstina, J.; Moad, G.; Postma, A.; Thang, S. H. *Macromolecules* **2000,** 33, (2), 243-245.

29. Thomas, D. B.; Convertine, A. J.; Myrick, L. J.; Scales, C. W.; Smith, A. E.; Lowe, A. B.; Vasilieva, Y. A.; Ayres, N.; McCormick, C. L. *Macromolecules* **2004,** 37, (24), 8941-8950.

30. Ferguson, C. J.; Hughes, R. J.; Nguyen, D.; Pham, B. T. T.; Gilbert, R. G.; Serelis, A. K.; Such, C. H.; Hawkett, B. S. *Macromolecules* **2005,** 38, (6), 2191-2204.

31. Abel, B. A.; McCormick, C. L. *Macromolecules* **2016,** 49, (2), 465-474.

CHAPTER V – REVERSIBLE AND EXCHANGEABLE SURFACE MODIFICATION VIA HYDRAZONE-FUNCTIONAL POLYMER BRUSH SURFACES

5.1 Introduction

The development of precisely engineered surfaces is necessary to achieve highly controlled surface properties (e.g. wettability, adhesion, optics, lubrication, etc.). Surface-initiated polymerization (SIP), in particular, has received much attention as a very effective and versatile means to tether polymers bearing specific functionality to surfaces in order to impart specific surface properties.[1-5] Polymer brush surfaces are characterized by covalently attached polymer chains with high grafting densities that lead to an extended brush conformation and functional homogeneity throughout the ultrathin film. These features provide significant advantages as compared to self-assembled monolayers (SAMs) which lack the robustness and functional complexity of polymer brush surfaces.

The SIP technique is more powerful, however, when combined with reversible-deactivation radical polymerization methods, such as surface-initiated atom transfer radical polymerization (SI-ATRP)[2, 5], and post-polymerization modification (PPM) processes.[6] The controlled radical process endows SIP with precise control over brush thickness by decreasing the dispersity of polymer chain lengths, whereas PPM greatly increases the range of functionalities that can be installed on a surface.[7, 8] PPM is based on the direct polymerization of monomers bearing chemoselective handles that are inert towards polymer conditions, but can be quantitatively converted to a broad range of functional groups in a subsequent step.[9] Our group, among others, has developed facile, efficient, and versatile surface platforms via PPM. For example, we have synthesized

polymers brushes with pendant thiols[10], alkynes[11], and isocyanates[12] for PPM by thiol-click reactions, allowing functionalization through a wide variety of reactions. These examples demonstrate the ability of different functional groups to control surface properties; however, the idea of reversible PPM, and subsequently reversible/dynamic surface properties or functions is increasingly desirable in order to fabricate smart surfaces that can undergo dynamic changes. Dynamic surface modifications utilize reversible covalent linkages to elicit specified responses or material behaviors via strategies such as attaching polymer brushes to surfaces via Diels-Alder linkages,[13] side chain modification via alkoxyamine bonds,[14] dual responsive phenylboronic acid polymer brush surfaces for cell capture,[15] and cleavage of dynamic covalent copolymers to generate porous thin films.[16]

Hydrazones are reversible bonds established through a thermodynamic equilibrium by reaction of a hydrazide and aldehyde/ketone and can be converted back to starting materials under acidic conditions. Among available dynamic covalent bonds, hydrazone linkages comprise one of the most versatile set of linkages considering their ability to react with a variety of aldehydes and ketones, stability at neutral pH, rapid bond formation/cleavage, and photoswitchable configurational isomerism.[17-19] Judicious choice of hydrazide and aldehyde or ketone can be used to tune the reaction rate, and aniline has been broadly employed as a catalyst for hydrazone formation and transimination reactions.[17, 20] Furthermore, hydrazone bond formation can occur in the presence of water despite generating water as a byproduct on the product side of the equilibrium.[17] These features have led to the use of hydrazones in applications such as self-healing materials,[21] photoswitches,[19] bioconjugation and coordination motifs,[22-25] and

actuation strategies.[26] Additionally, hydrazones have been employed for surface modification as monolayers[22, 27] and as pendant groups on nanoparticles or polymeric vesicles.[28, 29] These examples illustrate the ability of hydrazones to provide modular surfaces for advanced purposes such as cell capture and functionalization with biologically relevant molecules. However, the monolayer approach would benefit from the application of SIP, in particular SI-ATRP, to provide a means to better control architecture, domain size, and functionality for the design of dynamic surfaces. To the best of our knowledge, there are no examples of polymer brush surfaces containing pendant hydrazides for hydrazone formation and exchange.

Herein, we report the synthesis of 2-hydroxyethyl methacrylate brush surfaces via SI-ATRP and subsequent PPM to yield hydrazide-functional brush surfaces with controlled architectures. Hydrazone formation and exchange reactions were explored with these surfaces to facilitate reversible control of surface properties. Hydrazone bonds were formed by the reaction with aliphatic and aryl aldehydes with both electron-donating and -withdrawing character in a variety of solvents. Dynamic exchange of aldehydes participating in hydrazone linkages was also demonstrated for a variety of aldehydes. The ability of the hydrazone exchange reactions to occur over multiple cycles was investigated and resulted in switchable hydrophobicity/hydrophilicity of hydrazide-functional substrates. Trifluoroacetic acid (TFA) was used to affect hydrazone reversal and exchange reactions in both aqueous and organic solvents and aniline was used as a catalyst. Temperature was shown to influence hydrazone bond reversal. This work provides access to versatile, dynamic polymer brush surfaces and is expected to lead to

advances in applications where stimuli-responsive capture/release or surface switchability is desired.

5.2 Results and Discussion

5.2.1 Synthesis of Dynamic Covalent Brush Surfaces

In order to investigate dynamic covalent hydrazone surfaces, hydrazide-functional polymer brushes were first synthesized through the combination of SI-ATRP and PPM (Scheme 5.1). It should be noted that schemes showing polymer brushes for simplicity only depict one side-chain as a representative for each unit in the polymer chain.

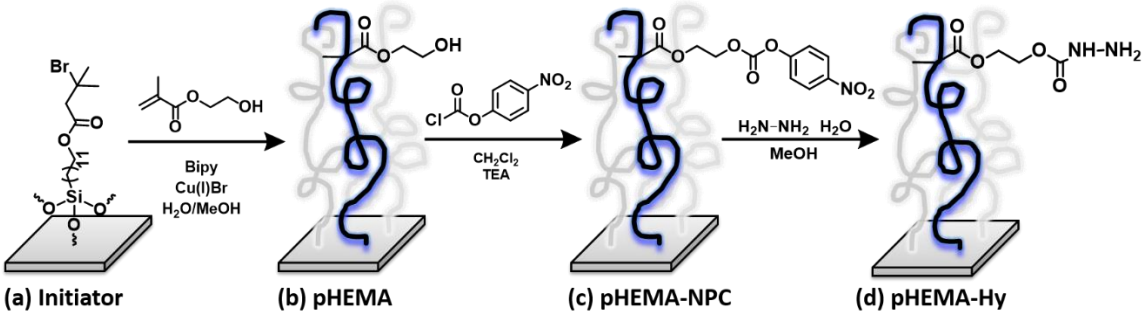

Scheme 5.1 Synthesis of hydrazide-functional polymer brush surfaces.

2-Hydroxyethyl methacrylate (HEMA) brushes (Scheme5.1b) were grown on silicon substrates (SS) and quartz substrates (QS) via SI-ATRP from an α-bromoisobutyryl bromide-based initiator (Scheme 5.1a). The hydroxyl containing side chains were then modified to form activated carbonate linkages by reaction with 4-nitrophenyl chloroformate (Scheme 5.1c). Hydrazine hydrate was used to replace the nitrophenyl leaving group at the activated carbonate, resulting in brushes with hydrazide containing side chains (denoted pHEMA-hy) (Scheme 5.1d). Synthesis and modification of pHEMA brushes on silicon substrates were monitored with gATR-FTIR spectroscopy, to confirm the presence of new chemical groups, and ellipsometry, to determine changes

in thickness as a result of brush modification. The gATR-FTIR spectrum in Figure 5.1a indicates the presence of HEMA brushes after SI-ATRP by the band at 3400 cm^{-1} corresponding to the hydroxyl group on HEMA side chains and the band at 1727 cm^{-1} corresponding to the carbonyl of the methacrylate. Modification of the HEMA brushes with 4-nitrophenyl chloroformate (Figure 5.1b) was confirmed by the disappearance of the band at 3400 cm^{-1} and appearance of three bands at 1770, 1527 and 1350 cm^{-1}. Upon substitution with hydrazine hydrate (Figure 5.1c), the bands at 1770, 1527 and 1350 cm^{-1} disappeared and a new band representative of the hydrazide moiety was found at 3346 cm^{-1}. Brush thicknesses change accordingly with each reaction step and are provided in Figure 5.1. The result of SI-ATRP of HEMA and subsequent simple, two-step modification was ultra-thin films with functional groups capable of forming dynamic covalent hydrazone linkages for reversible control of surfaces.

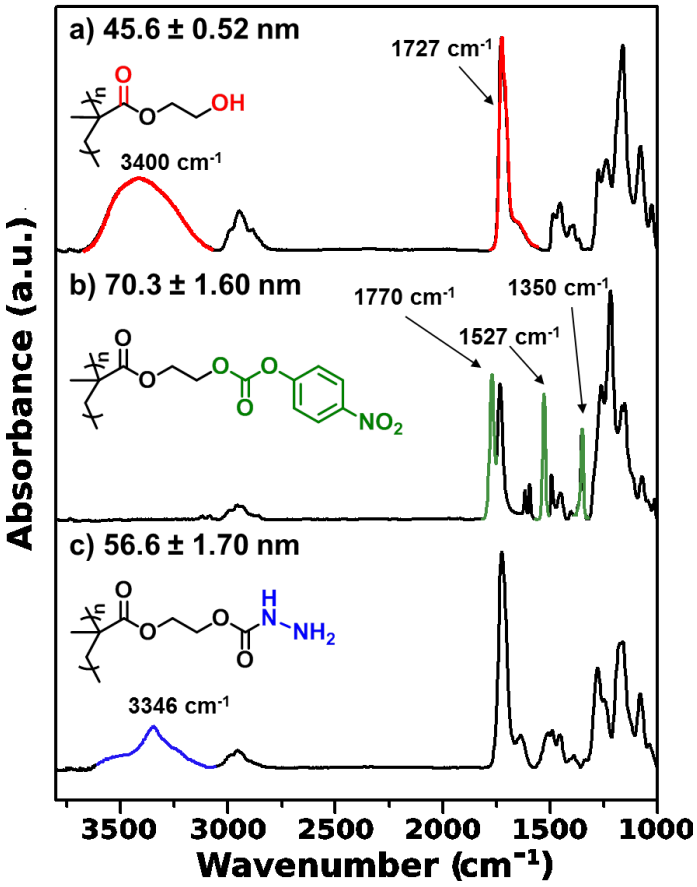

Figure 5.1 gATR-FTIR spectroscopy of (a) HEMA brushes on silicon substrates grown by SI-ATRP, (b) pHEMA brushes after modification with 4-nitrophenyl chloroformate (pHEMA-NPC), and (c) pHEMA-NPC brushes after modification with hydrazine hydrate (pHEMA-Hy).

5.2.2 Hydrazone Formation on Brush Surfaces

After successfully synthesizing hydrazide functional brushes, formation and cleavage reactions of pH-responsive hydrazone linkages were investigated. General hydrazone formation on brush surfaces is shown in Scheme 5.2 as well as selected aldehydes used for formation reactions and exchange reactions, discussed further in the following section. Aldehydes were selected rather than ketones for investigating hydrazone reactions due to their greater reactivity towards hydrazides and subsequent generation of more stable hydrazone linkages.[17]

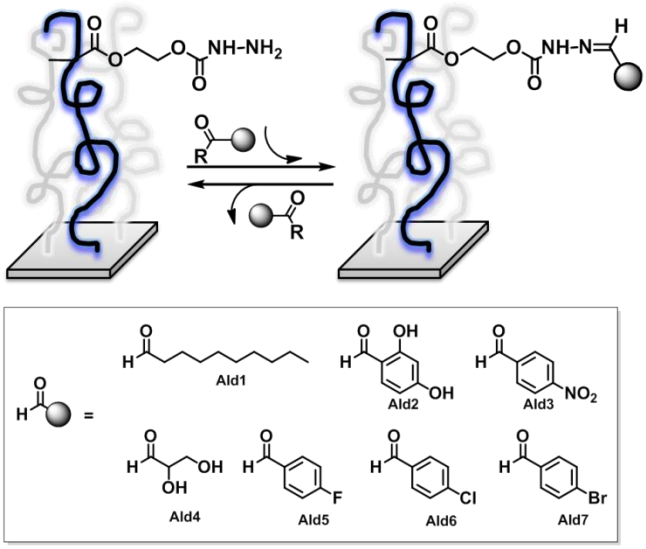

Scheme 5.2 Route to hydrazone formation with various aldehydes.

Hydrazone formation reactions were carried out by placing a silicon substrate with HEMA-hydrazide brushes in a test tube containing methanol or THF (depending on the solubility of the aldehyde modifier) and aldehyde modifier (0.1 M). gATR-FTIR spectroscopy was used to determine the presence of new hydrazone bonds after modification with aldehydes denoted Ald1-Ald5 (Figure 5.2). IR bands representative of each aldehyde modifier are labeled in Figure 5.2 to highlight the success of each formation reaction. Changes in brush thickness with hydrazone formation were also monitored and are summarized in Table 5.1. Both IR and thickness measurements are indicative of successful hydrazone formations with aliphatic and aryl aldehyde modifiers.

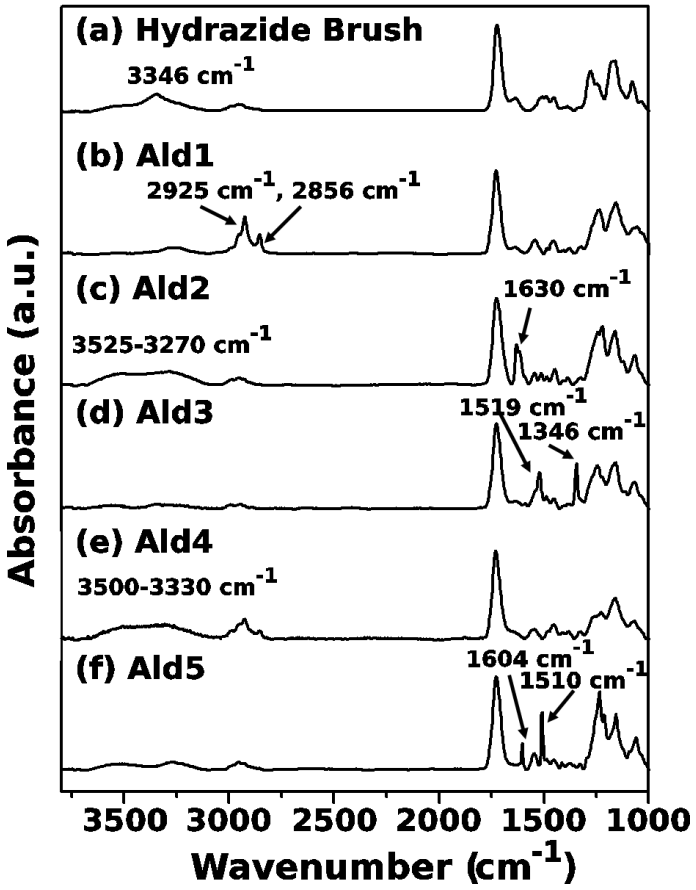

Figure 5.2 gATR-FTIR spectra of a (a) hydrazide-brush surface and hydrazone formation after reaction with (b) Ald1, (c) Ald2, (d) Ald3, (e) Ald4, and (f) Ald5.

Table 5.1

Thickness measurements of hydrazide functional brush surfaces before and after hydrazone formation with Ald1-Ald5.

Modifier	Thickness (before) (nm)	Thickness (after) (nm)
Ald1	53.34 ± 2.64	82.70 ± 3.34
Ald2	50.89 ± 1.07	70.93 ± 1.51
Ald3	75.25 ± 1.30	101.67 ± 1.65
Ald4	26.49 ± 0.35	30.27 ± 0.43
Ald5	26.49 ± 0.35	34.31 ± 0.58

As an example of the reversibility of hydrazone brush surfaces back to original hydrazide functional groups, a hydrazone brush surface modified with decanal was treated with TFA (1 M) in a mixture of THF and methanol (5:1, v:v) to achieve an acidic environment and trigger reversal of the hydrazone bonds. The reverse reaction was monitored with static water contact angle (WCA) (Figure 5.3). The WCA for an unmodified hydrazide-functional polymer brush surface is 62.6º ± 1.9 (Figure 5.3a), which increased to 81.0º ± 1.8 after modification with decanal (Figure 5.3b) as the hydrophobic content on the surfaces increased. The WCA decreased back to 63.4º ± 1.4 (Figure 5.3c) after reversal of the hydrazone bonds with TFA (1 M) to the original hydrazide-functional groups. The final WCA is within 1º of the initial value for a hydrazide-functional brush suggesting nearly complete reversal of the hydrazone bonds was achieved.

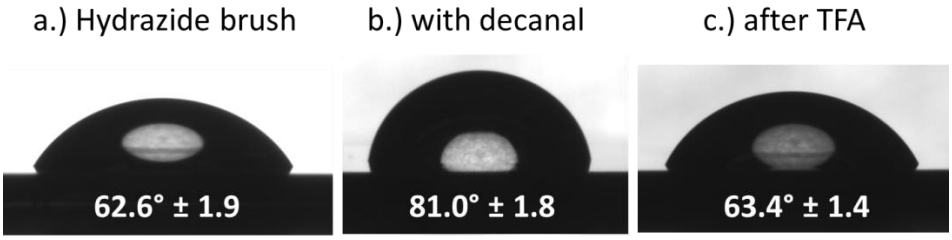

Figure 5.3 Static water contact angles of (a) a hydrazide-functional brush surface (b) after hydrazone formation with decanal (c) and hydrazone cleavage with TFA to regenerate hydrazide-functional polymer brushes.

To ensure that thickness changes are primarily a result of polymer modification and that unmodified brushes are stable in TFA (1 M), a control experiment was performed where a hydrazide brush surface was submerged in TFA (1 M) and THF for 2 h. The initial HEMA-hydrazide brush had a thickness of 23.92 nm ± 0.69 nm. After 2 h in solvent with acid present, the final brush thickness was determined to be 23.49 nm ±

0.38 nm by ellipsometry. This result shows that there was not a significant contribution to brush thickness from solvent swelling. Additionally, no decrease in thickness was observed that would indicate degradation of the polymer brushes in the presence of TFA.

5.2.3 Dynamic Surface Modification via Hydrazone Exchange Reactions

After determining successful hydrazone formation conditions, we next sought to employ hydrazone exchange reactions to dynamically change surface chemistry for control of surface properties and functions. The established equilibrium during hydrazone formation also allows exchange, or transimination, reactions to be driven towards the desired hydrazone product by addition of an excess of the new aldehyde to be exchanged. A large excess of aldehyde is simple to achieve in our case due to the inherently low concentration of polymers attached to surfaces in ultrathin films established by SIP techniques. In addition to establishing conditions for hydrazone exchange, we examined the ability of these exchange reaction on brush surfaces to perform over multiple cycles. A general representation of hydrazone exchange on brush surfaces is shown in Scheme 5.3.

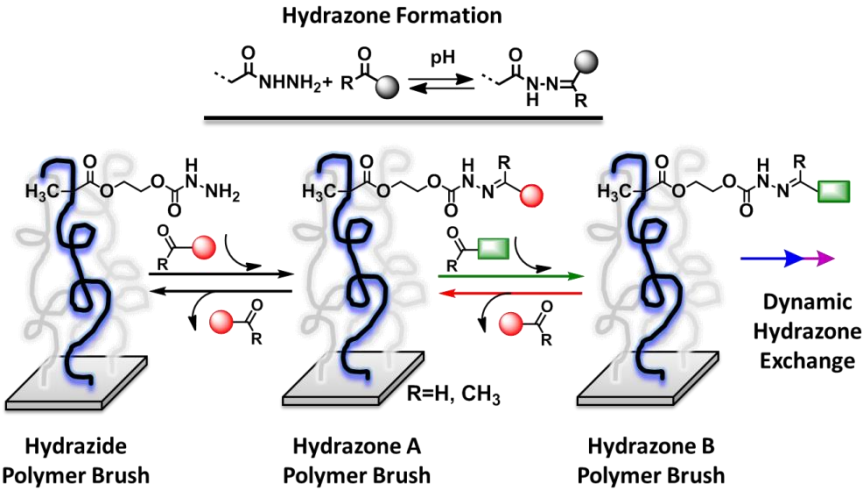

Scheme 5.3 Dynamic surface modification via hydrazone exchange.

Hydrazone exchange reactions over multiple cycles were first monitored by x-ray photoelectron spectroscopy (XPS). For each exchange reaction, a hydrazone brush surface was submerged in test tube containing a 5:1 mixture of THF and methanol with 1 M TFA, 0.1 M aldehyde modifier, and 10 mM aniline as a catalyst. These exchange reactions were carried out overnight at room temperature. XPS was then used to monitor change in elemental content on the brush surfaces as exchange reactions progressed between decanal, 4-fluorobenzaldehyde, 4-chlorobenzaldehyde, and 4-bromobenzaldehyde. Starting with a decanal-modified hydrazone brush surface, the XPS spectrum in Figure 5.4a reveals peaks at 285, 401, and 533 eV that are representative of the carbon, nitrogen, and oxygen character, respectively. When exchanging decanal for 4-fluorobenzaldehyde, a peak appeared at 687 eV corresponding to the fluorine atom in 4-fluorobenzaldehyde indicating that exchange was successful (Figure 5.4b). 4-fluorobenzaldehyde was then exchanged with 4-chlorobenzaldehyde which was reflected in the XPS spectrum (Figure 5.4c) by the disappearance of the fluorine peak at 687 eV and the appearance of chlorine peaks at 201 eV and 271 eV. The same trend was seen as 4-chlorobenzaldehyde was exchanged for 4-bromobenzaldehyde and the chlorine peaks at 200 and 280 eV disappeared to be replaced by bromine peaks at 71 eV, 184 eV, and 258 eV for 4-bromobenzaldehyde (Figure 5.4d). These results illustrate that exchange reactions can be readily employed over multiple cycles.

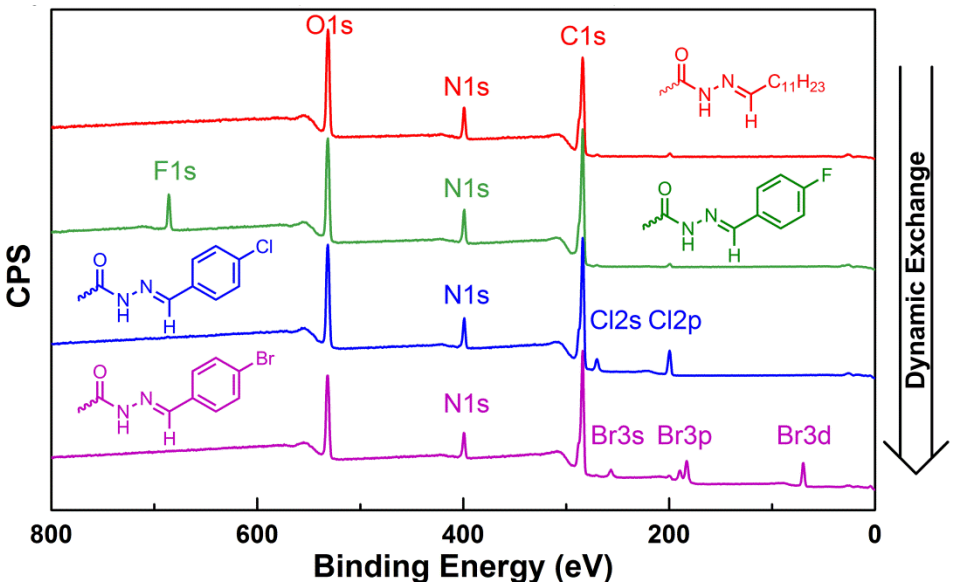

Figure 5.4 Survey XPS spectra of the dynamic exchange of aldehydes with pHEMA-hydrazone brushes. (a) hydrazone formation with Ald1, (b) hydrazone exchange of Ald1 with Ald5, (c) exchange of Ald5 with Ald6, (d) exchange of Ald6 with Ald7.

After confirming successful exchange reactions by XPS, we investigated the hydrazone exchange as a means to change surface wettability in a reversible fashion. Wettability was selected as a surface property to monitor due to the ability to readily observe the influence of changing surface chemistry on surface properties. By switching surface functionality between a hydrophobic aldehyde, decanal, and a hydrophilic aldehyde, 2,4-dihydroxybenzaldehyde, we demonstrated the capacity to reversibly control surface properties over multiple cycles. HEMA-hydrazide brushes on a silicon substrate were modified with decanal and then exchanged with 2,4-dihidroxybenzaldehyde (Scheme 5.4). 1 M TFA and 10 mM aniline were used to carry out hydrazone exchange reactions. Additionally, the reaction test tubes with substrates were heated to 40 ºC for 3 h before allowing exchange reactions to proceed at room temperature overnight aid to aid in aldehyde exchange. Three exchange cycles were performed and monitored by gATR-FTIR spectroscopy, ellipsometry, and WCA. The

gATR-FTIR spectra in Figure 5.5 illustrate that exchange occurs during each cycle by the appearance and disappearance of decanal peaks at 2925 cm^{-1} and 2856 cm^{-1} (regions highlighted by a red dotted line) and 2,4-dihydroxybenzaldehyde peaks at 1630 cm^{-1} and 3270 cm^{-1} (regions highlighted by blue dotted lines). Static WCA measurements also change according to the aldehyde participating in the hydrazone linkage over three cycles, increasing when hydrophobic decanal hydrazones are formed and decreasing as the hydrophilic 2,4-dihydroxybenzaldehyde is exchanged (Figure 5.6). While the exchange of aldehydes occurs during each cycle, the magnitude of the difference between the more hydrophobic state and the more hydrophilic state decreases slightly with increasing number of exchange reactions. gATR-FTIR spectra (Figure 5.5) also show, as exchange cycles progress, some residual aldehyde that is not exchanged. Factors like steric congestion may be responsible for trapped aldehydes and/or unreacted moieties that result in an incomplete exchange reaction near the surface layer of the brush.[30]

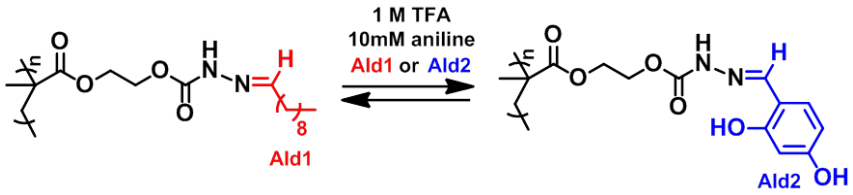

Scheme 5.4 Exchange reaction between decanal (Ald1) and 2,4-dihydroxybenzaldehyde (Ald2).

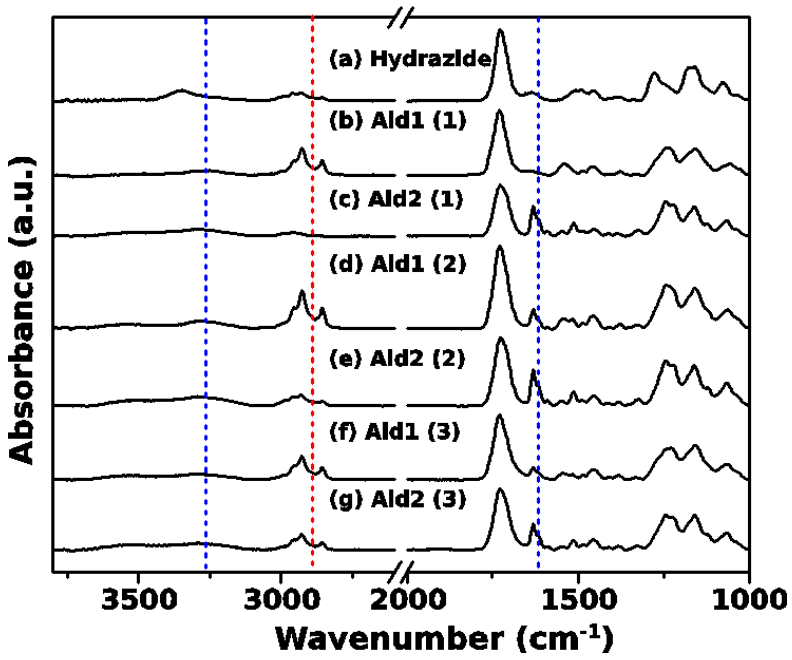

Figure 5.5 gATR-FTIR spectra of exchange reaction between decanal (Ald1) and 2,4-dihydroxybenzaldehyde (Ald2).

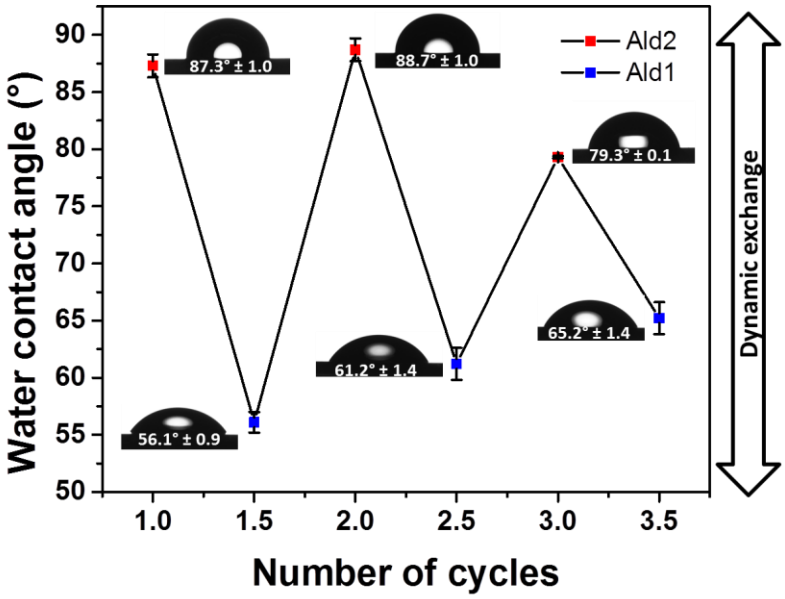

Figure 5.6 Water contact angle as a function of cycles where the hydrazone functional group changes between cycles from decanal (Ald1) to 2,4-dihydroxybenzaldehyde (Ald2).

Another factor that may contribute to incomplete exchange reactions is the nature of the aldehyde being used. It has been shown that aromatic aldehydes, particularly those with electron donating character, form more stable hydrazone linkages making them more difficult to exchange.[17] Despite some residual aldehyde after exchange, our strategy for dynamically changing surface chemistry was successful even for more stable hydrazone bonds, such as 2,4-dihydroxybenzaldehyde.

5.3 Conclusions

In summary, we report the synthesis of dynamic hydrazide-functional polymer brush surfaces with defined architectures via a simple, efficient combination of SI-ATRP and PPM. Successful hydrazone formation and exchange reactions were achieved with aliphatic and aryl aldehydes including those containing electron-donating or electron-withdrawing substituents. Additionally, exchange reactions were extended to multiple cycles to demonstrate the utility of these materials for applications such as capture/ release. Furthermore, surface hydrophobicity/ hydrophilicity was switched by exchanging hydrophobic aldehydes with hydrophilic ones to show that strategy provides dynamic control of surface properties. Hydrazide-functional brush surfaces provide a versatile approach to the design of dynamic covalent surfaces. Additionally, tuning the identity of the aldehydes and structure of the hydrazide (i.e. aryl acyl hydrazide, aliphatic hydrazide) will allow further investigation into improving rates and conversions of hydrazone exchange reactions.

5.4 Experimental

5.4.1 Materials

Reagent chemicals were purchased from Sigma-Aldrich Company and used without further purification unless otherwise indicated. Single-side polished silicon wafers were purchased from University Wafers and quartz microscope slides were purchased from Chemglass. 2-hydroxyethyl methacrylate (HEMA, 97% Sigma-Aldrich) was passed through a neutral alumina plug prior to use to remove inhibitor.

5.4.2 Characterization

A Varian Mercury Plus 300MHz NMR spectrometer operating at a frequency of 300 MHz with VNMR 6.1C software was used for proton and carbon analysis. Wettability of the unmodified and modified polymer brushes were monitored by a Ramé-hart 200-00 Std.-Tilting B. goniometer. Static (θsw) contact angles were measured using 10 μL water droplets in combination with DROPimage Standard software. Ellipsometric measurements were carried out using a Gaertner Scientific Corporation LSE ellipsometer with a 632.8 nm laser at 70° from the normal. Refractive index values of 3.86, 1.45, 1.43 and 1.5 for silicon, oxide layer, photoinitiator monolayer and all polymer layers, respectively, were used to build the layer model and calculate layer thicknesses.[31, 32] The chemical nature of the polymer brush surfaces was characterized by Fourier transform infrared spectroscopy (FTIR) in grazing-angle attenuated total reflectance mode (gATR-FTIR) using a ThermoScientific FTIR instrument (Nicolet 8700) equipped with a VariGATR™ accessory (grazing angle 65°, germanium crystal; Harrick Scientific). Spectra were collected with a resolution of 4 cm^{-1} by accumulating a minimum of 128 scans per sample. All spectra were collected while purging the VariGATR™ attachment

and FTIR instrument with N_2 gas along the infrared beam path to minimize the peaks corresponding to atmospheric moisture and CO2. Spectra were analyzed and processed using Omnic software. Atomic force microscopy (AFM) images were collected with a Bruker Dimension Icon operating in contact mode using Bruker SNL-10 probes (silicon tip; silicon nitride cantilever, spring constant: 0.350 N/m). A Lambda 35 UV-vis spectrometer was used to collect UV-Vis spectra of functionalized quartz substrates. Absorbance values were collected over a wavelength range of 200 - 700 nm. Quartz substrates were secured in 1 mm cuvette holders for analysis and an unmodified quartz substrate was used as a reference. XPS measurements were performed a Kratos Axis Ultra Spectrometer (Kratos Analytical, Manchester, UK) with a monochromatic Al K X-ray source (1486.6 eV) operating at 150 W under 1.0 × 10-9 Torr. Measurements were performed in hybrid mode using electrostatic and magnetic lenses, and the pass energy of the analyzer was set at 40 eV for high resolution spectra and 160 eV for survey scans, with energy resolutions of 0.1 eV and 0.5 eV, respectively. Generally, total acquisition times of 180 s and 440 s were used to obtain high resolution and survey spectra, respectively. For a 0° take off angle (angle between sample surface normal and the electron optical axis of the spectrometer), the maximum information depth of the measurements was approximately 8 nm1 All XPS spectra were recorded using the Kratos Vision II software; data files were translated to VAMAS format and processed using the CasaXPS software package (v. 2.3.12). Binding energies were calibrated with respect to C 1s at 285 eV.

5.4.3 Synthesis of pHEMA Brush Surfaces by Surface-Initiated Atom-Transfer Radical Polymerization

First, synthesis of 10-undecen-1-yl 2-bromo-2-methylpropionate (ATRP initiator precursor), (11-(2-bromo-2-methyl)propionyloxy)undecyltrichlorosilane (ATRP initiator-trichlorosilane), and immobilization of SI-ATRP initiator on silicon surfaces were performed according to literature procedure.[10] Then, in a vacuum purged test tube, SI-ATRP was carried out in the presence of HEMA followed by extensive washing in methanol, THF, and toluene. A typical polymerization procedure is as follows: initiator functionalized substrates were submerged into a reaction solution containing HEMA, 2,2'-bipyridyl, copper(I)bromide, (40:1:0.5 mol% monomer/ligand/Cu(I)Br) in deionized water and methanol (1:4 v/v) at room temperature. Prior to the polymerization, the monomer solution, Cu/ligand complex, and initiator functionalized substrates were degassed separately by either bubbling nitrogen through the solution or vacuum/purge cycles. Reaction times were varied to obtain the desired thickness of HEMA brushes.

5.4.4 Synthesis of Hydrazide-Functional Brush Surfaces via Post-Polymerization Modification

The pHEMA brush surfaces were modified with 4-nitrophenyl chloroformate to yield activated carbonate functional brushes. pHEMA modified substrates and dry dichloromethane (8 mL) were added to a test tube equipped with rubber septa and purged with N_2. Triethylamine (0.1M, 80.95 mg) was added followed by 4-nitrophenyl chloroformate(0.1M, 161.25 mg) dissolved in a small amount of dry dichloromethane. The test tube was then placed in a shaker overnight. After reaction, substrates were removed and washed with dichloromethane, 0.5 M HCl, and DI water followed by

sonication in THF and additional solvent rinses with THF and, lastly, toluene. The reactive carbonate functional brushes, formed by reaction of HEMA with 4-nitrophenyl chloroformate, were submerged in a methanol solution containing hydrazine hydrate (0.1 M, 40.04 mg) and allowed to react overnight to insure completion. After reaction, the substrates were sonicated in methanol followed by rinses with THF and, lastly, toluene.

5.4.5 Formation of Hydrazones on Brush Surfaces

Hydrazone formation was achieved in organic media (THF or methanol depending on solubility) by submersion of hydrazide functional brushes in a test tube with a solution containing desired aldehyde (0.1 M). The reactions were allowed to proceed overnight to insure complete reaction, rinsed and sonicated in THF or methanol, and finally rinsed with THF and toluene to remove any residual aldehyde.

5.4.6 Hydrazone Reverse and Exchange Reactions

Hydrazone exchange reactions were carried out in a THF/methanol solution (5:1 v:v). Trifluoroacetic acid (TFA, 1M) and aniline (10 mM) were added to a test tube containing the solvent mixture followed by the addition of the aldehyde (Ald1-Ald7) (0.1 M) to participate in the exchange reaction. Exchange reactions were carried out overnight to insure completion. Reactions were conducted at room temperature unless otherwise noted.

5.5 References

1. Koberstein, J. T. *Journal of Polymer Science Part B: Polymer Physics* **2004,** 42, (16), 2942-2956.

2. Barbey, R.; Lavanant, L.; Paripovic, D.; Schüwer, N.; Sugnaux, C.; Tugulu, S.; Klok, H.-A. *Chemical Reviews* **2009,** 109, (11), 5437-5527.

3. Krishnamoorthy, M.; Hakobyan, S.; Ramstedt, M.; Gautrot, J. E. *Chemical Reviews* **2014,** 114, (21), 10976-11026.

4. Wu, L.; Glebe, U.; Boker, A. *Polymer Chemistry* **2015,** 6, (29), 5143-5184.

5. Khabibullin, A.; Mastan, E.; Matyjaszewski, K.; Zhu, S., Surface-Initiated Atom Transfer Radical Polymerization. In *Controlled Radical Polymerization at and from Solid Surfaces*, Vana, P., Ed. Springer International Publishing: Cham, 2016; pp 29-76.

6. Jo, H.; Theato, P., Post-polymerization Modification of Surface-Bound Polymers. In *Controlled Radical Polymerization at and from Solid Surfaces*, Vana, P., Ed. Springer International Publishing: Cham, 2016; pp 163-192.

7. Arnold, R. M.; Huddleston, N. E.; Locklin, J. *Journal of Materials Chemistry* **2012,** 22, (37), 19357-19365.

8. Galvin, C. J.; Genzer, J. *Progress in Polymer Science* **2012,** 37, (7), 871-906.

9. Gauthier, M. A.; Gibson, M. I.; Klok, H.-A. *Angewandte Chemie International Edition* **2009,** 48, (1), 48-58.

10. Hensarling, R. M.; Hoff, E. A.; LeBlanc, A. P.; Guo, W.; Rahane, S. B.; Patton, D. L. *Journal of Polymer Science Part A: Polymer Chemistry* **2013,** 51, (5), 1079-1090.

11. Hensarling, R. M.; Doughty, V. A.; Chan, J. W.; Patton, D. L. *Journal of the American Chemical Society* **2009,** 131, (41), 14673-14675.

12. Hensarling, R. M.; Rahane, S. B.; LeBlanc, A. P.; Sparks, B. J.; White, E. M.; Locklin, J.; Patton, D. L. *Polymer Chemistry* **2011,** 2, (1), 88-90.

13. Preuss, C. M.; Goldmann, A. S.; Trouillet, V.; Walther, A.; Barner-Kowollik, C. *Macromolecular Rapid Communications* **2013,** 34, (8), 640-644.

14. Sato, T.; Amamoto, Y.; Yamaguchi, H.; Ohishi, T.; Takahara, A.; Otsuka, H. *Polymer Chemistry* **2012,** 3, (11), 3077-3083.

15. Liu, H.; Li, Y.; Sun, K.; Fan, J.; Zhang, P.; Meng, J.; Wang, S.; Jiang, L. *Journal of the American Chemical Society* **2013,** 135, (20), 7603-7609.

16. Rao, J.; Khan, A. *Polymer Chemistry* **2013,** 4, (9), 2691-2695.

17. Kool, E. T.; Park, D.-H.; Crisalli, P. *Journal of the American Chemical Society* **2013,** 135, (47), 17663-17666.

18. Su, X.; Aprahamian, I. *Chemical Society Reviews* **2014,** 43, (6), 1963-1981.

19. van Dijken, D. J.; Kovaříček, P.; Ihrig, S. P.; Hecht, S. *Journal of the American Chemical Society* **2015,** 137, (47), 14982-14991.

20. Dirksen, A.; Dirksen, S.; Hackeng, T. M.; Dawson, P. E. *Journal of the American Chemical Society* **2006,** 128, (49), 15602-15603.

21. Deng, G.; Li, F.; Yu, H.; Liu, F.; Liu, C.; Sun, W.; Jiang, H.; Chen, Y. *ACS Macro Letters* **2012,** 1, (2), 275-279.

22. Zhi, Z.-l.; Powell, A. K.; Turnbull, J. E. *Analytical Chemistry* **2006,** 78, (14), 4786-4793.

23. Ballard, N.; Bon, S. A. F. *Polymer Chemistry* **2014,** 5, (23), 6789-6796.

24. Iwasaki, Y.; Maie, H.; Akiyoshi, K. *Biomacromolecules* **2007,** 8, (10), 3162-3168.

25. Iwasaki, Y.; Tabata, E.; Kurita, K.; Akiyoshi, K. *Bioconjugate Chemistry* **2005,** 16, (3), 567-575.

26. von Delius, M.; Geertsema, E. M.; Leigh, D. A.; Tang, D.-T. D. *Journal of the American Chemical Society* **2010,** 132, (45), 16134-16145.

27. Yang, S. J.; Zhang, H. *Analytical Chemistry* **2012,** 84, (5), 2232-2238.

28. Jin, J.; Liu, J.; Lian, X.; Sun, P.; Zhao, H. *RSC Advances* **2013,** 3, (19), 7023-7029.

29. Brinkhuis, R. P.; de Graaf, F.; Hansen, M. B.; Visser, T. R.; Rutjes, F. P. J. T.; van Hest, J. C. M. *Polymer Chemistry* **2013,** 4, (5), 1345-1350.

30. Schuh, C.; Rühe, J. *Macromolecules* **2011,** 44, (9), 3502-3510.

31. Beinhoff, M.; Frommer, J.; Carter, K. R. *Chemistry of Materials* **2006,** 18, (15), 3425-3431.

32. Schuh, C.; Santer, S.; Prucker, O.; Rühe, J. *Advanced Materials* **2009,** 21, (46), 4706-4710.

CHAPTER VI – CONCLUSIONS AND FUTURE WORK

In summary, this dissertation focused on the design and synthesis of polymer scaffolds in solution and on surfaces bearing reactive functional groups with dynamic character. The research described herein addressed limitations in isocyanate PPM strategies (Chapter III), controlled polymerization of monomers possessing nucleophilic functional groups with low pK_a values (Chapter IV), and dynamic covalent surface modification based on pH-responsive hydrazone chemistry (VI).

In Chapter III, the synthesis of well-defined polymethacrylate scaffolds containing pendent N-heterocycle-blocked isocyanates via low temperature RAFT polymerization is reported. The reactivity of the azole-*N*-carboxamide moieties towards nucleophiles was tuned simply by varying the structure of the azole blocking agents (reactivity order: pyrazole < imidazole < triazole) to achieve rapid and efficient post-polymerization modification with thiols and amines at ambient temperature via chemical deblocking. Differences in the latent reactivity of triazole- and pyrazole-blocked NCO methacrylates were used to attain sequential post-polymerization modification. The work reported in this section provides an efficient and versatile approach to obtain multifunctional materials from a broad selection of thiol and amine modifiers using mild, room temperature conditions. Furthermore, this platform may be expanded to include additional blocking agents of varying reactivity. In ongoing work, blocked isocyanates are being investigated as a surface modification strategy in combination with SIP.

In the next chapter, acyl hydrazide methacrylamides and 4-vinylimidazole were synthesized in order to investigate low pH (< 1) aqueous RAFT polymerization of monomers with nucleophilic functional groups with low pK_a values. Additionally, a

novel imidazolium CTA was synthesized that demonstrated excellent hydrolytic stability and ability to mediate aRAFT polymerization at low pH values. Successful aRAFT polymerizations of an unprotected acyl hydrazide methacrylamide and 4-vinylimidazole were achieved at pH = 0 and yielded polymers with well-defined molecular weights and low dispersities. This marks the first report of the controlled polymerization of an unprotected acyl hydrazide-containing monomer and is expected to open the door to important hydrazide-functional polymer scaffolds for applications such as bioconjugation. Chain extension polymerizations of MAEH and 4VIM were performed and demonstrated that aRAFT polymerization at low pH afforded chain-end retention for block copolymer applications. Future directions include investigation of the formation of hydrazones from acyl hydrazide aRAFT polymers as well as the synthesis and controlled polymerization of alkyl hydrazides and phenacylhydrazides. Additionally, upon obtaining polymers with varying structures of the pendent hydrazides, the influence of hydrazide structure on rates and stabilities of pendent hydrazone formation and exchange reactions may be studied.

In the last chapter of this dissertation, hydrazide-functional polymer brush surfaces were synthesized via SI-ATRP of 2-hydroxyethyl methacrylate and subsequent PPM. The hydrazide-containing side chains on these brush surfaces were then used to successfully generate dynamic covalent hydrazone linkages from a variety of both aliphatic and aryl aldehydes. Additionally, hydrazone reverse and exchange reactions were demonstrated in the presence of TFA and used to control surface wettability. Hydrazone exchange reactions performed over multiple cycles were followed with XPS, gATR-FTIR spectroscopy, and WCA measurements. XPS measurements revealed

dynamic exchange between decanal, 4-fluorobenzaldehyde, 4-bromobenzaldehyde, and 4-chlorobenzadehyde. As exchange cycles between decanal and 2,4-dihydroxybenzaldehyde progressed some residual unexchanged aldehyde was observed, which may be the result of electronic effects influencing hydrazone stability or steric hindrance as a function of brush density. Despite some residual aldehyde during exchange cycles, hydrazide-functional brushes were easily obtained and used for dynamic surface modification to control surface properties. Future work will investigate the influence of hydrazide structure on exchange rates and conversion. Additionally, kinetic investigations of hydrazone formation, cleavage, and exchange will be explored on brush surfaces.

APPENDIX A – RAFT Polymerization of "Splitters" and "Cryptos": Exploiting Azole-*N*-Carboxamides as Blocked Isocyanates for Ambient Temperature Post-Polymerization Modification

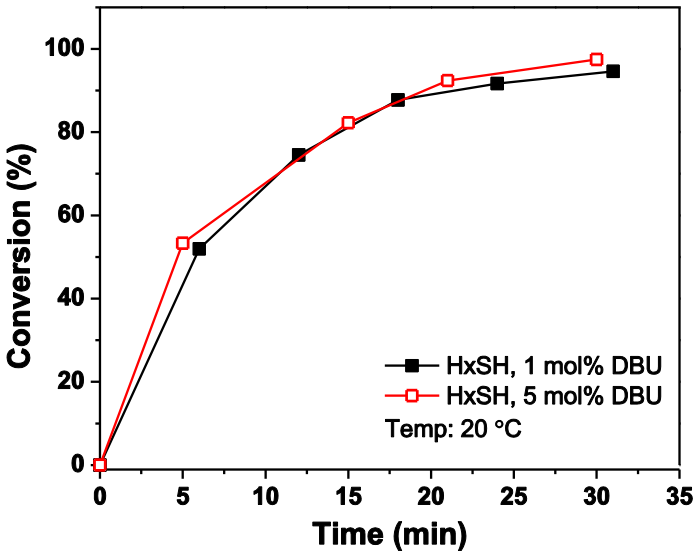

Figure A.1 Conversion versus time plots for model reactions of (■) mNCOT + 1-hexanethiol (HxSH) + 1 mol% DBU at 20ºC and (□) mNCOI + HxSH + 5 mol% DBU at 20ºC.

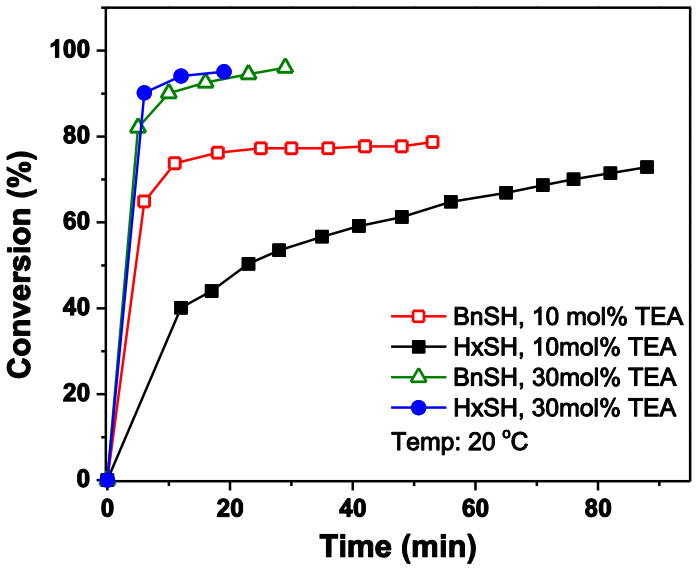

Figure A.2 Conversion versus time plots for model reactions of mNCOT with (□) benzyl mercaptan (BnSH) + 10 mol% TEA, (■) 1-hexanethiol (HxSH) + 10 mol% TEA, (Δ) BnSH + 30 mol% TEA, and (●) HxSH + 30 mol% TEA carried out at 20 ºC.

Table A.1

Influence of polymerization temperature on conversion, molecular weight, and $Đ_M$ for blocked NCO polymers made by RAFT.

Entry	Polymer	Temp.[a] (ºC)	Time[a] (min)	Conversion[b] (%)	$M_{n,theory}$ (kg/mol)	$M_{n,exp}$[c] (kg/mol)	$Đ_M$[c]
1a	pNCOP	25	300	18.7	14.3	23.2	1.10
1b	pNCOP	30		39.7	30.2	41.3	1.04
2a	pNCOI	25	300	8.6	6.0	26.7	1.19
2b	pNCOI	30		23.2	16.4	40.7	1.11
3a	pNCOT	25	300	37.9	26.5	35.3	1.08
3b	pNCOT	30		63.4	42.9	59.2	1.08

[a]Refers to polymerization time or temperature. [b]As determined by ^{1}H NMR. [c]As determined by SEC-MALLS (DMF with 20 mM LiBr) pNCOI and pNCOT samples were modified with PrSH prior to SEC analysis.

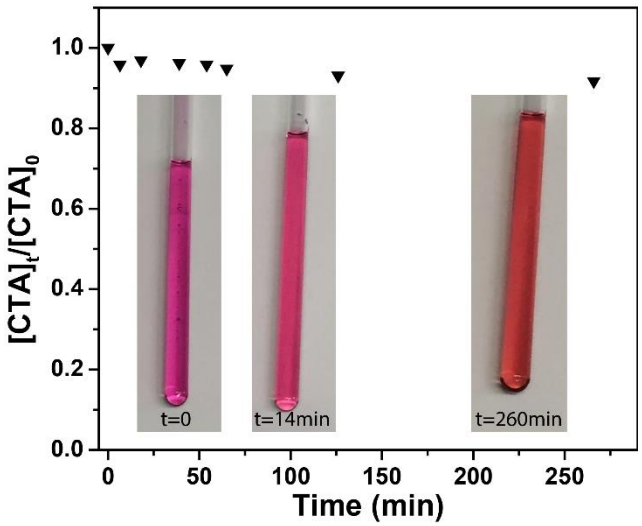

Figure A.3 CTA stability in the presence of NCOI monomer (10:1 [M]:[CTA]) as followed by ^{1}H NMR. Insets show the color change that occurs upon addition of NCOI

to the CTA. The color change was similar to that observed under polymerization conditions (300:1 [M]:[CTA]), however, degradation could not be determined with accuracy at 300:1 [M]:[CTA].

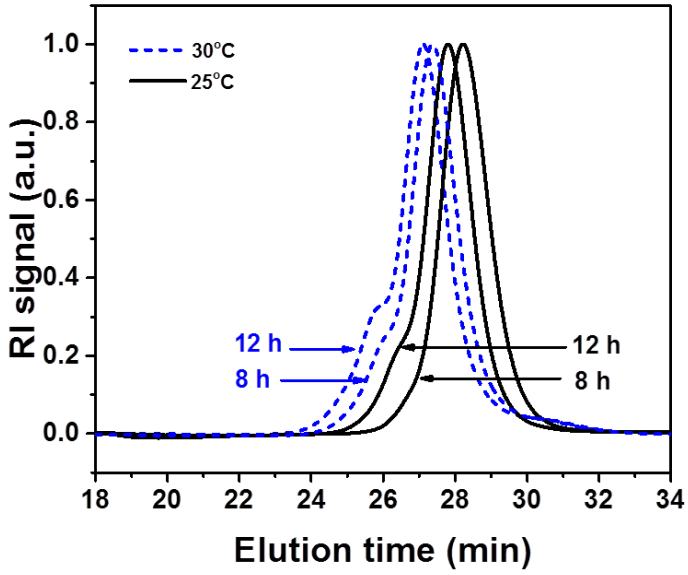

Figure A.4 SEC traces for aliquots of the RAFT polymerization of NCOT at 25ºC and 30ºC after 8 h and 12 h. The pNCOT was modified with PrSH prior to SEC analysis.

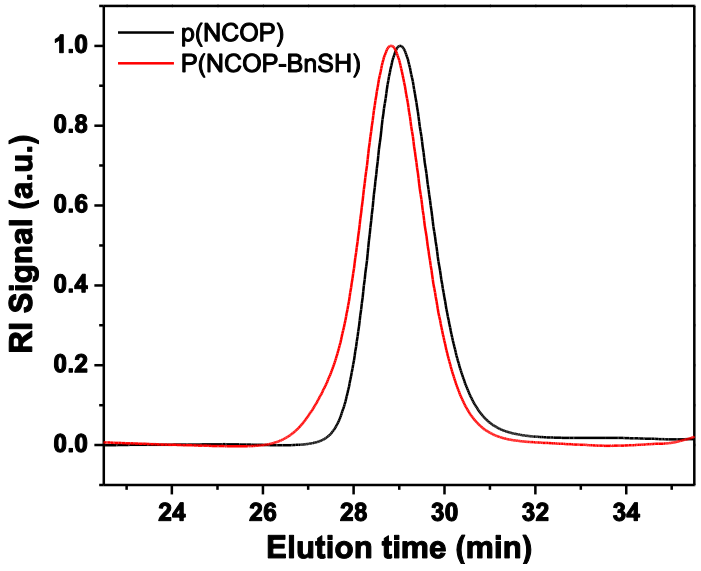

Figure A.5 SEC traces of pNCOP before ($Đ_M$ = 1.09) and after ($Đ_M$ = 1.10) modification with benzyl mercaptan at 50ºC.

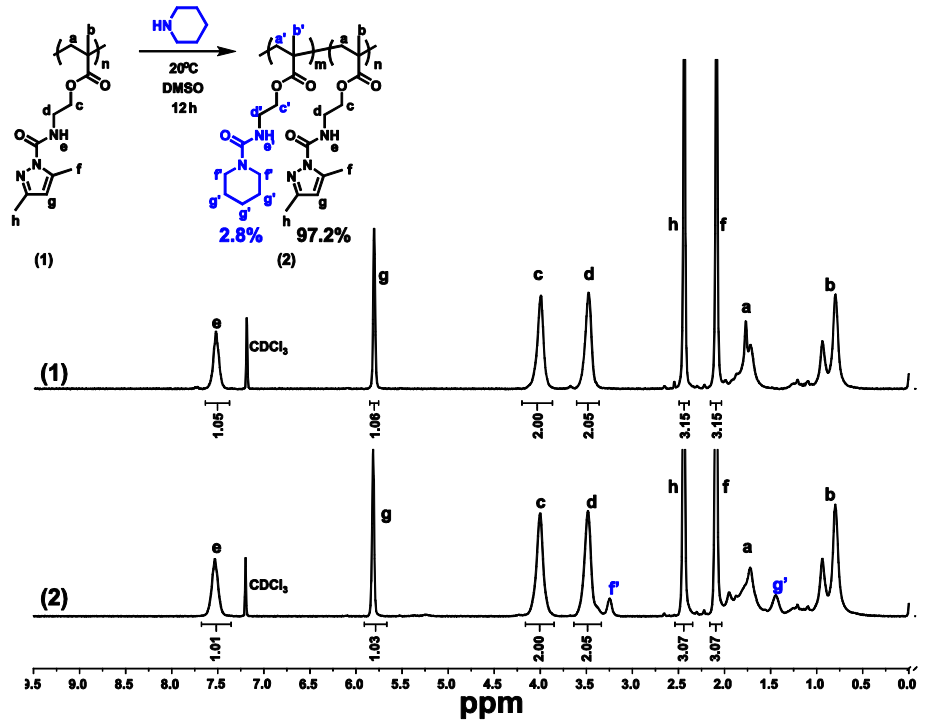

Figure A.6 ^{1}H NMR spectra of pNCOP homopolymer (1) before and after (2) modification with piperidine. Integration shows less than 3% of the pyrazole blocking agents are displaced by piperidine at 20 °C.

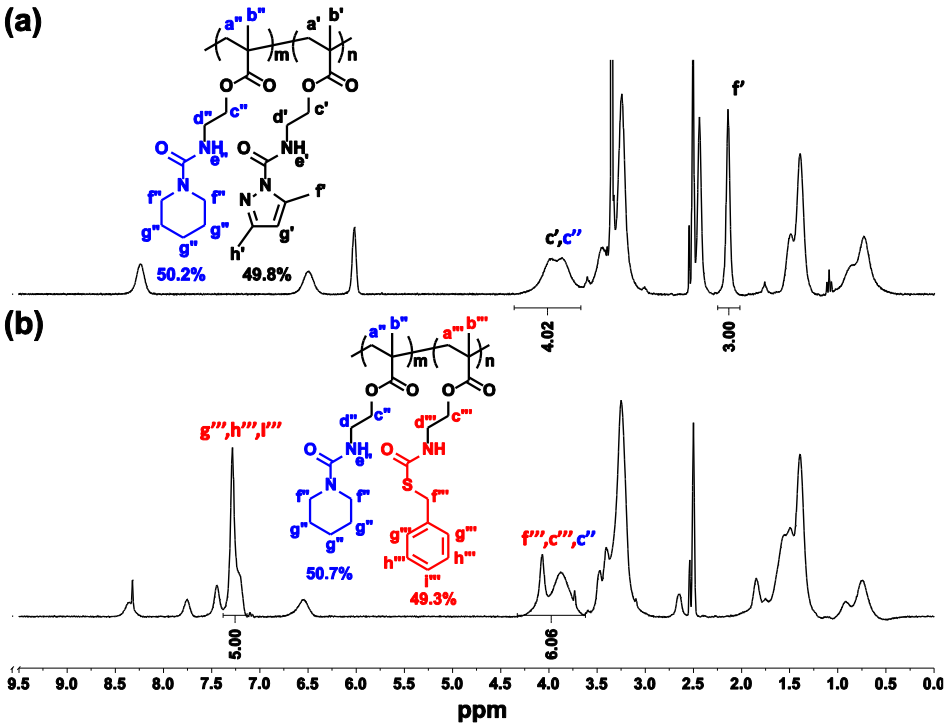

Figure A.7 ^{1}H NMR spectra of p(NCOT-PD-*co*-NCOP) after the first modification with piperidine and (b) after the second modification with benzyl mercaptan.

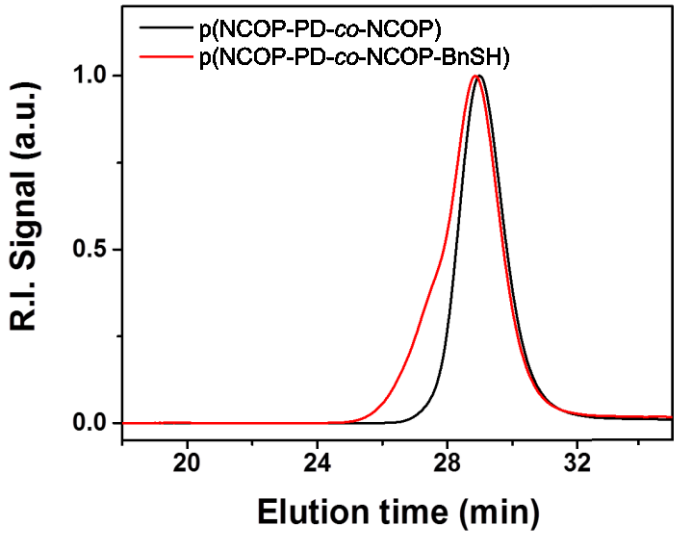

Figure A.8 SEC traces of the sequential modification of p(NCOT-*co*-NCOP) after modification of the NCOT units with piperidine at 20ºC (M_n= 43.4 kg/mol, $Đ_M$ = 1.05) (black) and after modification of the NCOP units with benzyl mercaptan at 50ºC (M_n= 52.7 kg/mol, $Đ_M$ = 1.24) (red).

APPENDIX B – Low pH Aqueous RAFT: Controlled Polymerization of Acyl hydrazide Methacrylamides and 4-Vinylimidazole

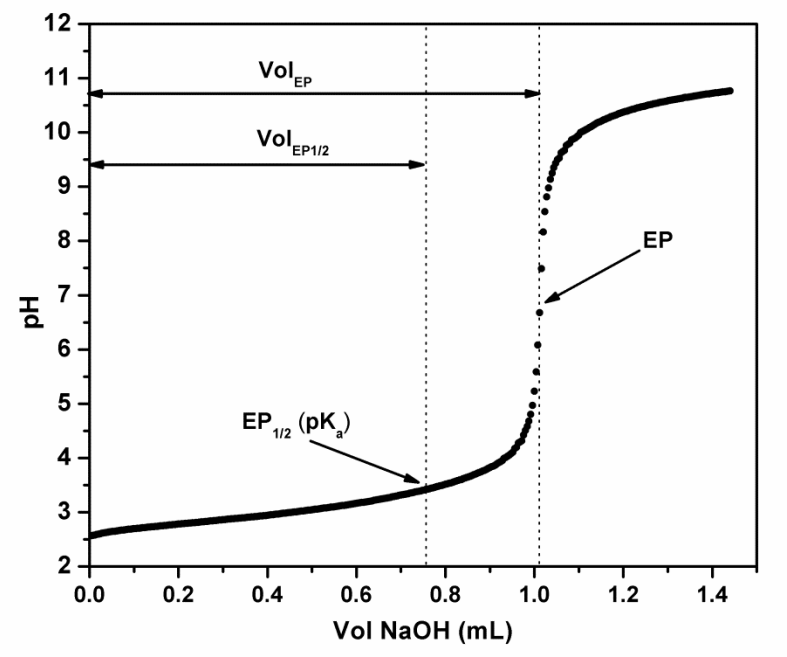

Figure B.1 EP and $EP_{1/2}$ locations on the titration curve of MAEH (1 mM) titrated against NaOH (0.05 N) at 25 °C using a Metrohm 848 Titrino Plus autotitrator.

Table B.1

pKa values determined for MAH, MAEH, and 4VIM and control pKa determination for imidazole via titration.

	EP run 1	**EP run 2**	**EP run 3**	**Summary**	
Monomer	**pK$_a$**	**pK$_a$**	**pK$_a$**	**Avg. pK$_a$**	**STD Dev.**
MAH	3.68	3.72	3.70	3.70	0.02
MAEH	3.42	3.43	3.43	3.43	0.01
4VIM	6.28	6.24	6.26	6.26	0.02

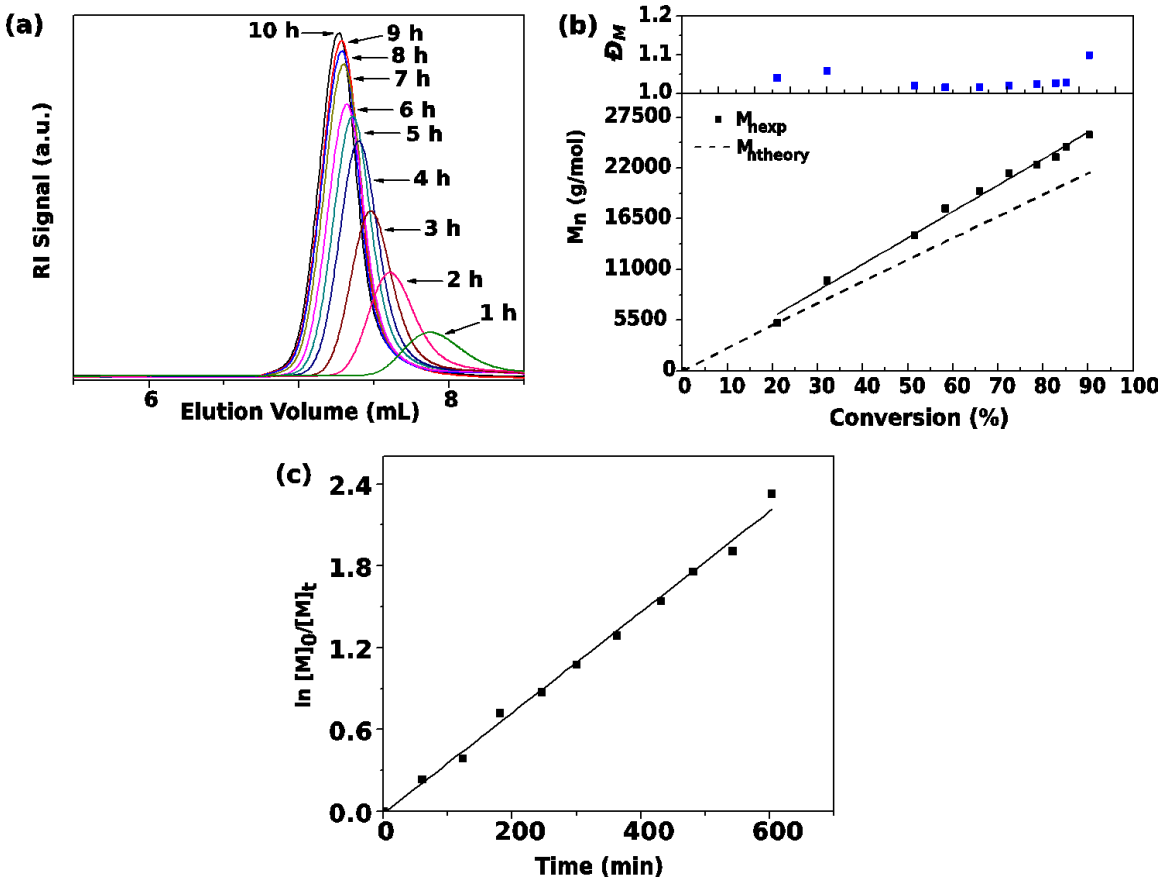

Figure B.2 (a) SEC traces for polymerization kinetics of 4VIM and inset scheme of low pH aRAFT polymerization of 4VIM, (b) dispersities and M_n vs. conversion plot, and (c) pseudo-first order kinetic plot for aRAFT polymerization of 4VIM in 2 M HCl with VA-044 and ImET at 40ºC.

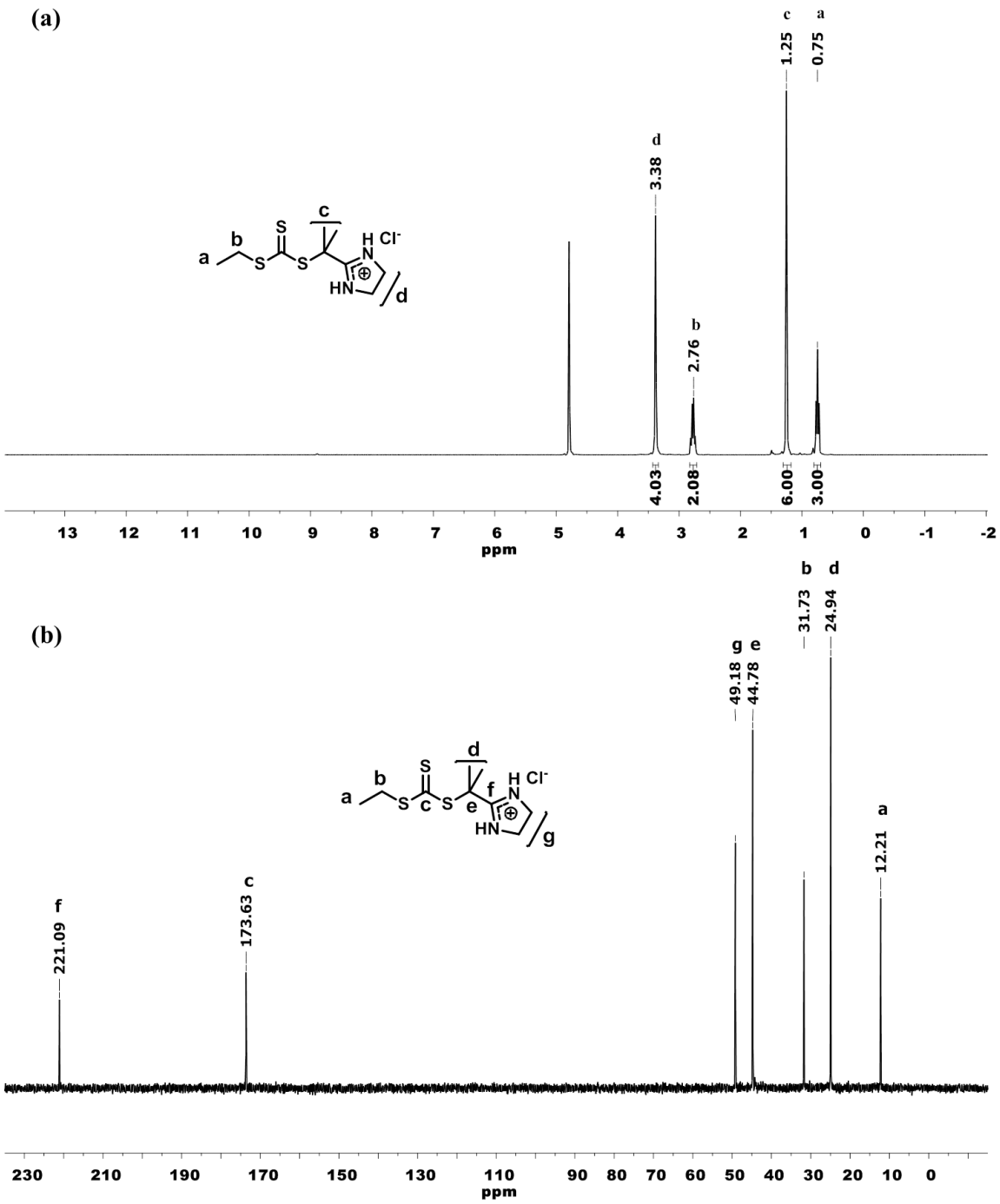

Figure B.3 (a) ^{1}H NMR and (b) ^{13}C NMR spectra of 2-(ethylthiocarbonothioylthio) 2-(2-imidazolin-2-yl)propane hydrochloride (ImET, 3).

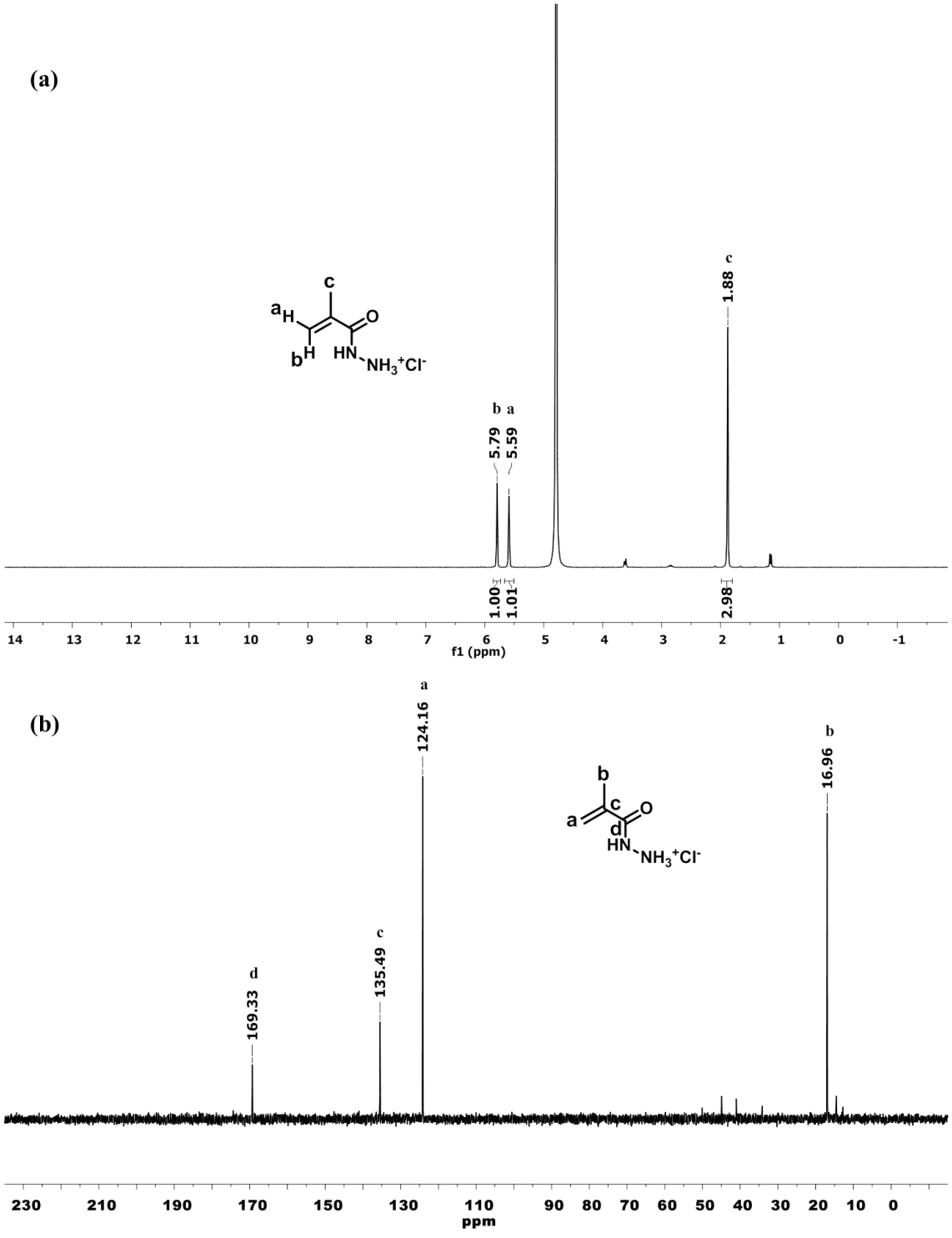

Figure B.4 (a) ^{1}H NMR and (b) ^{13}C NMR spectra of methacryloyl hydrazide hydrochloride (MAH, 5).

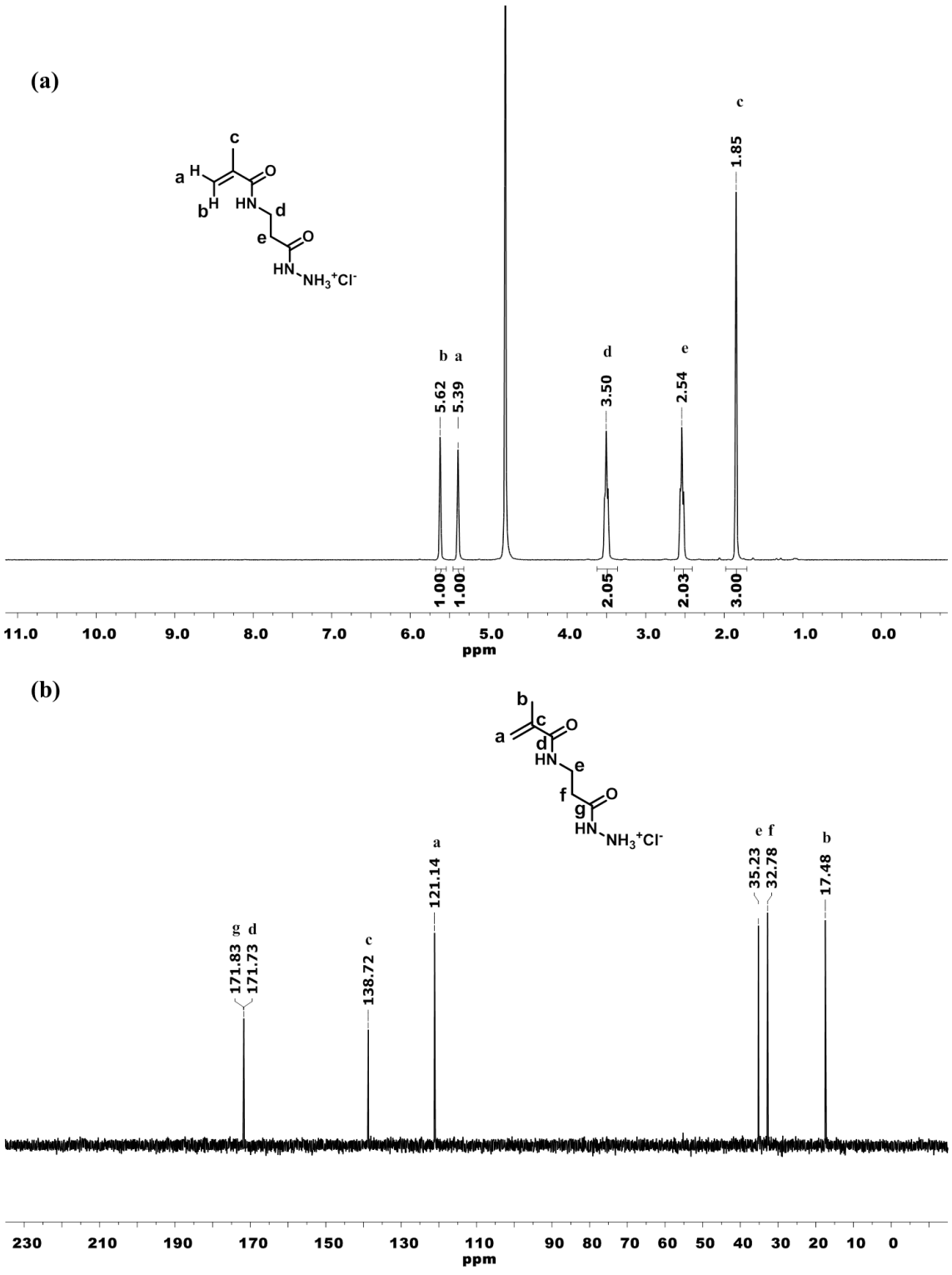

Figure B.5 (a) ^{1}H NMR and (b) ^{13}C NMR spectra of (2-methacrylamidoethyl) carbohydrazide hydrochloride (MAEH, 8).

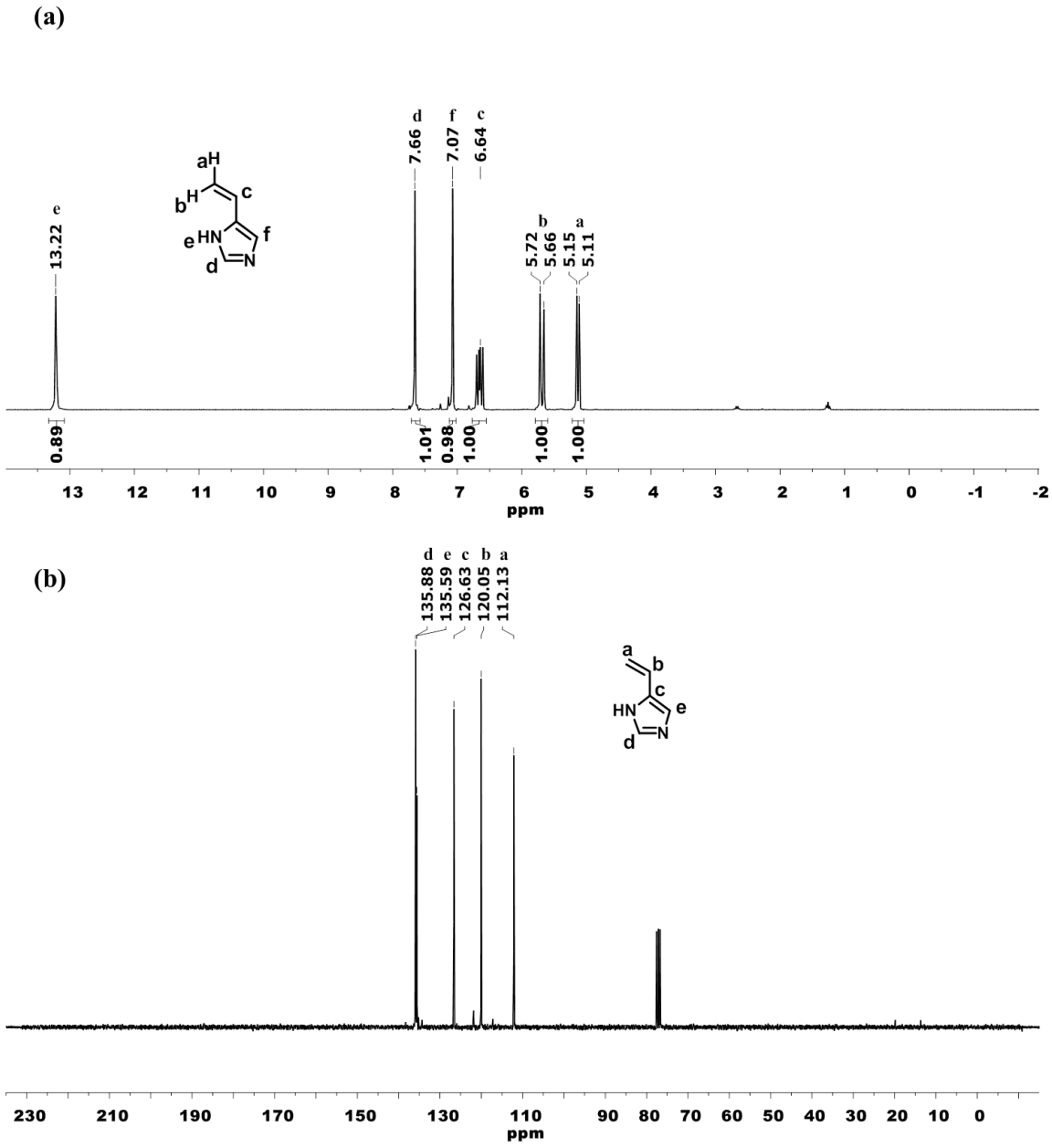

Figure B.6 (a) ^{1}H NMR and (b) ^{13}C NMR spectra of 4-vinylimidazole (4VIM, 9).

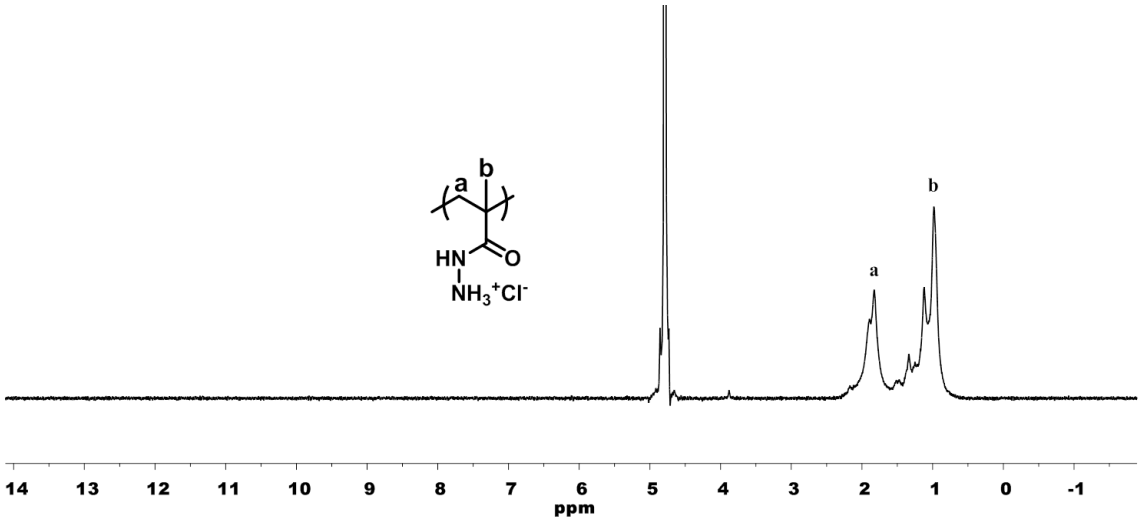

Figure B.7 ^{1}H NMR of pMAH.

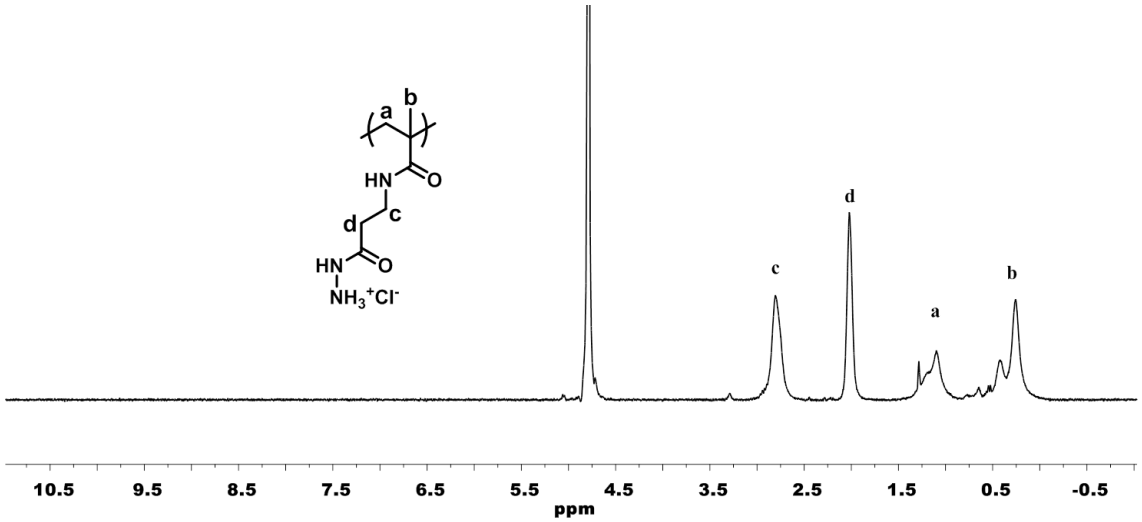

Figure B.8 ^{1}H NMR of pMAEH.